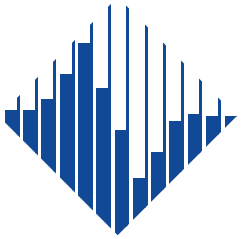

PACIFIC EARTHQUAKE ENGINEERING
RESEARCH CENTER

Influence of Vertical Ground Motion on Bridges Isolated with Spherical Sliding Bearings

Rushil Mojidra

Keri L. Ryan

Department of Civil and Environmental Engineering
University of Nevada, Reno

PEER Report No. 2019/08
Pacific Earthquake Engineering Research Center
Headquarters at the University of California, Berkeley

December 2019

PEER 2019/08
December 2019

Influence of Vertical Ground Motion on Bridges Isolated with Spherical Sliding Bearings

Rushil Mojidra

Keri L. Ryan

Department of Civil and Environmental Engineering
University of Nevada, Reno

PEER Report 2019/08
Pacific Earthquake Engineering Research Center
Headquarters at the University of California, Berkeley

December 2019

ABSTRACT

The motivation for this project developed from testing of a full scale building isolated with triple friction pendulum bearings on the E-defense shake table in Japan. The test demonstrated experimentally that the vertical component of ground motion can amplify both the base shear and the story acceleration in the isolated building. Vertical shaking introduced high-frequency variation in the axial force of the bearings, and, consequently, a high-frequency component in the bearing lateral force, which excited higher structural modes in the building. Since vertical bridges are flexible in the vertical direction because of long spans, similar effects may be observed in bridges.

The objectives of this study are to develop a physical understanding of the amplification of responses and develop a simplified method to predict amplification of base shear in three-dimensional (3D) shaking relative to two-dimensional (2D) shaking, for bridges isolated with spherical sliding bearings. A series of ground motions with a wide range of vertical shaking intensity were applied to 3D models of bridges isolated with triple pendulum bearings (TPBs), both excluding the vertical component (2D motion) and including the vertical component (3D motion). This enabled the comparison of the bridge response under 2D and 3D shaking such that the direct effect of vertical shaking could be investigated. The selected ground motions were fit to target spectra in the horizontal and vertical directions, and divided into three groups based on vertical peak ground acceleration (PGA_V). Multi-span concrete box girder bridges were selected for this study, as they are a prominent bridge type in California, and are suitable for seismic isolation. Models were developed for a 3-span, 45-ft wide, multi-column Base Model bridge; various superstructure and isolation-system parameter variations were implemented to evaluate the effect of these variations on the amplification of base shear. Response histories were compared for a representative motion from each ground-motion group under 2D and 3D shaking. Modal and spectral analyses were conducted to understand dynamic properties and behavior of the bridge under vertical motion. Based on simplified theory, a method to estimate the amplification of base shear due to vertical shaking was developed. The accuracy of the simplified method was assessed through a base shear normalized error metric, and different amplification factors were considered.

Response history analysis showed significant amplification of base shear under 3D motion implying that exclusion of vertical component could lead to under estimation of demand shear forces on bridge piers. Deck acceleration spectral response at different locations revealed that a transverse-vertical modal coupling response was present in the Base Model bridge, which led to amplification of deck accelerations in addition to base shear due to excitation of the superstructure transverse mode. The simplified method predicted that in addition to the peak vertical ground acceleration base shear amplification depended on the isolation-system period (radius of curvature) and friction coefficient. The error in the simplified method was approximately constant across the range of isolation-system parameters. Variations in the bridge

superstructure or substructure modeling parameters had only a minor effect on the base shear since the deck acts as a single mass sliding on isolators; therefore, the simplified method can be applied to a range of bridge models. The simplified method includes an amplification factor that indirectly represents the dynamic amplification of vertical acceleration from the ground to the isolation system. An amplification factor of 1.0 was found to be sufficiently conservative to estimate the base shear due to 3D shaking. The lack of apparent dynamic amplification could mean that the peak vertical acceleration is out-of-phase with the base shear. The simplified method is more likely to be unconservative for high-intensity vertical ground motions due to the complexities associated with uplift and pounding. Further investigation is recommended to determine the threshold shaking intensity limit for the simplified method.

ACKNOWLEDGMENTS

This study was sponsored by the Pacific Earthquake Engineering Research Center (PEER) with funding from the State of California through the Transportation Systems Research Program under Contract No. 1134-NCTRRY. The authors are grateful for this support. The authors recognize advisory committee members Allaoua Kartoum (Caltrans), Bijan Khalegi (vitiated), and Mason Walters (Forell-Elsesser) for providing feedback on the design of the study. Furthermore, feedback from Dr. Ian Buckle at the first author's M.S. thesis defense led to significant improvements in the simplified method to estimate base shear

Any opinions, findings, and recommendations expressed in this material are that of the authors and do not necessarily express those of the funding agency, PEER, or the Regents of the University of California..

CONTENTS

LIST OF TABLES

LIST OF FIGURES

1 Introduction

1.1 MOTIVATION AND BACKGROUND

Seismic isolation is a very effective approach to reduce the damaging effects of earthquakes on bridges, buildings, and other structural or nonstructural components. Isolation devices physically detach and uncouple the structure from the ground motion, thus reducing the forces transmitted to the structure by an earthquake. When applied to a bridge, the devices isolate the superstructure from horizontal ground shaking, significantly reducing the demand on the substructure. In order to isolate the superstructure, flexible devices are installed between the superstructure and substructure. Figure 1.1 compares a conventional bridge and isolated bridge response under earthquake loading.

An isolation system lengthens the natural period of the structure, significantly reducing the spectral acceleration demands (Figure 1.2). This reduction of spectral acceleration reduces inertial forces on the superstructure and allows the substructure—typically multi-column bents—to be designed to remain elastic. The lengthened natural period of the structure increases the displacement demands, which are accommodated by isolation devices. As a consequence, wider expansion joints and increased seat length may be required to accommodate displacement demands.

Isolation devices incorporate energy-dissipation mechanisms designed to limit the displacements demands to a reasonable level. Figure 1.3 shows a bilinear force-displacement curve, which is generally representative of several types of energy-dissipating isolation devices. The area under the closed curve represents the energy dissipated during each cycle of motion of the isolators. Isolation devices are also designed to provide high initial stiffness to resist service loads, e.g., wind loads or vehicle breaking forces. Isolation bearings remain elastic under wind loads and vehicle breaking forces, and exhibit nonlinear response under earthquake forces.

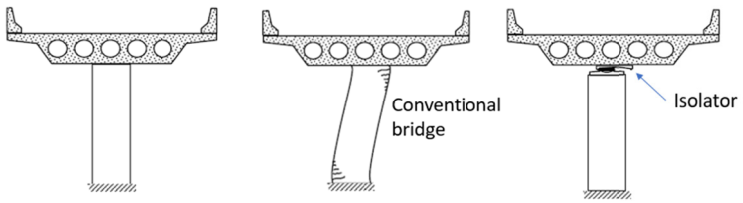

Figure 1.1 Behavior of conventional and seismically isolated bridge [Buckle et al. 2006].

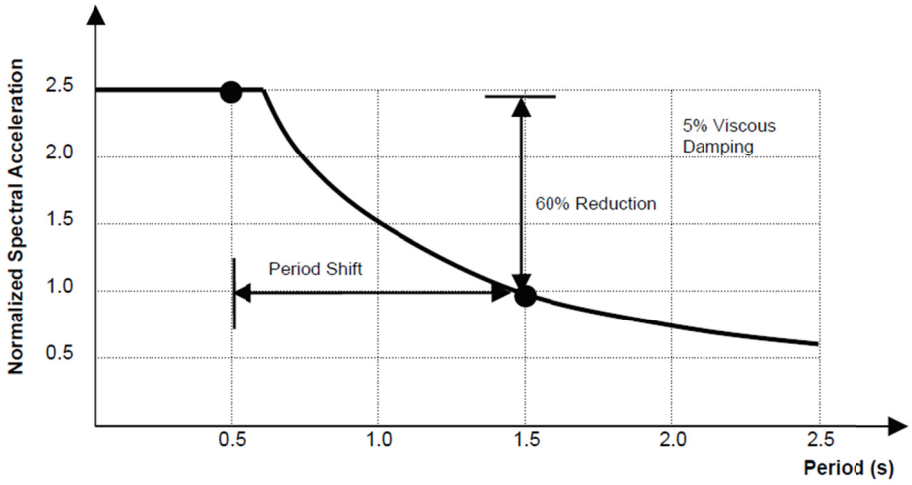

Figure 1.2 Effect of seismic isolation on bridge response [Buckle et al. 2006].

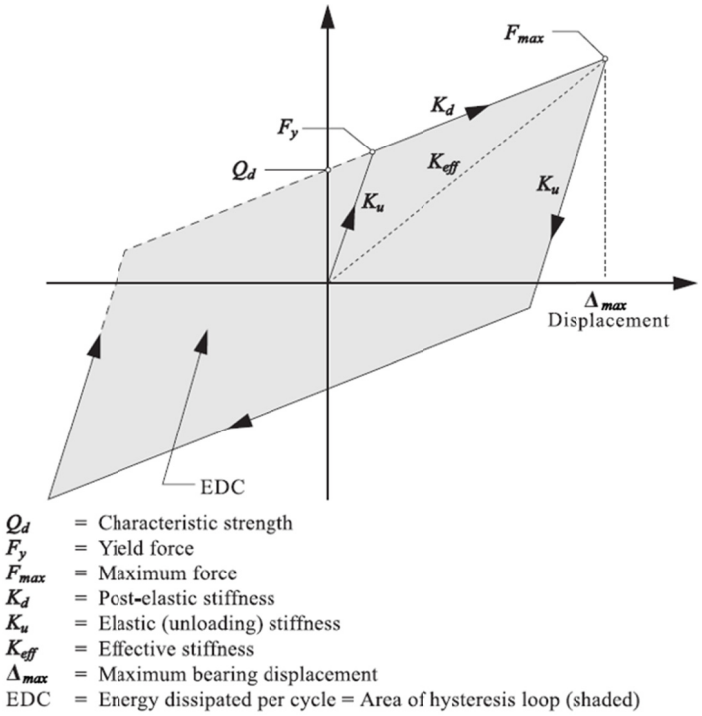

Figure 1.3 Bilinear force-displacement behavior [AASHTO 2010].

Primarily, there are two classes of bearings commonly used as isolation devices: lead–rubber bearings (LRBs) and spherical sliding bearings. Lead–rubber bearings incorporate alternating layers of rubber with steel shims; the rubber layers provide flexibility and the steel shims prevent bulging under vertical loads. The LRB also uses a lead core press fit into the

center as part of the energy-dissipation mechanism. Large diameter LRBs are required to maintain stability under large lateral displacements and high axial loads; however, increasing the diameter increases the bearing stiffness, which may undermine the seismic isolation objective. In the design of LRBs, balancing the competing needs to achieve both stability and the required bearing flexibility can be difficult.

Spherical sliding bearings use a frictional slider on a spherical surface. The natural period of a structure isolated with spherical sliding bearings is independent of the weight and determined only by the radius or radii of curvature of the spherical surface(s). Various types of spherical sliding bearings are manufactured by Earthquake Protection Systems and are classified as Friction Pendulum™ bearings (FPB). Figure 1.4 shows two types of FPBs: single pendulum bearings (SPBs) [Figure 1.4(a)], and triple pendulum bearings (TPBs) [Figure 1.4(b)]. Single pendulum bearings consist of a single slider that slides over a spherical surface, resulting in a single pendulum mechanism. A TPB embeds an inner double pendulum mechanism (articulated slider sandwiched between spherical sliding surfaces on the top and bottom) within an outer double pendulum mechanism. Hence, there are four spherical surfaces on which sliding occurs. Note that although the two inner sliding surfaces are identical, the two outer surfaces may have distinct radii of curvature, which in the most general case results in three pendulum mechanisms. Multi-spherical sliding bearings such as the TPB can provide displacement capacity comparable to an SPB with a reduced bearing diameter.

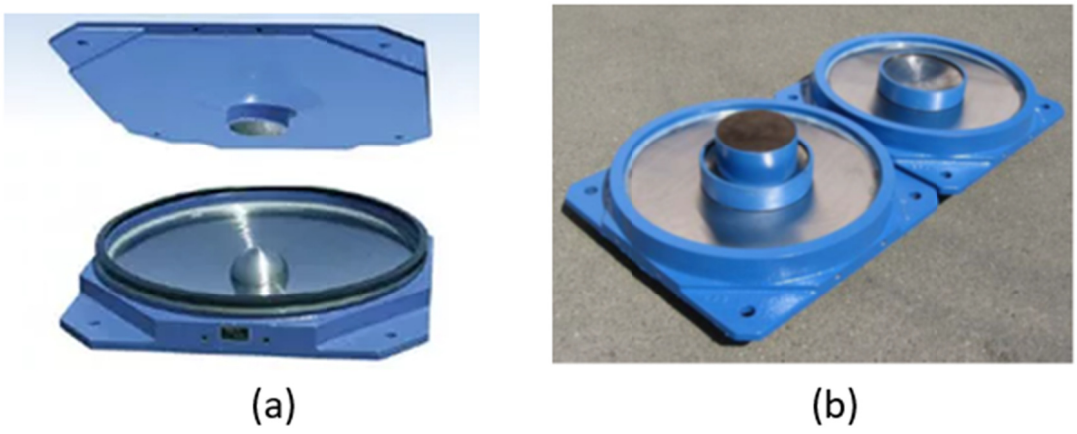

Figure 1.4 (a) Single pendulum bearings; and (b) triple pendulum bearings (EPS, n.d.).

Figure 1.5 is an idealized schematic of the equilibrium of the SPB in the displaced configuration. From Figure 1.5, the force-deformation relationship of the bearing is derived as:

$$F = u\frac{w}{R} + \mu W \tag{1.1}$$

where R is the radius of curvature, μ the friction coefficient, and u the lateral displacement. Although the term W generally symbolizes weight, it should be interpreted as the instantaneous axial force on the bearing. Thus, the horizontal force of the isolator depends on instantaneous axial force acting on it, implying that vertical motion might affect the horizontal response of the structure significantly.

The significant influence of vertical shaking was observed in a full-scale test of a five-story steel moment frame building (Figure 1.6) isolated by TPBs at Japan's E-Defense facility in August 2011 [Dao and Ryan 2015]. The anticipated outcome of the full-scale test was to prove the effectiveness of the isolation system to protect both the structure and nonstructural components. Based on the test results, however, nonstructural components were shown to be vulnerable to the vertical component of shaking [Ryan and Dao 2015; Soroushian et al. 2015], and horizontal-vertical coupling effects were also noted in the response [Ryan and Dao 2015]. The test program included 19 independent test simulations—or trials—each with a different input motion. Input ground motions incorporated a sine wave, a variety of recorded ground motions, and one simulated motion. The ground motions included representative broadband frequency shaking, shaking in the near-fault region, and shaking from a long-duration subduction motion. Some input motions were applied with vertical shaking and some were applied without, although few direct comparisons (same motion with and without vertical shaking) were applied.

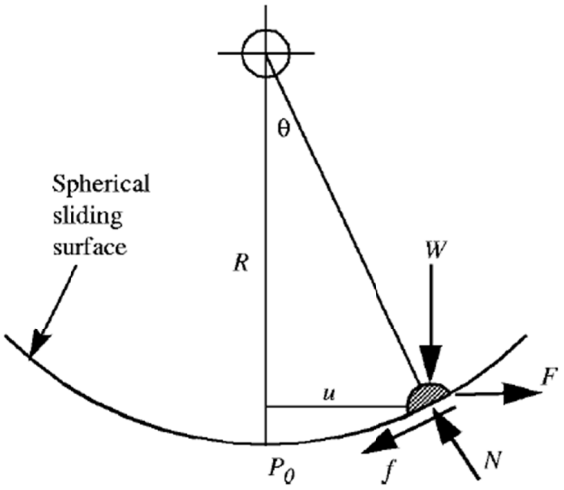

Figure 1.5 Idealized equilibrium of slider in displaced configuration [Mosqueda et al. 2004].

Figure 1.6 Full-scale five-story steel moment frame test specimen [Dao and Ryan 2015].

The results of the test program demonstrated two direct effects of vertical shaking that may need to be considered in the lateral design of isolated structures. The effects are believed to be generally applicable to structures with spherical sliding bearings and even flat sliding bearings. The first effect was an increase in base shear, which occurs because the bearing horizontal force is proportional to the instantaneous axial force or normal force on the bearing.

To demonstrate, Figure 1.7 compares the recorded histories of base shear in *X* and *Y*, and total axial force of the building under the 1999 ChiChi, Taiwan, earthquake recorded at TCU station [TCU80(XY)] and the 1978 Tabas, Iran, earthquake recorded at Tabas station (TAB80). TCU80(XY) and TAB 80 are representative of two-dimensional (2D) (without vertical) and three-dimensional (3D) (with vertical) motions, respectively, that were applied during the test program. The number 80 indicates both records were scaled to 80% of their recorded intensity. The axial force is almost constant under the 2D motion TCU80(XY), and the shear force is

dominated by longer period cycles; however, under the 3D motion TAB80, the axial force history contains high-frequency variation due to the vertical shaking. This high-frequency content was also transferred to the bearing lateral force. As a result, the base-shear history contains high-frequency content at peak locations.

Figure 1.8 compares the recorded base shear for both 2D and 3D shaking under 88% of the motion recorded at Rinaldi Receiving Station (RRS) in the 1994 Northridge, California, earthquake. This was the only direct comparison with the same motion applied both with and without the vertical component of shaking. The intensity of the vertical component was greater than 1g [vertical peak ground acceleration (PGA) or PGA_V = 1.2g]. This caused a complete uplift excursion of the bearings. Although the total axial force dropped to zero, the system recovered; see Figure 1.8(c). The high-frequency component of the base shear for 3D shaking (with a period around 0.16 sec), which is absent in 2D shaking, was in sync with the total axial force variation for 3D shaking; see Figure 1.8.

The second observed effect was an amplification of horizontal floor accelerations due to the expression of higher modes activated by horizontal–vertical coupling. Specifically, the high-frequency component introduced into the base shear by the vertical motion caused the activation of higher structural modes. Figure 1.9 shows floor spectra for the 3D recorded motion from 1995 Kobe, Japan, earthquake at Takatori Station, generated from both test data and numerical simulation using the validated computational model. These spectra provide evidence of a response in Mode 8 (the second structural mode) and determined to have a period of 0.17 sec based on modal analysis. In the Mode 8 displaced shape, floors 2 and 5 are nearly stationary; see Figure 1.9. The floor acceleration response spectra at Floors 1, 3, 4, and 6 show spectral peaks around 0.17 sec (the period of Mode 8), whereas Floors 2 and 5 (the nodal locations in Mode 8) are not amplified. Thus, Mode 8 was amplified in the presence of vertical shaking because its period was closely tuned to the period of vertical shaking. In bridges isolated with spherical sliding bearings, a similar amplification of higher mode(s) due to vertical shaking is possible.

In summary, the effect of vertical motion on structures isolated with spherical sliding bearings, especially for isolated bridges, is a relatively unexplored topic, and past research has been very limited. The next section documents previous studies on the effect of vertical shaking on isolated structures, with an emphasis on those with spherical sliding bearings.

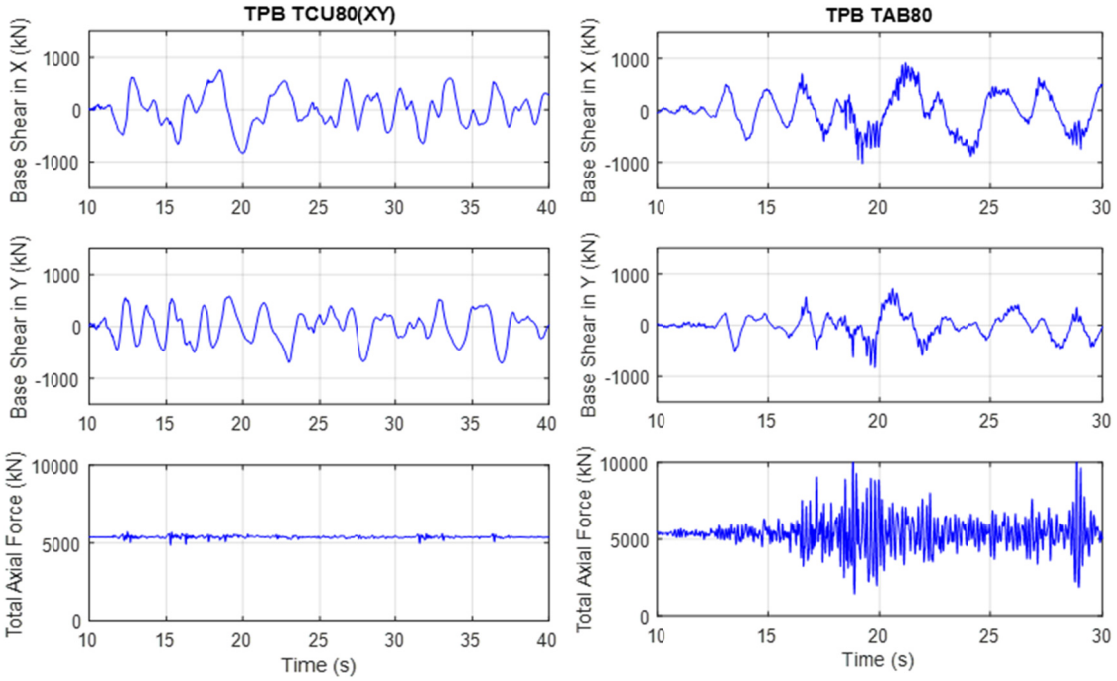

Figure 1.7 Base-shear history of the building under TCU80(XY) and TAB80 ground motion.

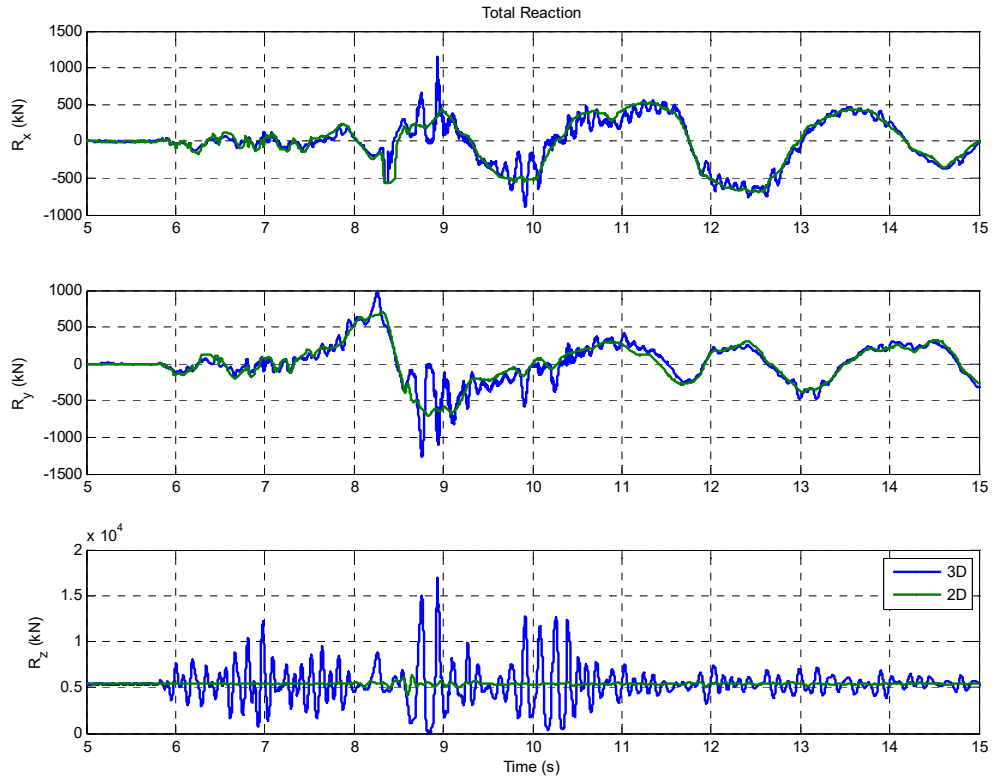

Figure 1.8 Total reaction history of the building under 88% Northridge-RRS ground motion.

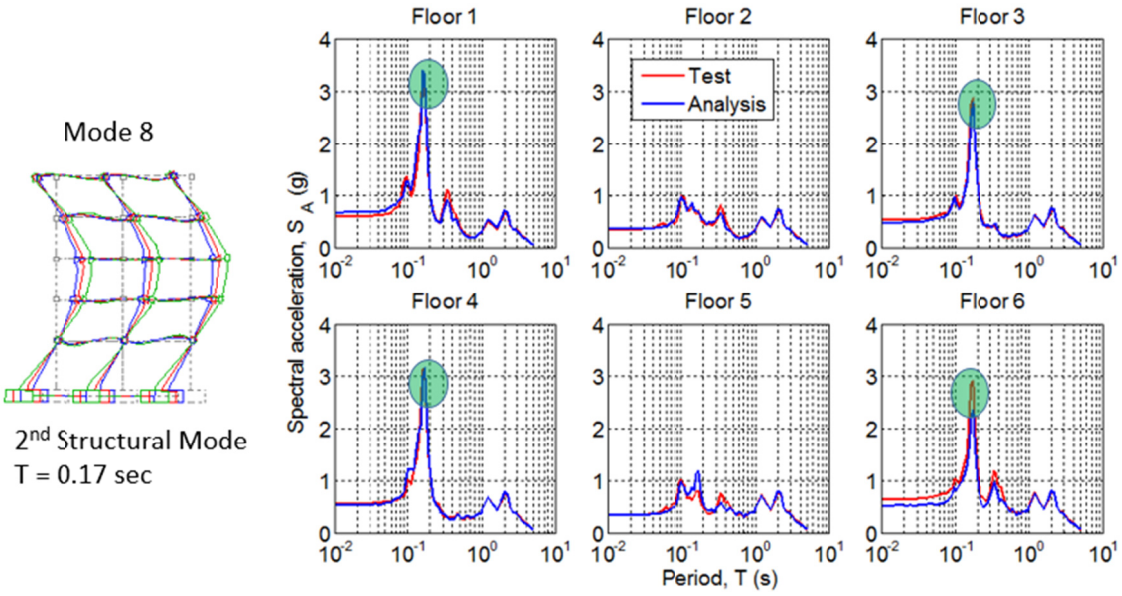

Figure 1.9 Floor spectra for Takatori motion in the *X*-direction.

1.2 LITERATURE REVIEW

A number of computational studies of structures with sliding isolation systems have raised the issue of potential amplification of various demand parameters in the presence of vertical shaking. Lin and Tadjbakhsh [1986] analytically simulated a rigid mass subjected to harmonic horizontal excitation with and without vertical excitation at the same frequency, considering soil–foundation interaction. The authors found that the response of the sliding mass was significantly affected by vertical ground motion; however, harmonic excitation of a structure at the same frequency in both horizontal and vertical directions is unrealistic. Shakib and Fuladgar [2003] performed an analytical study on an asymmetric building isolated by a pure friction isolation system (e.g., flat sliding bearings), wherein the building was idealized as a 3D single-story building. The authors concluded that the isolation system was less effective when the vertical component was included compared to the isolated asymmetric building subjected to horizontal motions only.

Analytical studies focused specifically on isolated bridges drew similar conclusions. Calvi et al. [2004] performed nonlinear dynamic analyses on different bridge configurations to determine the effect of axial force variations on the seismic response of bridges isolated with SPBs. In the case of curved bridges, the vertical component had more significant effects on the response compared to bridges with a "straight" configuration. The authors concluded that vertical shaking may increase significantly the shear force demand on piers, but the variation of displacement demand on isolators is negligible. Eroz [2007] modeled typical highway bridges isolated with SPBs. The isolator model accounted for the variation of normal force and friction coefficient, large deformation effects, and coupling of vertical and horizontal responses during

ground shaking. Computational simulations performed on a 3D concrete bridge model showed that peak isolator forces were underestimated when the vertical component was excluded, but the vertical shaking had a negligible effect on the column drift.

Rabiei and Khoushnoudian [2011] were the first researchers to suggest that increases in the base shear of friction pendulum bearings due to vertical excitation may be amplified further in the horizontal floor accelerations of a multi-story building. In this study, a four-story shear type building isolated with SPBs was subjected to vertical and horizontal components of recorded earthquakes. The authors calculated the error in the responses for single-component (horizontal only) shaking relative to horizontal plus vertical shaking. The maximum error observed (over all ground motions) by neglecting vertical motion was 36% and 50.12% for base shear and top floor acceleration, respectively. The authors concluded that for a low-period superstructure, the top floor acceleration was significantly affected by vertical acceleration and neglecting vertical shaking may lead to underestimation of the base shear.

Politopoulus and Moussallam [2012] performed a 3D analysis of a nuclear plant with low-damping bearings. They compared the horizontal floor spectra under two horizontal components and all three components of ground motion, and observed that non-isolated higher modes were amplified due to coupling between vertical excitation and horizontal response. This behavior was explained conceptually by a simple two-degree-of-freedom model.

As discussed above, a number of numerical studies have suggested that vertical shaking may lead to significant amplification of the horizontal responses in base-isolated structures, particularly those with spherical sliding bearings, as reported by the experimental results of the E-Defense tests. In contrast, experimental research has not, in general, corroborated these analytical claims. For example, vertical excitation had little influence on the horizontal force or displacement of the isolation system in a test of a single-story structure with SPBs [Zayas et al. 1987]. Mosqueda et al. [2004] performed displacement-controlled tests on a rigid block supported by four SPBs under 2D and 3D motions. The test apparatus consisted of four bearings supporting a 1.82 m × 2.59 m rigid frame loaded with concrete and lead weighing 290 kN. Six different orbits were used for displacement-controlled test. The authors concluded that the inclusion of vertical shaking had only a small effect on the lateral force of the SPBs. The horizontal displacements of the rigid block were the same in both cases.

Iemura et al. [2005] conducted shake table tests on two scaled models of highway bridges seismically isolated with a combined rubber and flat sliding bearing system to investigate the effect of axial force variation due to overturning and vertical acceleration. This hybrid system of rubber and sliding bearings was referred to as a “resilient” sliding isolation system because it provided a restoring force. The tested models included a reduced-scale portion of a bridge deck that could not capture the vertical vibration characteristics of a full-scale deck. The test results suggested that normal force variation on bearings would be much higher due to overturning than due to vertical acceleration. Furthermore, vertical acceleration had only a minor effect on force-deformation hysteresis loops in these tests.

Fenz and Constantinou [2008] formulated and validated a general model for multi-spherical sliding bearings that can be used for response history analysis (RHA). The model specialized for TPBs was validated with experimental results of a quarter-scale six-story seismically isolated steel structure. The authors concluded that the effect of vertical shaking on peak displacement, peak base shear, and peak superstructure response was minor; however, results presented in the report show that base shear was amplified up to 25% and horizontal floor acceleration was amplified by up to a factor of two in some cases. The peak vertical table acceleration was moderate, ranging from 0.1 to 0.45g.

In addition, Morgan and Mahin [2011] performed analytical and experimental investigations on multi-stage spherical sliding isolation bearings. Experimental testing included a shake table test of a one-quarter-scale three-story seismically isolated steel braced frame on multi-spherical sliding bearings. The authors observed no difference in the peak shear force, peak displacement demand, or total energy dissipated when vertical acceleration was included; the change in the total vertical load on all isolators when vertical acceleration was excluded versus included was insignificant, which appears to be due to a significant noise in the vertical signal. In summary, most experimental studies have not shown any significant effect of vertical motion on horizontal responses.

Only one study has attempted to conduct a comprehensive statistical evaluation to quantify broadly the effects of vertical shaking on the isolation system base shear. Using a model of a simple rigid block on an FPB, Cilsalar and Constantinou [2017] evaluated the ratio of isolator displacement and base shear with vertical ground motion to that with vertical ground motion neglected. The study employed the FEMA P-695 [FEMA 2009a] far-field and near-fault ground-motion sets; a statistically significant number of analyses were conducted and distributions were generated. System variables included the pendulum period, friction coefficient, and amount of viscous damping in the system. The 85th percentile base-shear ratio (recommended for design) was found to vary from 1.06 to 1.22 for far-field motions, and from 1.15 to 1.48 for near-fault motions; ratios were highest in systems without added viscous damping. While the study suggested the results could be implemented by codes such as ASCE 7-16 [ASCE 2017] to approximate the base-shear amplification due to vertical shaking in simplified methods, the study did not directly consider the dependence of the base-shear ratio to the intensity of vertical shaking.

1.3 OBJECTIVE AND SCOPE

As outlined above, although quite a few previous experimental studies reported no significant influence of vertical motion on the horizontal response isolated structures, the experimental test on a full-scale five-story steel moment frame building isolated with TPBs at E-defense demonstrated that vertical shaking can increase the base shear and horizontal acceleration. This observation is supported by a number of analytical studies that predict that horizontal responses

can be increased by 3D excitation. These effects are anticipated to have direct significance to bridges, wherein the amplified horizontal force of the TPBs will lead to increased base-shear demand on bridge piers. Furthermore, potential coupling between vertical and horizontal vibration modes might occur, which can increase horizontal acceleration and associated spectra due to the activation of a higher structural mode. Design methods or simplified methods that can account for amplification of seismic responses due to vertical shaking are needed. Bridges are conceptually simpler dynamically; therefore, they should be the natural starting point for a comprehensive treatment of the subject.

The primary objectives of this study are as follows: (1) to develop a physical understanding of the phenomena by which responses in bridges isolated with spherical sliding bearings are amplified due to vertical shaking; and (2) to develop a simplified method to estimate the amplification of the base-shear coefficient for this class of bridges.

This report is organized as follows: Chapter 1 documents the motivation and background of this study with a review of relevant literature. For this study, a ground-motion suite was selected that has a wide range of horizontal and vertical intensity ground-motion components. The detailed procedure for selection and scaling of the ground motions is presented in Chapter 2. Chapter 3 identifies the prominent bridge type used in California suitable for seismic isolation; describes the geometry, properties and modeling assumptions of a Base Model bridge, and identifies parameter variations to be applied to the bridge and the isolation system. Chapter 4 discusses fundamental dynamic properties of the Base Model bridge, and presents histories of various responses under representative ground motions, amplification of responses based on vertical PGA, and spectral responses to identify coupling between horizontal and vertical modes. Chapter 5 describes the proposed simplified method for estimating base-shear amplification and error analysis to validate the method. Chapter 6 validates the method considering various isolation-system parameters and bridge-parameter variations. Key conclusions from this study are presented in Chapter 7.

2 Ground-Motion Selection and Scaling

Ground motions play a crucial role in modeling and predicting the response of structural systems. For most investigations, ground motions are selected and scaled for a target intensity or target spectrum in the horizontal direction only, without regard to the vertical component. There are very limited studies evaluating the effect of vertical ground motions on bridges. In addition, most literature on ground-motion selection focuses on horizontal components of motion only.

2.1 DESCRIPTION OF A GROUND-MOTION SUITE

To avoid challenges in selecting and scaling ground-motion triplets, the strategy used herein was to select a well-vetted, pre-defined suite of horizontal strong ground-motion records that were fit to a target spectrum. For this study, the vertical components of those records were amplitude-scaled independently to best fit a target vertical spectrum that corresponded to the target horizontal spectrum. The selected suite consisted of 11 recorded ground motions corresponding to shallow crustal earthquakes in active tectonic regions that incorporate near-fault effects [Carlton 2014].

The motions were amplitude scaled to match a 5%-damped target acceleration response spectrum based on the 2008 NGA ground-motion prediction equations (GMPEs) given by Abrahamson and Silva [2008], Boore and Atkinson [2008], Campbell and Bozorgnia [2008], Chiou and Youngs [2008], and Idriss [2008]. Parameters used for estimating this spectrum were M_w = 6.7 (a moment magnitude of 6.7), F_{RV} = 1 and F_{NM} = 0 (a reverse-type-fault failing mechanism), Z_{TOR} = 0 (surface rupture), and δ = 45 (45° fault plane). Figure 2.1 shows the target median (μ) and median plus/minus ± one standard deviation ($\mu \pm \sigma$) spectral acceleration.

The procedure used to scale the ground motions to best fit the target spectrum was as follows [Carlton 2014]: first, motions were rotated to the direction that maximized the spectral acceleration at a period T = 1 sec. The code SigmaSpectra [IICGE 2019] was used to select the best suite of ground motions from a larger pool of rotated motions. Individual motions were amplitude scaled to minimize the sum-square-of-the-error relative to the target spectrum. The root-mean-square-error (RMSE) for a suite of scaled motions is defined as:

$$RMSE = \sqrt{\frac{1}{n_p}\sum_{i=1}^{n_p}\left[\ln\left(S_{a,avg,i}^{scaled}\right) - \ln\left(S_{a,tar,i}\right)\right]^2} \tag{2.1}$$

where n_p is the number of points (periods) in the response spectra to be targeted; and $S_{a,tar,i}$ and $S_{a,avg,i}^{scaled}$ are the target spectral acceleration and the mean spectral acceleration of the suite of scaled ground motions for the *i*th period, respectively. The spectral values are assumed to be log-normally distributed. Motions were selected such that RMSE for the suite was minimized.

After the suite of motions was selected, scale factors for individual motions were further increased or decreased while keeping the average scaling factors constant so that the suite as a whole also matched the target standard deviation. The best scaling factor for each record were determined by the Centroid Method as illustrated by Kottke and Rathje [2008]. Table 2.1 below lists the ground motions selected by Carlton [2014] and their relevant statistics. The motions can also be found in the database created for the PEER transportation research program; see Baker et al. [2011].

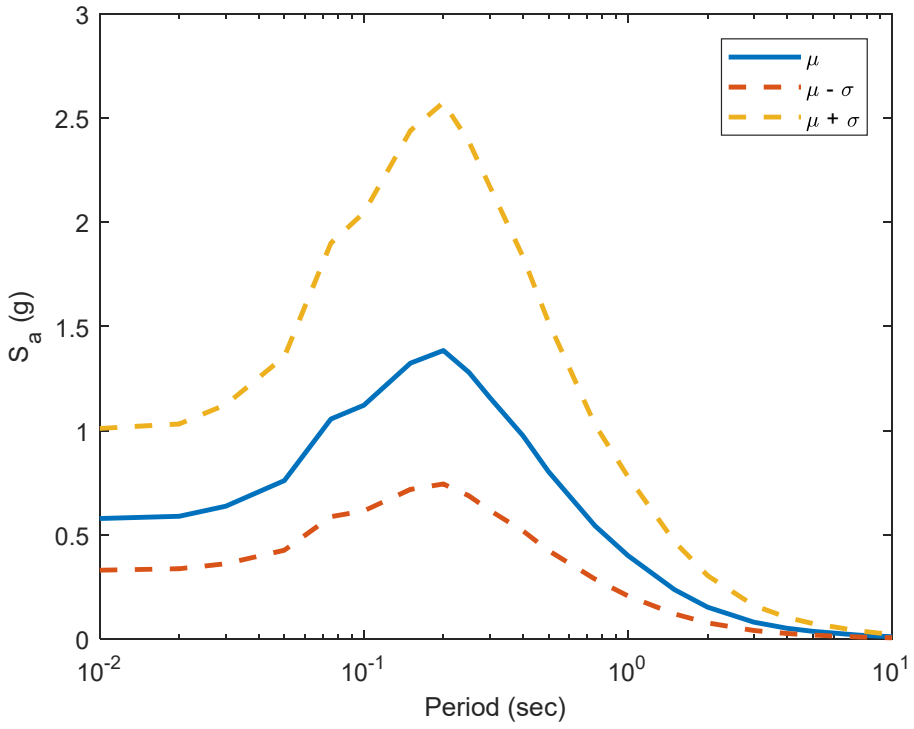

Figure 2.1 Target response spectrum with and without standard deviation.

Table 2.1 Selected ground motions with their abbreviation.

Motion	NGA #	Event	Year	Station	M_W	R_{rup} (km)	V_{s30} (m/sec)
SFPU	77	San Fernando	1971	Pacoima Dam (upper left abut)	6.61	1.81	2016
IIB	285	Irpinia, Italy-01	1980	Bagnoli Irpinio	6.9	8.18	1000
IIS	292	Irpinia, Italy-01	1980	Sturno	6.9	10.8	1000
LPG	763	Loma Prieta	1989	Gilroy - Gavilan Coll.	6.9	9.96	729.7
CAM	825	Cape Mendocino	1992	Cape Mendocino	7.0	6.96	513.7
LAL	879	Landers	1992	Lucerne	7.2	2.19	1369
NPD	1050	Northridge-01	1994	Pacoima Dam (downstr)	6.6	7.01	2016.1
NPA	1051	Northridge-01	1994	Pacoima Dam (upper left)	6.6	7.01	2016.1
KCL	1148	Kocaeli, Turkey	1999	Arcelik	7.5	13.4	523
CT46	1486	Chi-Chi, Taiwan	1999	TCU046	7.6	16.7	465.6
CT78	3473	Chi-Chi,Taiwan-06	1999	TCU078	6.3	11.5	443

2.2 SCALING OF VERTICAL COMPONENTS

Since vertical motions were not considered in development of the ground-motion suite [Carlton 2014], a similar procedure was adopted herein to scale the vertical motions. First, the target vertical spectral acceleration, $S_{a,V}$ was developed from the target horizontal spectrum based on NEHRP recommended seismic provisions [FEMA 2009(b)]. Figure 2.2 shows a vertical response spectrum according to these guidelines. The vertical spectral shape resembles a standard code horizontal spectrum [ASCE 2017] but with fixed transition periods at 0.05 sec and 0.15 sec that determine the start and end of the constant acceleration region. For periods $T > 0.15$ sec, $S_{a,V}$ is calculated as

$$S_{a,V} = 0.8 C_V S_{DS} \left(0.15 / T_V\right)^{0.75} \tag{2.2}$$

where C_V is the vertical coefficient that depends on site class and ranges from 0.7 to 1.5; S_{DS} is the design spectral response acceleration parameter at short periods and represents the largest horizontal spectral acceleration. When C_V takes the value of 1.5, the peak vertical spectral acceleration $S_{a,V} = 1.2 S_{DS}$, i.e., the vertical to horizontal (V/H) ratio = 1.2.

The NEHRP vertical spectrum is based on a standard design spectrum that has constant spectral acceleration over a range of short periods. Because the target horizontal spectrum of Carlton [2014] reflects the GMPE and does not have a constant spectral acceleration region, the shape of the target vertical spectrum developed here was modified from the NEHRP spectrum. Two regions for the target vertical spectrum were defined. In the first region, $S_{a,V}$ varies linearly

from $0.3C_VS_{DS}$ at T = 0 sec to $0.8C_VS_{DS}$ at T = 0.15 sec, which resembles the shape of the horizontal spectrum. For T > 0.15 sec, $S_{a,V}$ is determined by Equation (2.2), which is consistent with the NEHRP target spectrum. Assumed coefficients were C_v = 1.5 and S_{DS} = 1.38, which is the largest spectral acceleration of the target horizontal spectrum at T = 0.2 sec. Figure 2.3 illustrates the target vertical spectrum.

To scale the vertical components to best fit this target spectrum, the following procedure was followed. First, a scale factor was identified for each horizontal rotated motion such that it best fit the median horizontal target spectrum. This scale factor is hereafter referred to as "horizontal best fit factor." A horizontal adjustment ratio A' was calculated by dividing the scale factor reported in Carlton [2014] by the horizontal best fit factor. The adjustment ratio represents the additional scaling of individual motions to represent the dispersion in the target spectrum. Likewise, the vertical components of these motions were also amplitude scaled to best fit the vertical target spectrum; this scale factor is referred to as "vertical best fit factor." Final vertical-component scale factors were derived by multiplying the vertical best fit factors by A'. Essentially, the scale factors for vertical motions were adjusted comparable to the horizontal motions to match the $\mu \pm \sigma$ target spectrum. This procedure ensures that motions with high-intensity horizontal components have high-intensity vertical components as well.

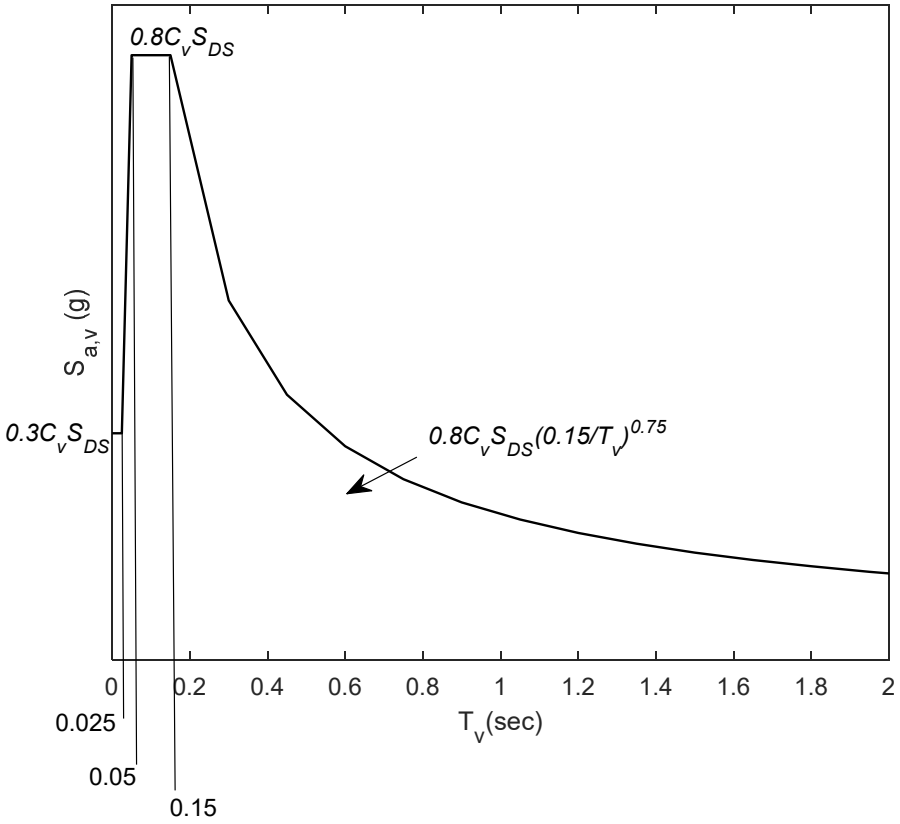

Figure 2.2 Design vertical response spectrum per FEMA guidelines [FEMA 2009(b)].

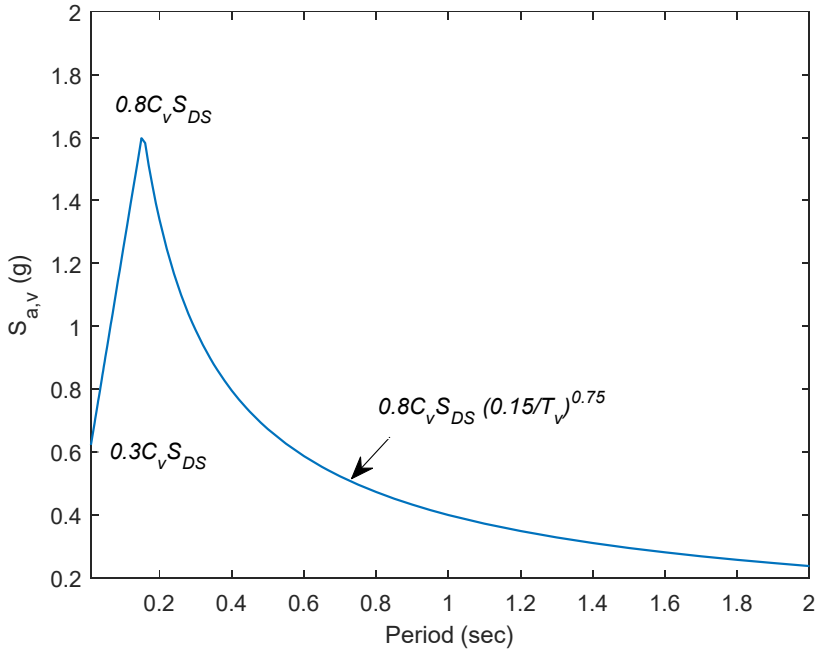

Figure 2.3 Vertical target spectrum.

Table 2.2 Ground-motion groups, scaled PGAs, scaling factors, and adjustment factors.

Group #	Motion	Scaled PGA			Scale Factor		Adjustment factor *A*'	
		PGA_V (g)	PGA_T (g)	PGA_L (g)	Horiz.	Vert.	Horiz.	Vert.
Group 1	SFPU	0.817	0.843	0.856	0.69	1.189	1.55	1.19
	CAM	1.10	1.116	0.776	0.75	1.490	0.42	1.49
	NPA	1.683	1.678	1.36	1.06	1.369	0.41	1.37
Group 2	LPG	0.62	0.47	0.43	1.31	3.228	1.2	3.23
	LAL	0.614	0.73	0.793	1.01	0.745	0.67	0.75
	NPD	0.597	0.544	0.568	1.31	3.133	1.02	3.13
	CT78	0.694	0.336	0.49	1.26	2.226	1.27	2.26
	IIS	0.543	0.27	0.382	1.19	2.313	1.27	2.31
Group 3	IIB	0.38	0.266	0.39	2.05	3.561	2.78	3.56
	KCL	0.272	0.424	0.271	2.02	3.282	3.19	3.28
	CT46	0.262	0.28	0.234	1.97	2.673	3.98	2.67

To better understand the influence of intensity on the bridge response, the ground motions have been divided into three groups based on scaled vertical PGA intensity ranges; see Table 2.2. The vertical PGA (PGA_V) intensity ranges are as follows: Group 1 = 0.8g and above (High Intensity), Group 2 = 0.5g to 0.7g (Moderate Intensity), and Group 3 = 0.2g to 0.4g (Low Intensity). Table 2.2 indicates the scaled PGA in the vertical direction and in the two horizontal directions (PGA_T and PGA_L to be applied in the bridge transverse and longitudinal directions, respectively), as well as the final scale factors and adjustment factors for horizontal and vertical components. Figures 2.4 and 2.5 show acceleration spectra for individual scaled motions plotted against the target spectrum for horizontal and vertical components, respectively. In each plot, the Group 1, Group 2, and Group 3 spectra are identified by color. By inspection, the spectral intensities of the vertical motions (per group) are roughly proportional to those of the horizontal motions. Furthermore, Group 1, Group 2, and Group 3 motions correlate well to $\mu + \sigma$, μ, and $\mu - \sigma$ horizontal target spectra, respectively; see Figure 2.4.

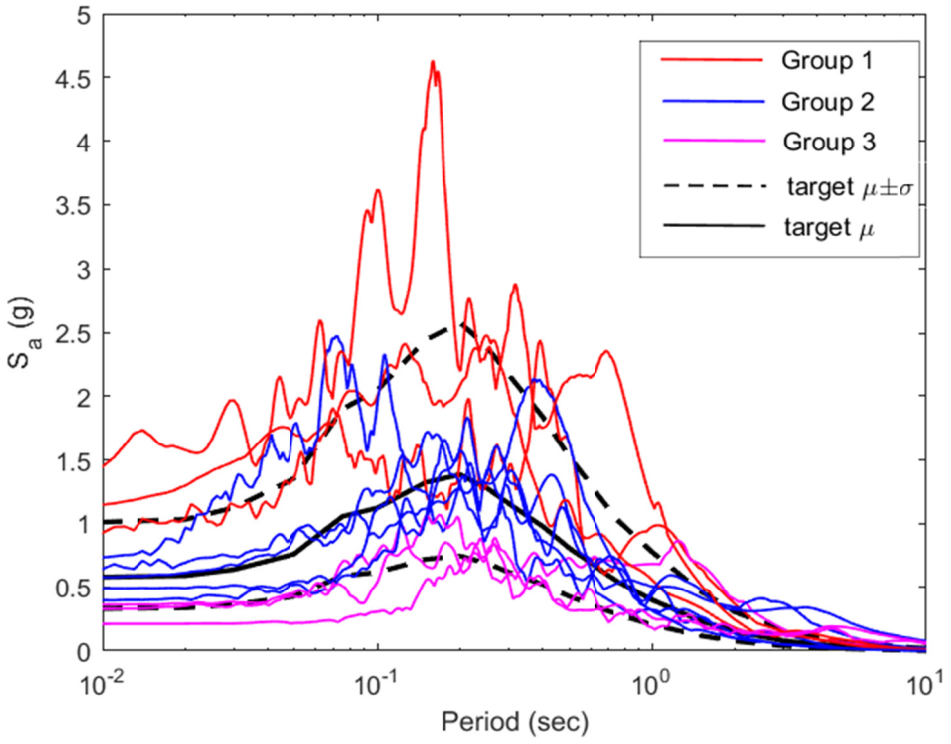

Figure 2.4 **Spectral acceleration of scaled rotated horizontal ground motions compared to median (μ) and median ± standard deviation ($\mu \pm \sigma$) target horizontal response spectra.**

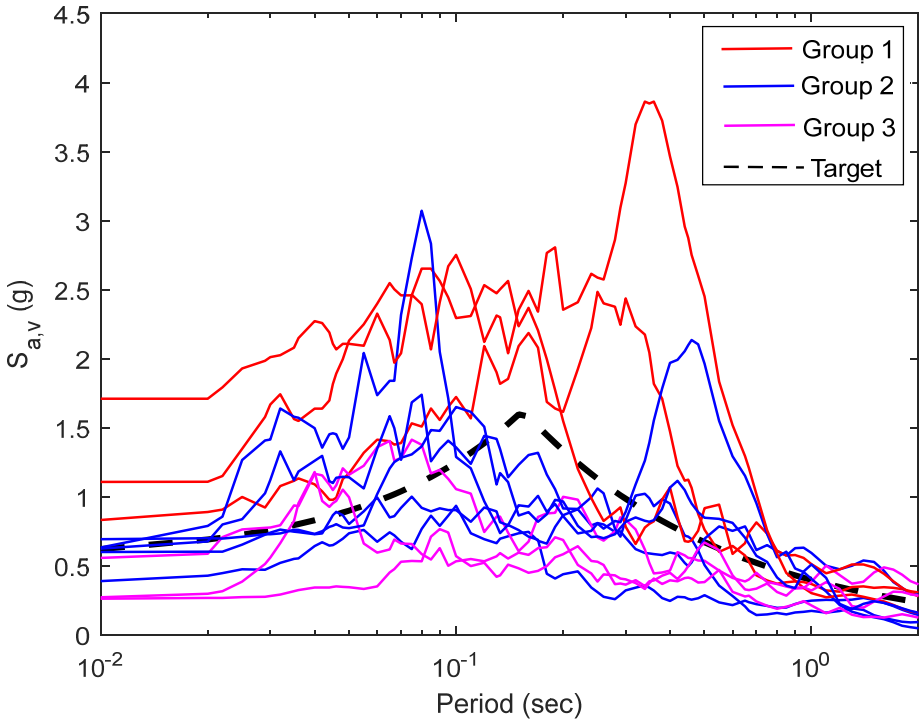

Figure 2.5 **Spectral acceleration of scaled vertical ground motion components compared to target vertical spectrum.**

3 Bridge Parameter Selection and Modeling

3.1 INTRODUCTION

Bridges are classified into various categories according to design and construction methodologies, materials used, and other characteristics such as single vs. multiple spans, integral vs. bearing connection of superstructure to substructure, etc. Ramanathan [2012] studied the California bridge inventory utilizing the National Bridge Inventory (NBI) database [2010]. According to that study, three classes of bridges (multi-span continuous concrete box-girder, multi-span continuous slab, and multi-span continuous concrete girder) account for 45% of the total bridge inventory. Other bridge classes in California include concrete and steel culverts, concrete tunnels, concrete and steel bridges with other structural systems, cast/wrought iron, masonry, wood/timber, and aluminum bridges. Table 3.1 shows the major bridge classes with their count and the percentage of total inventory.

The objective of this study is to investigate the effect of vertical motion on isolated bridges. With that goal in mind, a variety of bridges archetypes, commonly found in the seismically active regions of California, were considered. Clearly, isolation is not suitable for bridge classes listed in Table 3.1. Multi-span continuous concrete box-girder bridges (MSCBG) and multi-span continuous steel or concrete girder bridges are the most suitable choice for seismic isolation because of the convenience of placing the isolators directly between the substructure bent cap and the superstructure girders. With simply supported bridges, different displacements can arise in each span, resulting in pounding. Pounding in isolated bridges is undesirable because it can induce additional shear forces in isolators. Because single-span bridges tend to be limited in length, they are not very flexible in the vertical direction and vertical shaking might not affect their response.

In California, MSCBG is the preferred bridge archetype for use with seismic isolation [Kartoum 2018]. In MSCBG bridges, isolation bearings are placed between the deck and the bent cap. A column cap provides support for the bearing installation. Bearings are also provided at the abutment. Figure 3.1 shows the typical assembly of bearings between the bent cap and the superstructure in MSCBG bridges. Only MSCBG bridges are investigated herein because of their wide presence and suitability for seismic isolation. Also, the bridge response is not expected to

be affected directly by the bridge type, but rather by variation in dynamic properties that arises from parameter variation.

Table 3.1 Prominent bridge classes in California [Ramanathan 2012].

Bridge class	Number of bridges	
	Count	Percentage
Multispan continuous concrete box-girder	5314	20.89
Single span concrete girder	4582	18.02
Multispan continuous slab	4004	15.74
Multispan continuous concrete girder	2164	8.51
Multispan simply supported steel girder	1085	4.27
Single span steel girder	936	3.68
Multispan simply supported concrete girder	900	3.54
Multispan simply supported concrete box-girder	398	1.56
Multispan simply supported slab	391	1.54
Multispan continuous steel girder	322	1.27
Multispan continuous concrete frame	8	0.03
Multispan simply supported concrete frame	4	0.02
Other	5326	20.94
Total	25434	100

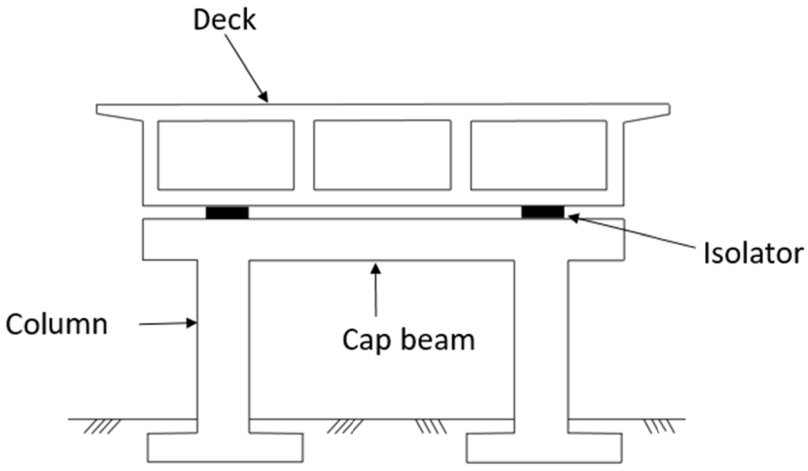

Figure 3.1 Configuration of isolated concrete box-girder bridge.

3.2 BRIDGE PARAMETER SELECTION

This section describes the parameter variations considered explored the influence of vertical motion on bridge response. Parameter variations include span length, number of spans, width of deck, number of columns per bent, and column height (substructure stiffness). Considering these parameter variations, eight different bridges were modeled and analyzed by changing one bridge parameter at a time and keeping the other parameters constant. All bridges were assumed to be isolated with TPBs. The bridges and their properties are tabulated in Table 3.2. The span length of the approach spans are 0.8 times the length of intermediate spans.

- Bridge 1 is a three-span bridge (120-ft-long spans) with two-column bents. Bridge 1 was considered a baseline to evaluate the effect of other parameter variations and is referred to as the Base Model bridge. Figure 3.2 details the Base Model bridge with dimensions.
- Bridge 2 is a four-span bridge and Bridge 3 is a two-span bridge.
- Bridges 4 and 5 are both three-span bridges but have increased span lengths of 135 ft and 160 ft, respectively, and increased depth of the deck to 5.4 ft and 6.4 ft, respectively.
- Bridge 6 has increased deck width (from 45 ft to 90 ft), 10 cells, and four columns per bent.
- Bridge 7 has a reduced deck width of 35 ft, two cells, and is reduced to a single 6-ft-diameter column bent.
- Relative to the standard column height (20 ft), Bridge 8 has a reduced column height of 15 ft.

Isolation system parameter variations were also applied to the Base Model bridge to investigate the influence of friction coefficient and isolation period on bridge response to combined horizontal and vertical ground motions. Table 3.3 lists the isolator parameter variations considered for Base Model bridge. The symbols μ_2 and T_2 correspond to friction coefficient and pendulum period, respectively, associated with sliding on the outer sliding surfaces. The TPB model is described more fully in Section 3.3. Other bridges in Table 3.2 were analyzed with the parameters of Iso System No. 6 in Table 3.3.

Table 3.2 Parameter variations for multi-span continuous concrete box-girder bridges.

Sr No.	Deck Width (ft)	No. of Cells	Depth (ft)	Deck Thickness (in)	Soffit Thickness (in.)	Wall Thickness (in.)	Wall C-C Spacing (ft)	Span Length (ft)	No. of Spans	Column Height (ft)	No. Column	Column Dia. (ft)
1	45	3	4.8	8.875	7	12	11.75	120	3	20	2	5
2	45	3	4.8	8.875	7	12	11.75	120	4	20	2	5
3	45	3	4.8	8.875	7	12	11.75	120	2	20	2	5
4	45	3	5.4	8.875	7	12	11.75	135	3	20	2	5
5	45	3	6.4	8.875	7	12	11.75	160	3	20	2	5
6	90	10	4.8	8.875	7	12	8.4	120	3	20	4	5
7	35	2	4.8	8.875	7	12	15	120	3	20	1	6
8	45	3	4.8	8.875	7	12	11.75	120	3	15	2	5

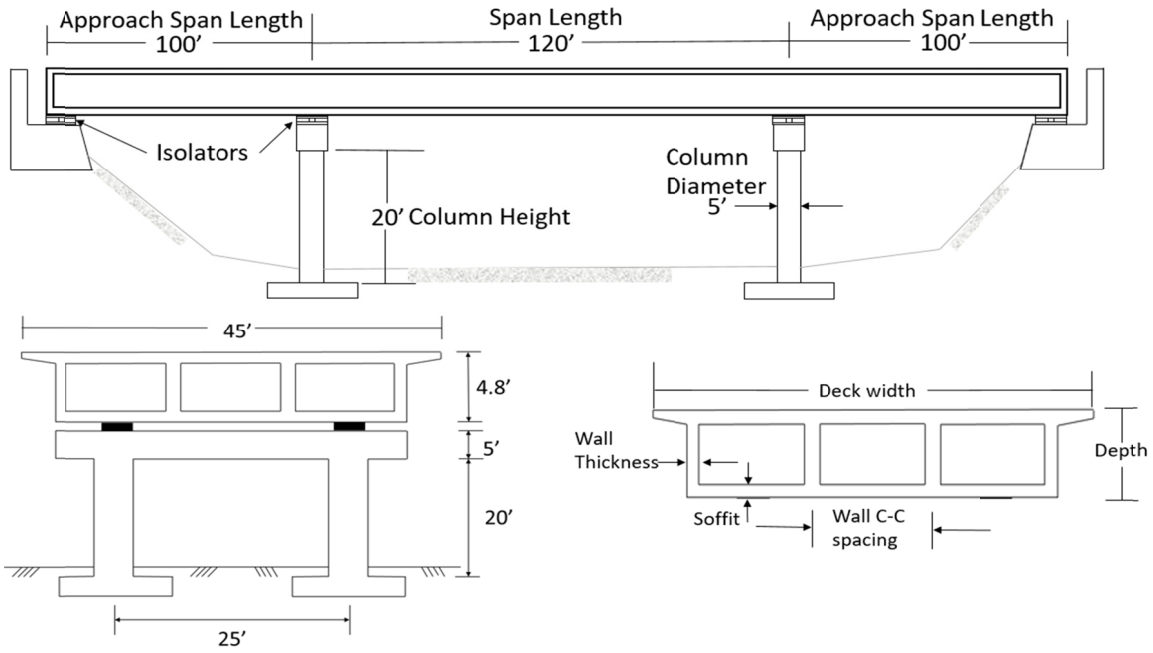

Figure 3.2 Base Model bridge dimensions and details.

Table 3.3 Isolation parameter variation for Base Model bridge.

Iso System No.	μ_2	T_2 (sec)
1	0.04	2
2	0.06	2
3	0.08	2
4	0.04	3.5
5	0.06	3.5
6	0.08	3.5
7	0.04	5
8	0.06	5
9	0.08	5

3.3 BRIDGE MODELING DETAILS

Three-dimensional computational models of the isolated bridge model variations presented above were developed in OpenSees [2019], partly based on Aviram et al. [2008]. Modeling assumptions for each bridge element are discussed below. Unless otherwise noted, assumptions are for the Base Model bridge, with implementation of parameter variations discussed as needed.

Figure 3.3 shows an overview of the Base Model bridge model. The bridge was modeled using the spine-model approach in OpenSees. The superstructure was divided into multiple elements per span, with the tributary mass lumped at the nodes. Superstructure nodes were connected to isolators with rigid links. Cap–beam elements were also connected to the base of the isolators and the top node of the column via rigid links. Cap beams and columns were modeled as elastic-frame elements. The column base was attached to translational and rotational springs representing the foundation stiffness. Abutments were modeled such that isolators can displace freely without restrictions; end nodes of abutments were attached to abutment foundation springs. Modeling details for each bridge member are discussed next.

3.1.1 Superstructure

The bridge superstructure (deck and girders) is capacity protected and assumed to remain elastic. The basic principle of isolation is to reduce the demands on the bridge structure and constrain the nonlinearity to the isolators. The bridge superstructure was modeled using elastic beam–column elements with uncracked section properties for prestressed concrete; the contribution of steel was neglected. Section properties were calculated separately for each bridge and assigned to 3D beam–column elements. The assumed section properties are tabulated in Table 3.4. I_{XX} and I_{YY} are the moments of inertia with respect to x- and y-axes respectively, and J is the torsional constant, of the deck with girders cross section.

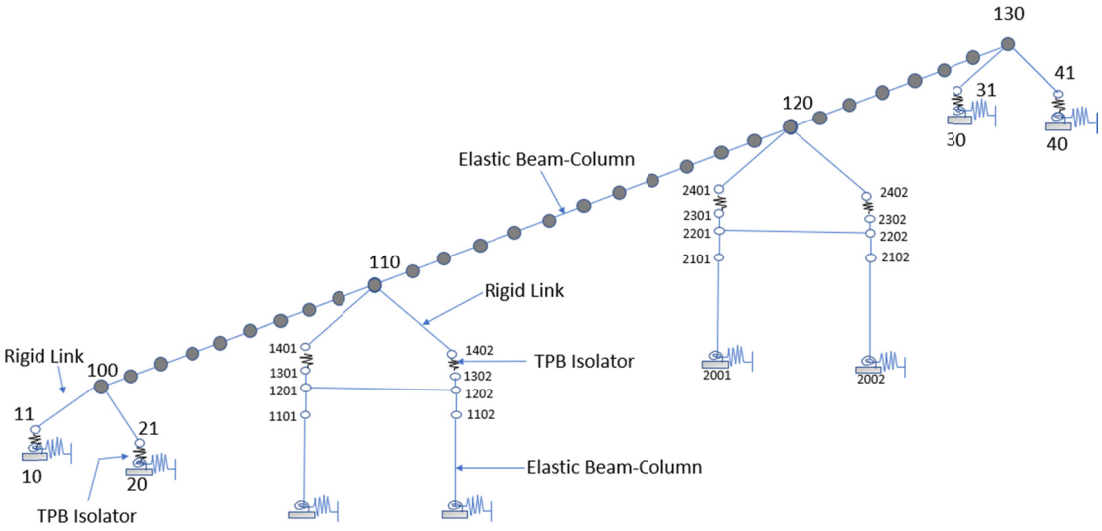

Figure 3.3 Overview of Base Model bridge model.

Table 3.4 Section properties of bridge superstructure elements.

Bridge no.	A_{deck} (in.^{2})	I_{XX} (in.^{4})	I_{YY} (in.^{4})	J (in.^{4})
1 (Base model)	9,862.56	4.951 x 10^6	2.111 x10^8	1.129 x 10^7
2	9,862.56	4.951 x 10^6	2.111 x10^8	1.129 x 10^7
3	9,862.56	4.951 x 10^6	2.111 x10^8	1.129 x 10^7
4	10,189.44	6.601 x 10^6	2.215 x10^8	1.458 x 10^7
5	10,722.24	4.857 x 10^6	2.316 x10^8	1.998 x 10^7
6	21,712	1.093 x 10^7	2.041 x10^9	2.442 x 10^7
7	7,765.92	3.998 x 10^6	1.126 x 10^8	1.05 x 10^7
8	9,862.56	4.951x10^6	2.111 x10^8	x 10^7

The superstructure node was assigned at the center-of-gravity of the section. The superstructure was divided into 10 elements per span, and translational masses were lumped at nodes based on the tributary length L_{trib} and cross-sectional area A_{deck}. The translational nodal mass was computed as:

$$M_{\text{node}} = mL_{\text{trib}}A_{\text{deck}} \tag{3.1}$$

The unit mass of concrete assigned to the material was m = 4.471 lb-sec^2/ft^4, based on the assumed weight of normal concrete w = 143.96 lb/ft^3 [Caltrans 2004]. For example, the nodal mass for Base Model bridge would be computed using a tributary length L_{trib} = 12 ft (one tenth of the intermediate span length of 120 ft) and the cross-sectional area A_{deck} from Table 3.4.

Rotational mass assignment is also important to capture fundamental mode shapes of the bridge in the transverse direction. The rotational mass of the superstructure about the longitudinal axis, M_{xx}, (Figure 3.4) was calculated and assigned using the following formula.

$$M_{xx} = \frac{mL_{\text{trib}}A_{\text{deck}}d_w^2}{12} \tag{3.2}$$

where d_w = superstructure width (average of top and bottom flange).

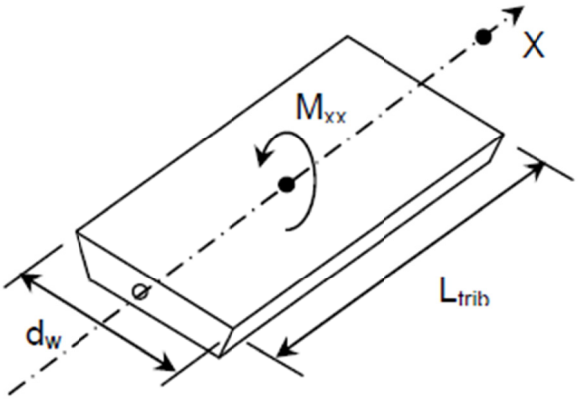

Figure 3.4 Rotational mass of superstructure [Aviram et al. 2008].

3.1.2 Single-Column and Multi-Column Bents

Most of the bridge models listed in Table 3.2 contain multi-column bents; only one bridge model used a single-column bent. The width of the deck dictates the number of columns in the bent. For isolated bridges, the column base must be fixed because the column top acts as a pinned support in the bridge longitudinal direction. The cap beam is a concrete element that ties the columns together and through framing action resists acting lateral loads and displacement in the transverse direction. The cap beam also facilitates isolator installation and connection between the superstructure and column bents in an isolated bridge.

Figure 3.5 illustrates the modeling details of the single and multi-column bent. The cap beam was modeled as an elastic beam–column element in OpenSees, with section properties representing the plan dimensions. The dropped cap beam was connected by a rigid link to both columns below and isolators above; see Figure 3.5. In this rigid link element, the constrained nodes move together in space as a rigid body. The rigid link connection facilitates moment and force transfer between the elements of the bent. Isolation reduces the demand on the sub-structure such that it remains elastic during dynamic loading. Hence, the columns were also modeled using 3D elastic beam–column elements.

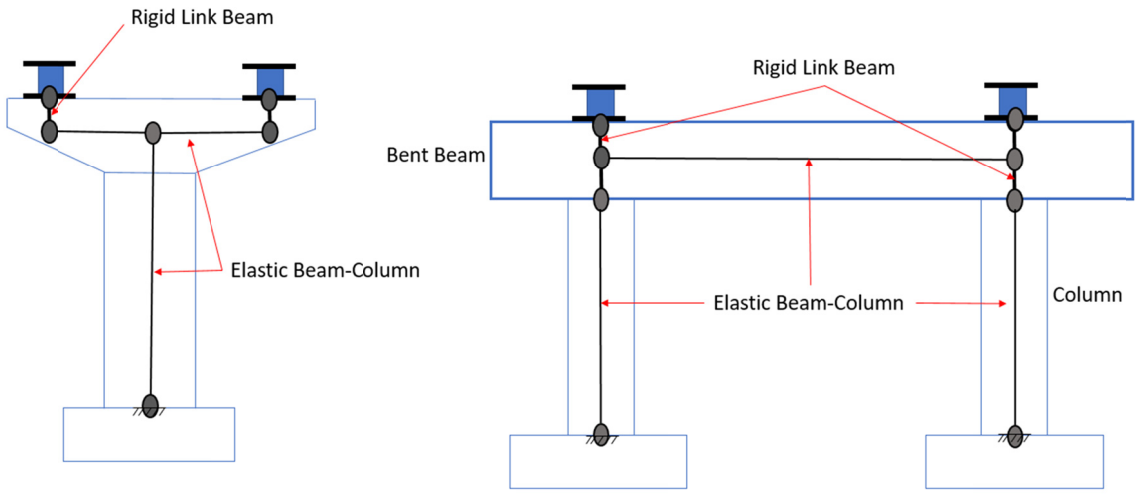

Figure 3.5 Single- and multi-column bent model detailing.

3.1.3 Abutment

The abutments facilitate access of traffic to and from the bridge. Typically, bridges have either seat-type abutments or integral-type abutments. In a seat-type abutment, the bridge superstructure load is transferred through bearings to the abutment seat, and the connection is designed as an expansion joint. Isolated bridges use seat-type abutments where the typical bearings are replaced by isolation bearings. In a non-isolated bridge, a seat-type abutment may have an unrestricted capacity for displacement across the joint or it may be restrained by the abutment backwall in the longitudinal direction and by shear keys in transverse direction. Seismically isolated bridges are generally designed to allow free movement of the superstructure and isolators at the abutments because pounding may introduce additional high shear forces in the isolators and hence the columns. Therefore, the isolators were modeled to move freely at both abutment ends without restriction. In the Base Model bridge, abutment base nodes were modeled with foundation springs, as described next.

3.1.4 Foundation

Foundations transmit the service and ultimate loads from the superstructure and columns to the underlying soil. Possible types of bridge foundations are spread footing, integral pile/column, and pile-supported footings. The type of bridge foundation is governed by loadings requirements, soil conditions, overhead clearance, existing utilities, and its proximity to existing facilities. Mangalathu [2017] performed a performance-based grouping methodology to group the box-girder bridges in California for regional seismic assessment. His study modeled and analyzed different foundation systems and soil profiles, and documented the development of statistical distribution functions to represent the variation of foundation translational and rotational stiffnesses for spread footings and pile foundations.

In this study, the Base Model bridge was modeled with spread footings below the columns and abutments. These spread footings were modeled as elastic translational and rotational springs located at the center-of-gravity of the footing; see Figure 3.6. The foundation springs were connected by a rigid link to the column base. The assumed translational spring stiffness, K_h, was 1000 kip/in. in both directions, and rotational spring stiffness, K_r, was 30×10^6 kip-in./rad for rotation about the transverse direction and 25×10^6 kip-in./rad for rotation about the longitudinal direction per column. These were based on mean values of the distribution functions for spread footings under a multiple column bent [Mangalathu 2017]. Foundation springs, added to the Base Model bridge only, were observed to have no effect on the axial force and base shear. Therefore, other bridges listed in Table 3.2 were modeled as fixed at the base without foundation springs.

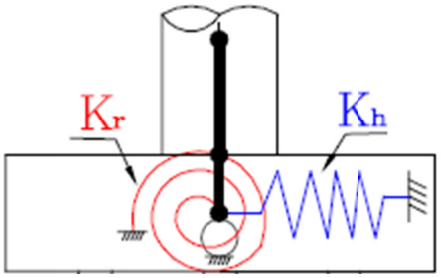

Figure 3.6 Foundation spring modeling detail [Choi 2002].

3.1.5 Triple Pendulum Bearings

As mentioned in Chapter 1, triple pendulum bearings or TPBs are a type of friction pendulum bearing characterized by multiple concave surfaces upon which sliding occurs. Due to multiple sliding surfaces, TPBs are more compact than other types of friction pendulum bearings. The bridges in this study were isolated with TPBs, although the observations regarding the influence of vertical shaking are expected to apply generally to any type of spherical sliding bearing.

Figure 3.7 presents a general configuration of a TPB, which consists of an inner slider, two articulated sliders, and two main concave surfaces. The radii of these curved surfaces, R_1, R_2, and R_3, and the friction coefficients of the sliding interfaces, μ_1, μ_2, and μ_3, determine the hysteretic response of the TPBs. Parameters d_1, d_2, and d_3 represent displacement limits of the pendulum mechanisms, and h_1, h_2, and h_3 are slider heights; see Figure 3.7. A TPB provides different pendulum mechanisms under different levels of shaking intensity. The normalized backbone curve of the TPB is presented in Figure 3.8, and the different related sliding mechanisms are shown in Figure 3.9 and explained hereafter.

The effective radii of the spherical surfaces are: $L_1 = R_1 - h_1$; $L_2 = R_2 - h_2$; and $L_3 = R_3 - h_3$. In the first stage, shown in Figure 3.9, sliding occurs between Interfaces 2 and 3 when the

normalized horizontal force, f_1^*, exceeds the friction coefficient μ_1. Here, f_1^* is the horizontal force that is normalized by the instantaneous acting axial force, not the constant weight of the superstructure. Since the axial force changes because of vertical motion, the horizontal force also changes accordingly. The inner slider has a small spherical radius, R_1, resulting in a relatively large normalized stiffness (stiffness normalized by axial force), $k_1 = 1/(2L_1)$ (Figure 3.8), and the maximum displacement is $u_2^* = 2L_1\ (\mu_2 - \mu_1)$. The friction coefficient μ_1 between these two surfaces is low, such that sliding takes place under small earthquake intensity.

In the second stage of sliding, the normalized horizontal force, f_2^*, exceeds the friction coefficient, μ_2, and the inner slider slides on the upper articulated slider (Interface 3), while, simultaneously, the lower articulated slider slides on the bottom concave plate (Interface 1) (Figure 3.9). The normalized stiffness of this stage is $k_2 = 1/(L_1 + L_2)$, and the maximum displacement is $u_3^* = L_1\ (\mu_2 + \mu_3 - 2\mu_1) + L_2\ (\mu_3 - \mu_2)$.

In the third stage of sliding (Figure 3.9), the lower articulated slider slides on the bottom concave plate (Interface 1), and the upper articulated slider slides on the top concave plate (Interface 4). The third stage of sliding starts when the normalized horizontal force f_3^* acting on the isolators exceeds the friction coefficient μ_3. The normalized stiffness of backbone curve of the third stage is $k_3 = 1/\ (L_2 + L_3)$, and the maximum displacement is $u_4^* = u_3^* + (d_2/L_2 + \mu_2 - \mu_3)\ (L_2 + L_3)$.

When the normalized horizontal force acting on the isolator exceeds $f_4^* = \mu_2 + d_2/L_2$, the fourth stage of sliding is initiated (Figure 3.9). The inner slider slides on the lower articulated slider (Interface 2), and the upper articulated slider slides on the top concave plate (Interface 4). In this fourth stage of sliding, the normalized stiffness of the backbone curve is $k_4 = 1/(L_1 + L_3)$, and the maximum displacement is $u_5^* = u_4^* + (d_3/L_3 + \mu_3 - d_2/L_2 - \mu_2)\ (L_1 + L_3)$.

The fifth stage of sliding is activated when the normalized horizontal force on the isolators exceeds $f_5^* = \mu_3 + d_3/L_3$. Sliding occurs between Interfaces 2 and 3: that is, the inner slider slides between the two articulated sliders. The normalized stiffness in this stage is $k_5 = 1/(2L_1)$, and the maximum displacement is $u_6^* = 2d_1 + d_2 + d_3 + (L_1/L_3)\ d_3 - (L_1/L_2)\ d_2$. This is the last stage of sliding before the bearing reaches its displacement limit; it comes in contact with the restraining rings of the articulated sliders and cannot go beyond without incurring damage. At the maximum displacement, u_6^*, the corresponding normalized horizontal force is $f_6^* = \mu_1 + d_1/L_1 + d_3/L_3$.

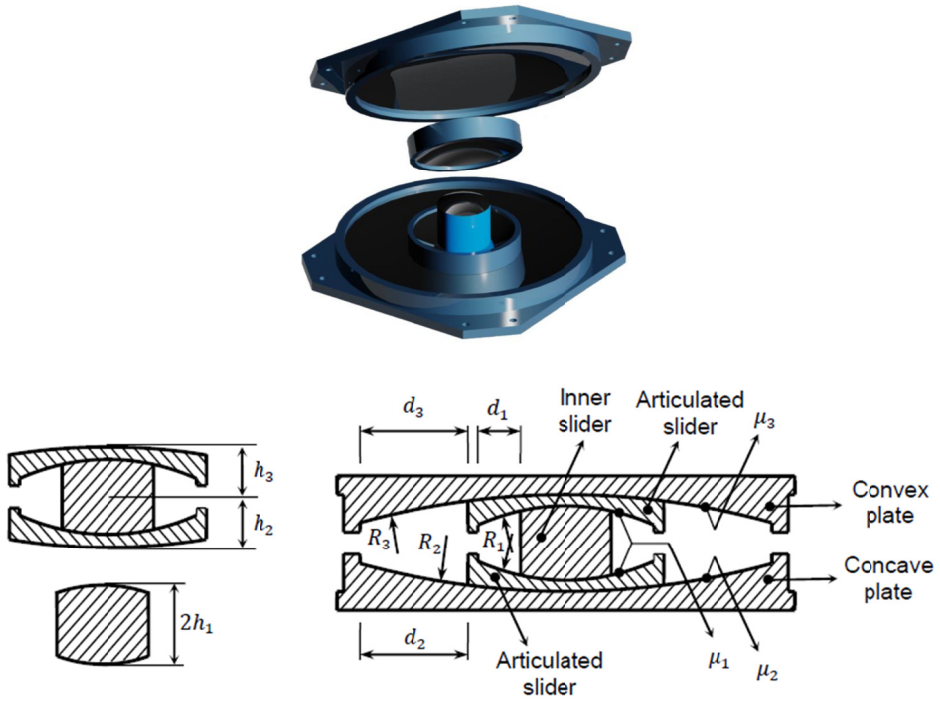

Figure 3.7 **3D and sectional view of triple pendulum bearing with basic parameters [Dao and Ryan 2015].**

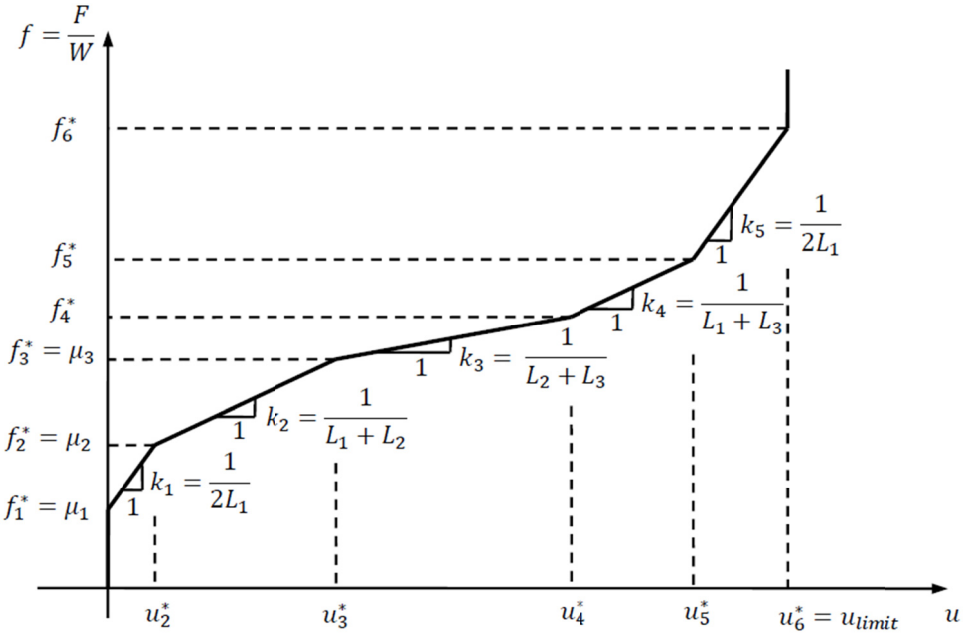

Figure 3.8 **Normalized backbone curve of a typical TPB [Dao and Ryan 2015].**

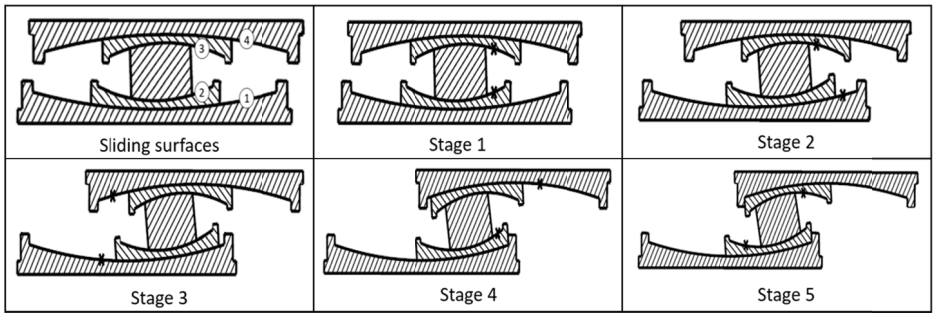

Figure 3.9 Sliding stages of a TPB [Dao and Ryan 2015].

The normalized backbone curve used in this study for the Base Model bridge is shown in Figure 3.10. The parameters were selected in such a way that sliding stages 2 through 4 collapse into a single stage. Specifically, the design parameters of the upper and lower concave plates were selected such that: effective lengths $L_2 = L_3$, friction coefficients $\mu_2 = \mu_3$, and displacement limits $d_2 = d_3$. Based on these assumptions, the normalized stiffnesses for the first and second stages of sliding are: $k_1 = 1/(2L_1)$, and $k_2 = 1/(2L_2)$. The periods associated with individual sliding stages on the normalized force-displacement curve are defined by:

$$T_i = 2\pi\sqrt{\frac{1}{k_i g}} = 2\pi\sqrt{\frac{2L_i}{g}} \tag{3.3}$$

where k_i is the normalized stiffness = $1/(2L_i)$, and g is the gravitational constant. For the normalized backbone curve shown in Figure 3.10, L_1 = 4.9 in. corresponding to T_1 = 1 sec, and L_2 = 60 in. corresponding to T_2 = 3.5 sec. The friction coefficients were selected as μ_1 = 0.02 and μ_2 = 0.08. Displacement capacities are d_1 = 0.8 in. and d_2 = 14.7 in., which were selected to provide sufficient displacement capacity so that large displacement stiffening would not be engaged. A vertical stiffness was assigned corresponding to a vertical period of 0.03 sec, as TPB bearings are very stiff in the vertical direction.

The TPBs were modeled using the *TripleFrictionPendulum* element [Dao et al. 2013] in OpenSees. This element is capable of capturing vertical–horizontal coupling and bidirectional coupling in the two horizontal directions. Past analytical studies using this element have replicated the response observed in the full-scale experiment at E-defense shake table in Japan.

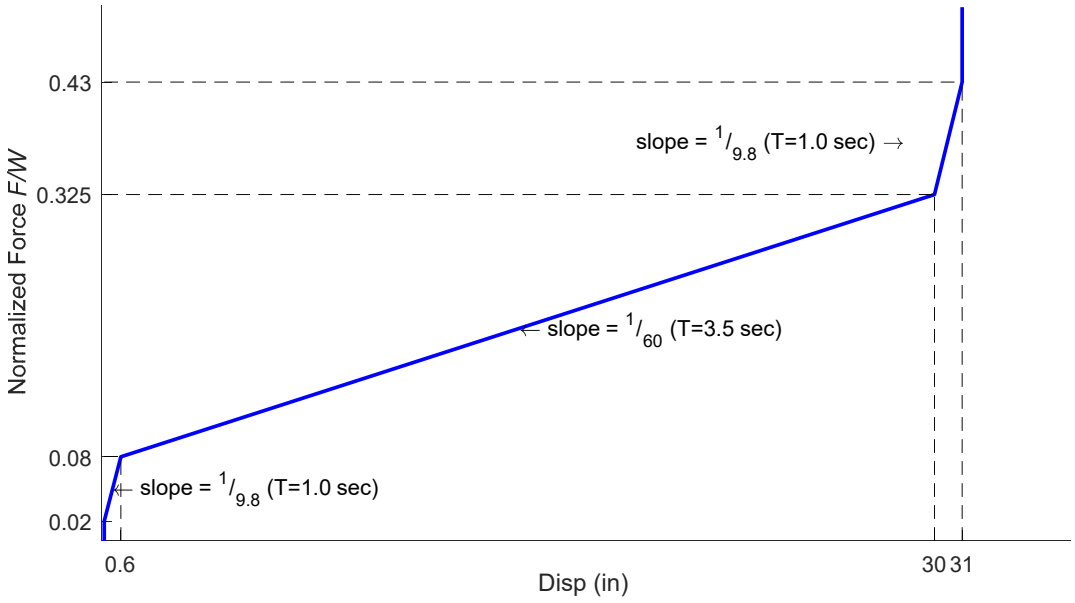

Figure 3.10 Design backbone curve for base model bridge.

4 Analysis of the Base Model Bridge Configuration

This chapter presents results of RHA and bearing force vs. displacement (hysteresis loops), and spectral responses of the Base Model bridge for each ground-motion group. Amplification of base shear in 3D motion (vertical and horizontal components) vs. ground-motion intensity are evaluated. Section 4.1 reports the various mode shapes and periods of the Base Model bridge to evaluate the behavior of the bridge under dynamic earthquake forces. Section 4.2 details various response histories, such as acceleration, shear force, displacement, and axial force, as well as bearing force-displacement for a representative motion selected from each of the three ground-motion groups. Section 4.3 reports peak shear force and acceleration responses for all selected ground motions. Section 4.4 examines in detail the spectral response of the Base Model bridge. This section demonstrates the existence of coupled horizontal and vertical modes, which are apparent in the deck spectra under combined horizontal and vertical shaking compared to horizontal shaking only.

4.1 EIGENVALUE ANALYSIS

Knowledge of the dynamic properties of the bridge is critical to evaluating its dynamic response, especially when the bridge is subjected to vertical shaking and potential horizontal–vertical coupling. An eigenvalue analysis of the Base Model bridge was performed in OpenSees to identify the frequencies and mode shapes of the participating modes. Also, a corresponding stick model of the bridge was built in SAP2000 [CSI 2017] and modal analysis performed for validation. Mode shapes and periods determined from each software were similar. The results shown here are from the OpenSees model. For modal analysis, the TPB models were replaced by linear springs with an effective stiffness representative of large displacement response. For this analysis, the effective period T_{eff} was assumed to be 3 sec. Isolators at bent and abutment locations carry different axial forces based on tributary area, and the effective stiffnesses, k_{eff}, of individual isolators were calculated according to the following equation:

$$k_{\text{eff}} = \left(\frac{2\pi}{T_{\text{eff}}}\right)^2 m_{\text{iso}} \tag{4.1}$$

where m_{iso} is the mass carried by the isolator.

The first ten modes shapes and corresponding periods are shown in Figure 4.1. The periods and corresponding modal mass participation factors in each direction are tabulated in Table 4.1. This information allows interpretation of the modal responses. The first three modes are isolation modes, which means the bridge deck moves as a single rigid mass sliding on the isolators. These three modes represent movement in the longitudinal, transverse, and torsional directions, respectively. Mode 4 is a first vertical mode, and Mode 5 is a second vertical mode. Mode 6 is a second transverse mode that activates significant bending of the deck about the vertical axis. Mode 7 is a vertical superstructure deformation mode (3C-shape). Vertical Modes 4 and 5 exhibit deck displacements in different directions and low mass participation; see Table 4.1. In contrast, the deformations in vertical Mode 7 are in-phase, and the mode has high mass participation around 80%; thus it is likely to be expressed in the dynamic response more than the other vertical modes. Modes 8 and 10 are rotational modes that rotate the deck in the clockwise direction, while Mode 9 is a deck torsional mode that rotates the deck in two different directions such that the deck twists.

Table 4.1 Periods and modal participation factors of base model bridge.

Mode	Period (sec)	Modal mass participation (%)		
		Longitudinal	Transverse	Vertical
1	3.03	100	0	0
2	3.01	0	100	0
3	2.69	0	0	0
4	0.35	0	0	0.02
5	0.25	0	0	0
6	0.21	0	0	0
7	0.20	0	0	79.42
8	0.14	0	0	0
9	0.12	0	0	0
10	0.11	0	0	0

4.2 REPRESENTATIVE RESPONSE HISTORIES AND BEARING HYSTERESIS LOOPS

Next, response history results are presented for the Base Model bridge incorporating the nonlinear TPB isolator element. The equations of motion were solved in OpenSees using Newmark's average acceleration integrator and the Newton–Raphson line search algorithm. Results are shown for a representative motion from each ground-motion group. The effect of vertical motion is defined by the amplification ratio, *AR*, defined as

$$AR = \frac{\chi_{o,3D}}{\chi_{o,2D}} \tag{4.2}$$

where $\chi_{o,3D}$ is the peak response (over time) during a 3D motion, and $\chi_{o,2D}$ is the peak response during the comparable 2D motion, with the vertical input omitted. Simply put, AR is the ratio of peak responses during 3D motion and 2D motion.

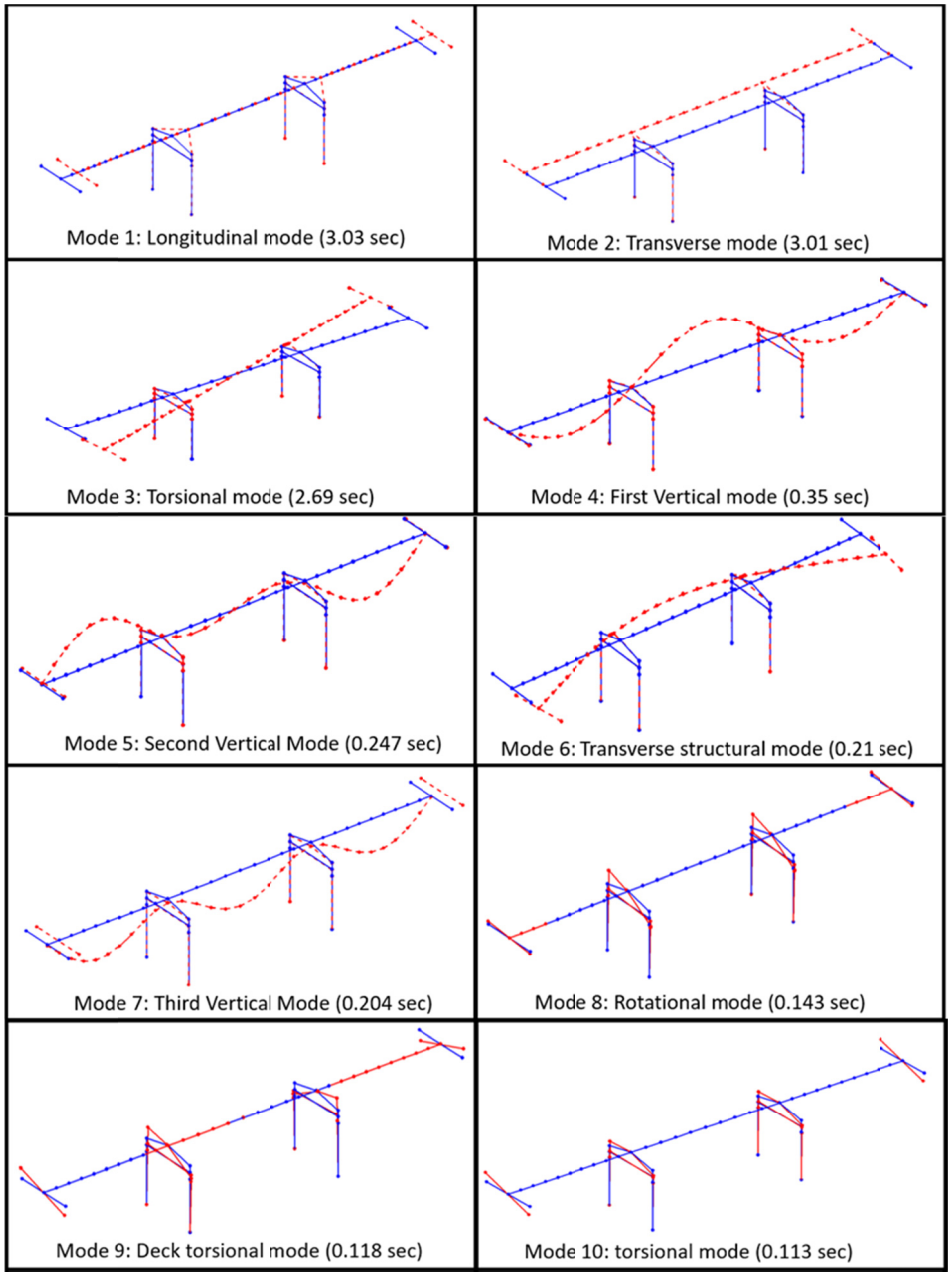

Figure 4.1 First ten periods and mode shapes of Base Model bridge.

4.2.1 Group 1 Motions

The vertical components of Group 1 motions had the greatest effect on bridge response since they have high vertical intensity. The SFPU motion (PGA_V = 0.817g) (Table 2.2) is selected as a representative motion from Group 1. Figure 4.2 shows the deck transverse and longitudinal direction acceleration histories at Bent 1. Peak accelerations are indicated by a circle and corresponding value for both 3D and 2D motions. The peak transverse direction accelerations during 3D and 2D motions are 0.35g and 0.14g, respectively. The peak longitudinal direction accelerations during 3D and 2D shaking are 0.21g and 0.11g, respectively. Thus, AR = 2.42 for transverse acceleration and 1.9 for longitudinal acceleration; see Equation (4.2). Accelerations under the 3D motion in both directions are affected by a high-frequency oscillation; as a result, the peak acceleration increases relative to the 2D motion.

Figure 4.3 represents transverse- and longitudinal-direction shear force histories of a column at Bent 1. Again, circles and corresponding values indicate the peak shear force. Shear-force histories are almost identical to acceleration histories, suggesting that the deck acted as a single mass sliding on the isolators. For the transverse base shear, AR = 2.56, and for longitudinal base shear, AR = 1.83. Figures 4.2 and 4.3 suggest that high-frequency vertical oscillation was transferred to the acceleration and base shear during 3D motion, which increased the shear force demand on the bridge piers.

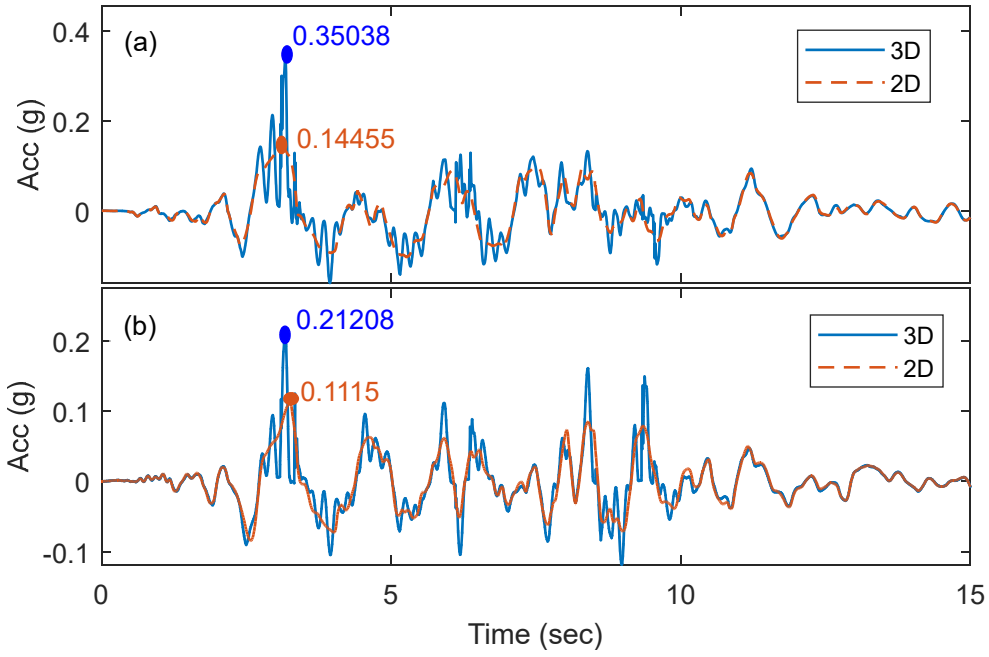

Figure 4.2 **(a) Transverse acceleration history and (b) longitudinal acceleration history at Bent 1 for SFPU motion (PGA_V = 0.817g).**

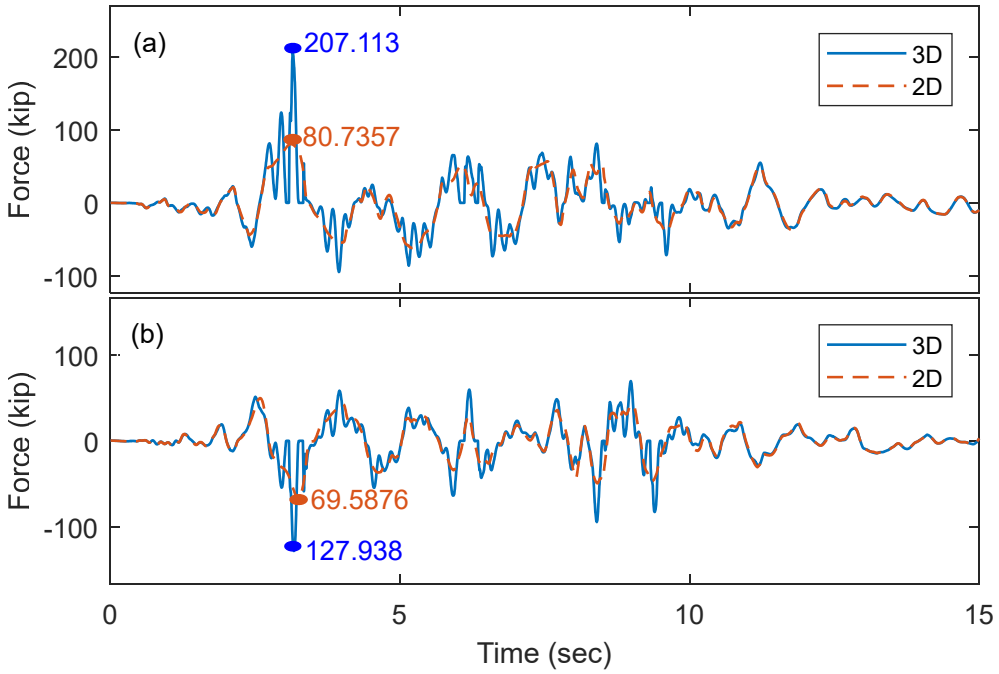

Figure 4.3 **(a) Transverse shear force history and (b) longitudinal shear force history at Bent 1 for SFPU motion (PGA_V = 0.817g).**

Figure 4.4 demonstrates Bent 1 column axial force history, vertical acceleration history, and longitudinal shear force history. Since TPB isolators do not have tension capacity, the isolator will experience uplift when they reach zero axial force. Uplift of the isolators occurs at approximately 3 sec, 3.2 sec, 6 sec, 6.3 sec, 8.5 sec, 9.3 sec, and 9.5 sec; see Figure 4.4(a). The uplift and subsequent pounding causes a spike in vertical acceleration, which is evident in Figure 4.4(b). Figure 4.4(c) illustrates a sudden increase in the shear force correlated to the uplift and spiked vertical acceleration.

Figure 4.5 compares the Bent 1 isolator displacement histories in each direction for 2D and 3D shaking due to SFPU ground motion. Unlike horizontal acceleration and base shear, vertical shaking has a minimal effect on isolator displacement. Figure 4.6 illustrates the total force-displacement hysteresis loops summed over all isolators for SFPU motion. When the bridge is subjected to 2D motion, the axial force variation is negligible [Figure 4.4(a)], and the isolator force-displacement loop is smooth; however, when the bridge is subjected to 3D motion, the axial force variation is high [Figure 4.4(a)], which causes a corresponding variation in the horizontal shear force. This results in local oscillation of the isolator force in the force-displacement loop and an overall increase in the peak base shear. The vertical component increases significantly the base shear. Thus omitting the vertical component may lead to underestimation of force demands.

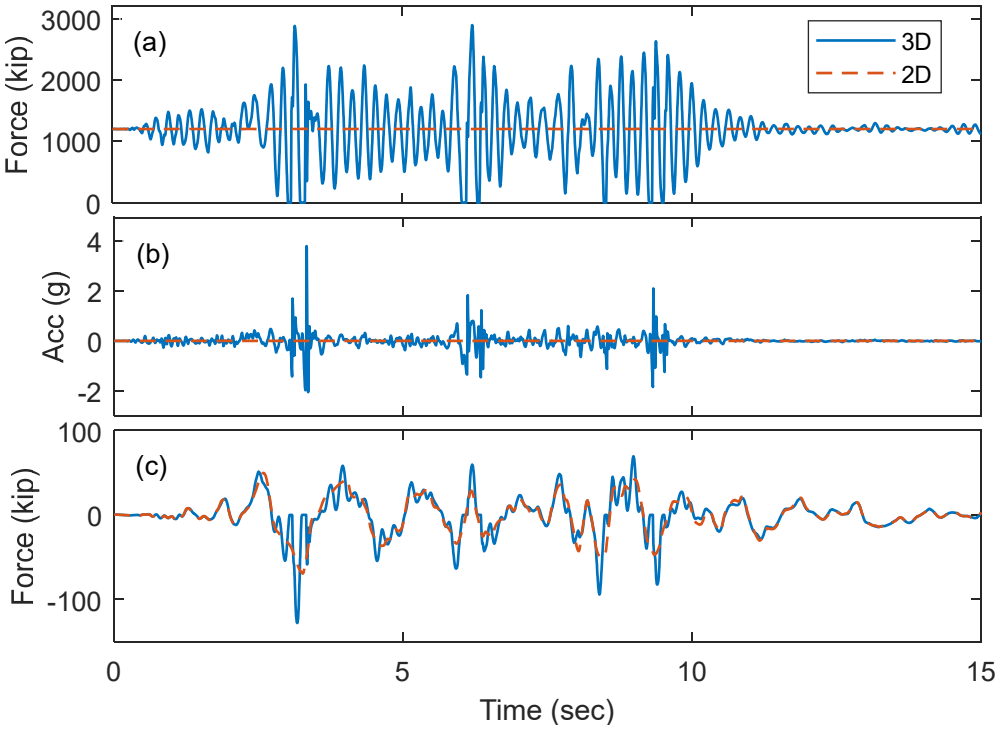

Figure 4.4 **(a) Total axial force history SFPU at Bent 1 column isolator; (b) vertical acceleration history at Bent 1; and (c) longitudinal shear force history at Bent 1 for SFPU motion (PGA_V = 0.817g).**

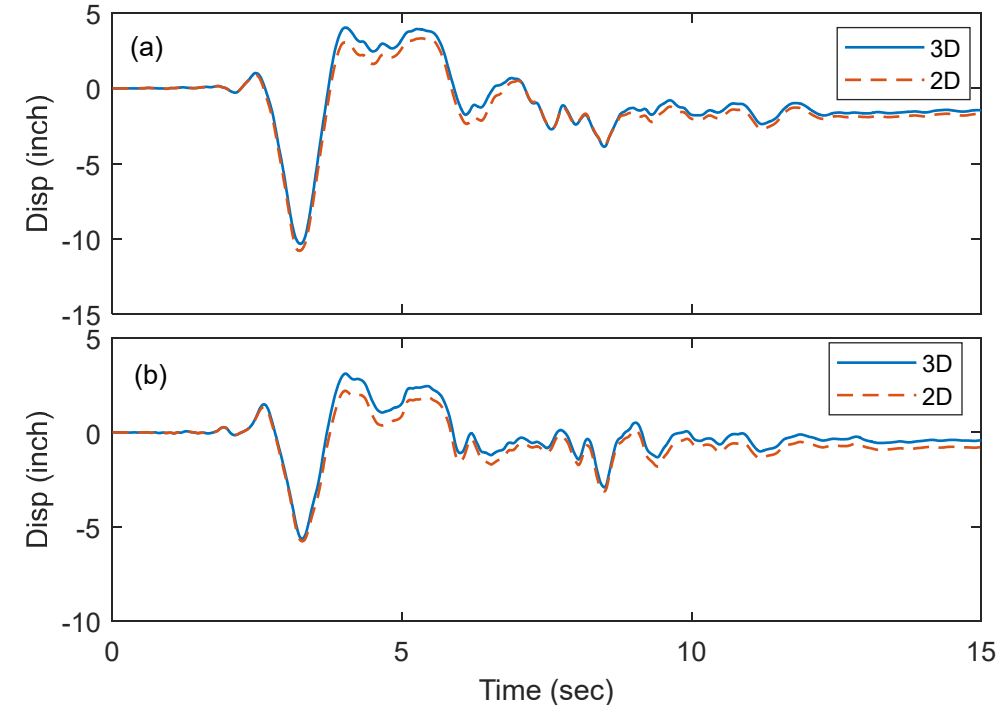

Figure 4.5 **(a) Transverse isolator displacement history; and (b) longitudinal isolator displacement history at Bent 1 for SFPU motion (PGA_V = 0.817g).**

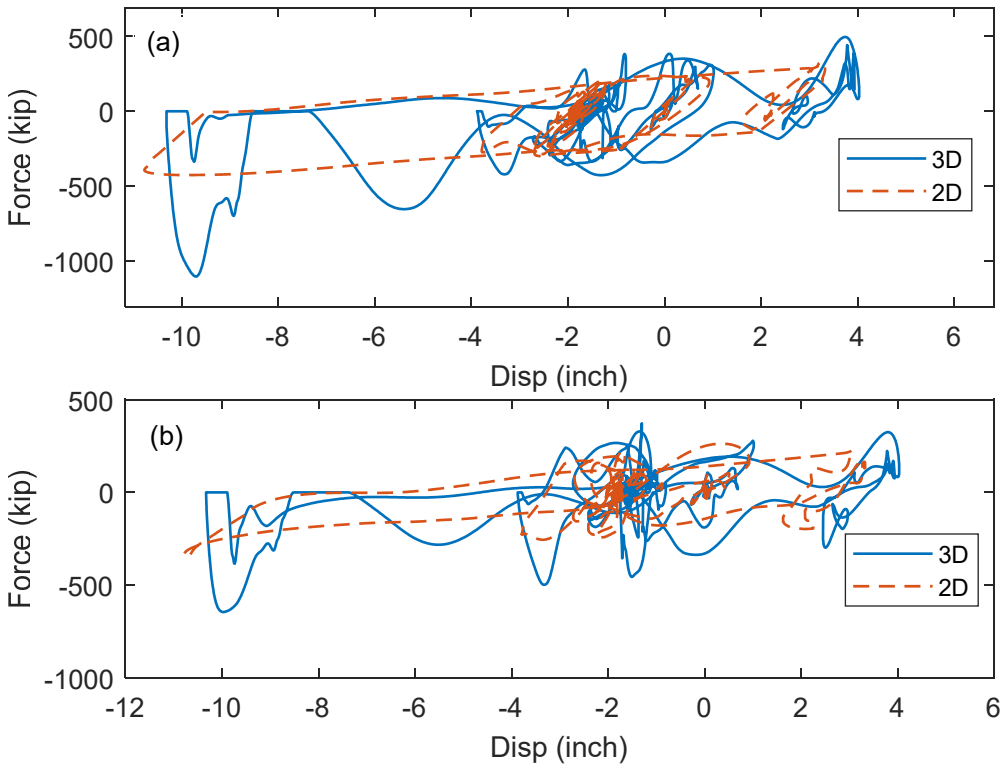

Figure 4.6 **Total force-displacement summed over all isolators in (a) transverse and (b) longitudinal direction for SFPU motion (PGA_V = 0.817g).**

4.2.2 Group 2 Motions

The LPG motion (PGA_V = 0.62g) was selected as a representative Group 2 ground motion. Group 2 motions have moderate vertical intensity; therefore, the *AR* is expected to be lower than Group 1 motions. Figure 4.7 presents horizontal acceleration histories in both directions for the LPG motion at Bent 1. Based on the observed peak accelerations, *AR* = 1.41 for the transverse acceleration and 1.18 for longitudinal direction acceleration. These amplifications are much less than the corresponding *AR* for Group 1 motion SFPU (2.7 for transverse acceleration and 1.9 for longitudinal acceleration). Overall, peak accelerations in the longitudinal and transverse directions during 2D motion are lower than exhibited by Group 1 (Figure 4.7 versus Figure 4.2) due to comparatively lower horizontal shaking intensities; during the 3D motion, they are lower due to comparatively lower PGA_V.

Figure 4.8 plots the shear-force histories in the transverse and longitudinal directions for a column at Bent 1 of the bridge. The base-shear *AR* is 1.43 for the transverse direction and 1.21 for the longitudinal direction. Here, the *AR* for base shear is almost the same as the *AR* for deck acceleration. Figure 4.9 shows the axial force history of an isolator at Bent 1; uplift did not occur due to this moderate-intensity vertical motion. As a result, spikes in the vertical acceleration history (not shown here) are not present, which correlate to lower amplification of the horizontal acceleration and base shear in both directions.

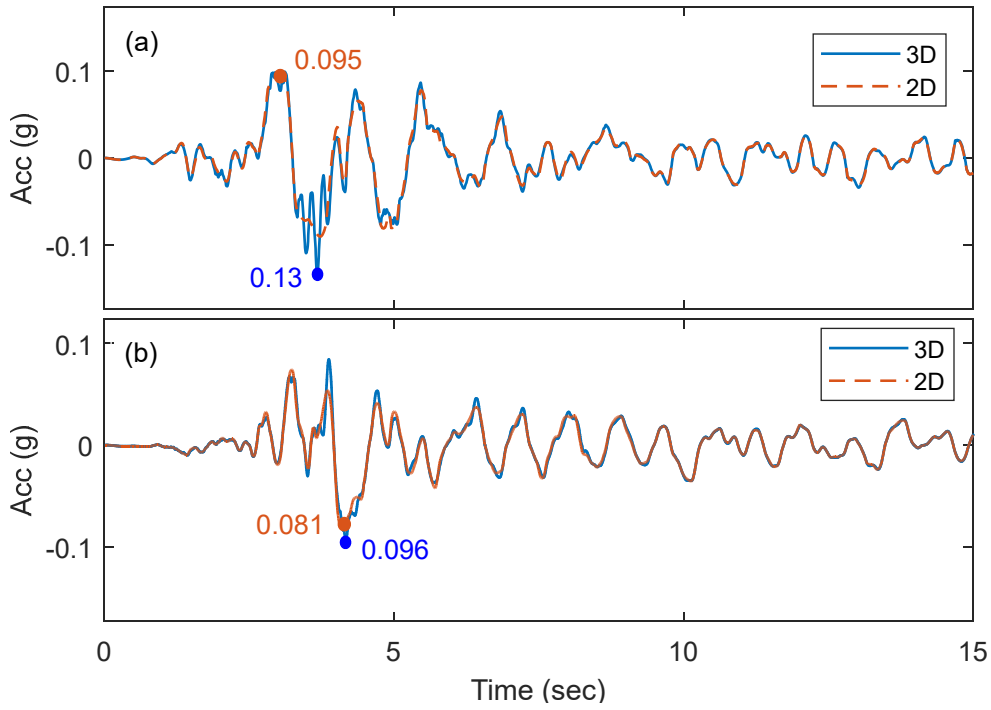

Figure 4.7 **(a) Transverse acceleration history at Bent 1; and (b) longitudinal acceleration history at Bent 1 under LPG motion (PGA_V = 0.62g).**

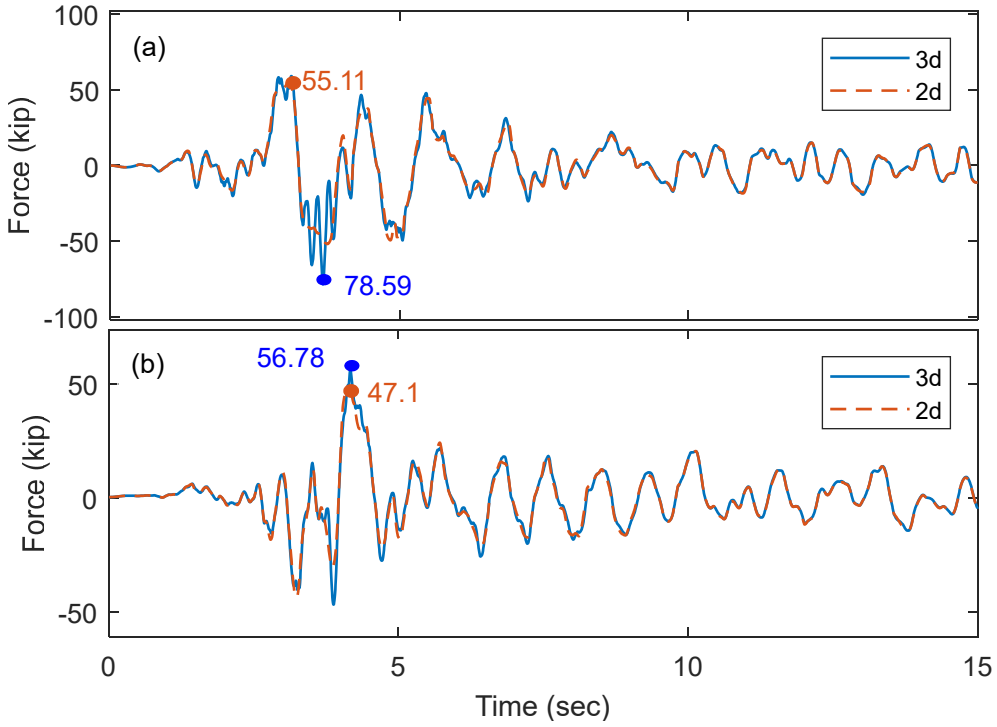

Figure 4.8 **(a) Transverse shear force history at Bent 1 column; and (b) longitudinal shear force history LPG motion at Bent 1 column under LPG motion (PGA_V = 0.62g).**

Figure 4.10 shows the displacement history of a TPB isolator at Bent 1 during the LPG motion. Consistent with earlier findings, the isolator displacement is not affected by the vertical component of ground shaking. Figure 4.11 shows the total isolator force-displacement hysteresis loops summed over all isolators for the LPG motion. The effect of the axial force variation on the isolator shear force for 3D shaking is also evident in this figure, although not as pronounced as in Figure 4.6. Specifically, axial force variation in transverse direction is greater, and the hysteresis loop in transverse direction shows increased base shear compared to the longitudinal direction.

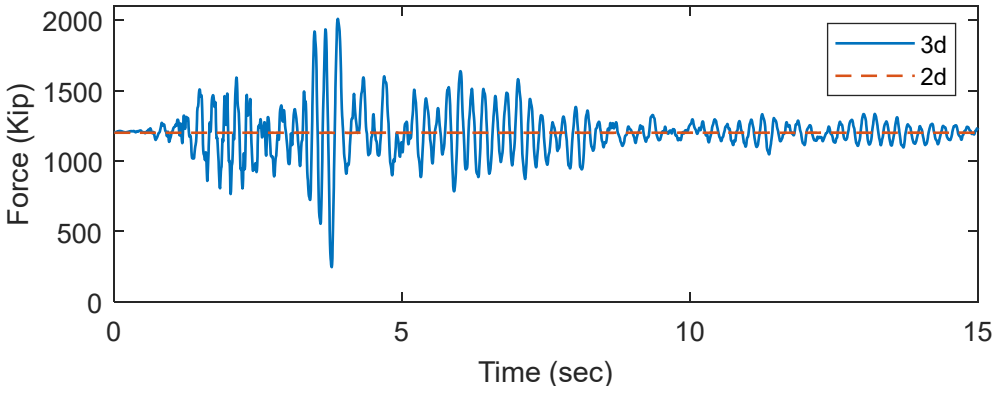

Figure 4.9 Axial force history for LPG (PGA_V = 0.62g) motion at Bent 1.

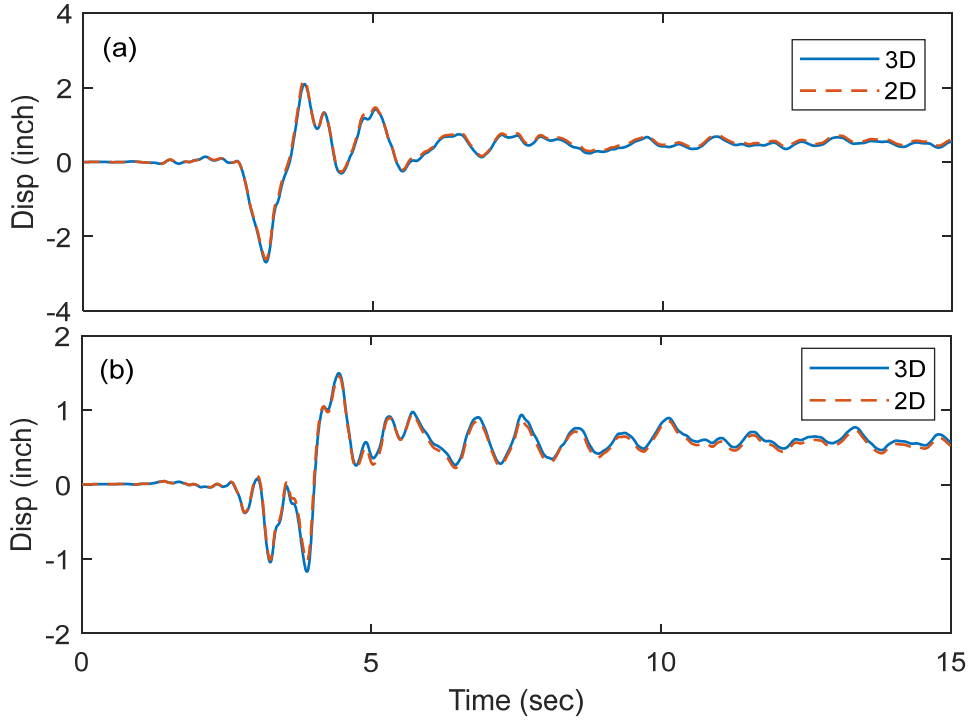

Figure 4.10 (a) Transverse and (b) longitudinal isolator displacement history at Bent 1 for LPG motion (PGA_V = 0.62g).

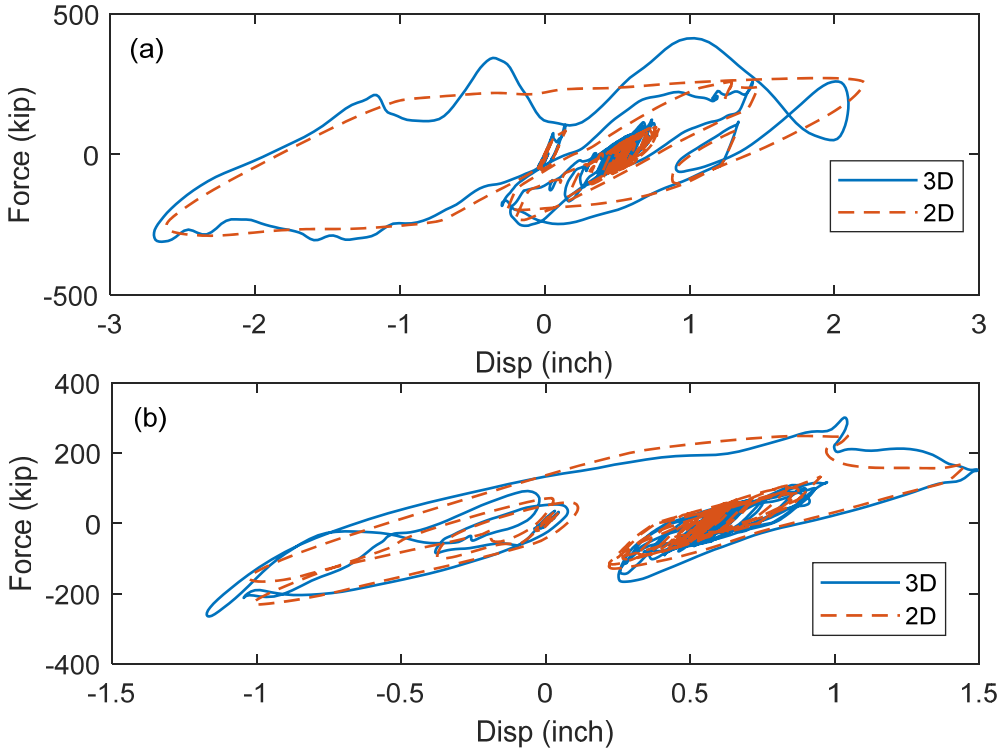

Figure 4.11 **Total force-displacement summed over all isolators in (a) transverse and (b) longitudinal direction under LPG motion (PGA_V = 0.62g).**

4.2.3 Group 3 Motions

This section presents response histories to the IIB motion (PGA_V = 0.38g) as a representative Group 3 motion. Motions from Group 3 have comparatively low vertical intensity. Figure 4.12 shows the horizontal acceleration histories for the IIB motion. The *AR* is 1.16 for the transverse direction acceleration and 1.42 for the longitudinal direction acceleration. Figure 4.13 shows the base-shear histories in the transverse and longitudinal directions in a column at Bent 1. The increase in acceleration for 3D motion is also reflected in base-shear histories; see Figure 4.13. The *AR* for transverse base shear is 1.22 and for longitudinal base shear is 1.42, which is almost the same as the *AR* for acceleration. Figure 4.14 displays the axial force history of a Bent 1 isolator. Similar to Group 2 (moderate-intensity) motions, no instances of isolator uplift during this motion are observed.

One notable difference in the response to this motion compared to the motions examined for Groups 1 and 2 is that the *AR* for longitudinal direction acceleration and base shear is higher than for the transverse direction. An inspection of the axial force history in Figure 4.14 shows that the peak axial force variation occurred around 5 sec. Thus, the timing of the strongest intensity vertical shaking is out-of-phase with the peak transverse direction acceleration [Figure 4.12(a)], but in-phase with the peak longitudinal direction acceleration [Figure 4.12(b)]. This implies that the *AR* is influenced by the relative phasing of horizontal and vertical shaking, and the peaks produced by horizontal and vertical shaking may not directly sum together.

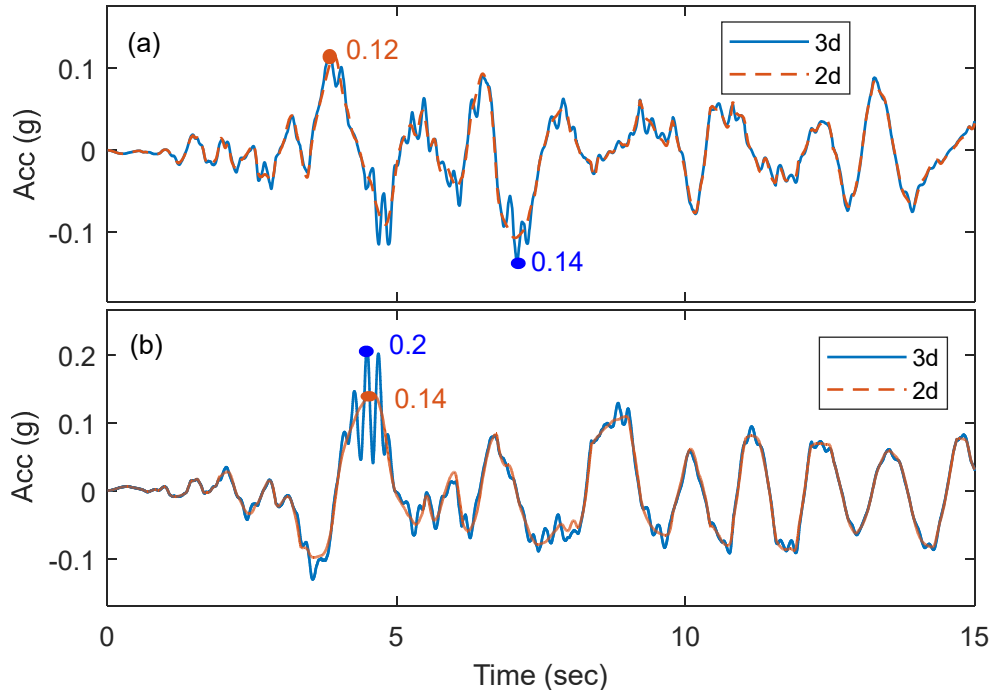

Figure 4.12 **(a) Transverse acceleration history and (b) longitudinal acceleration history at Bent1 under IIB motion (PGA_V = 0.38g).**

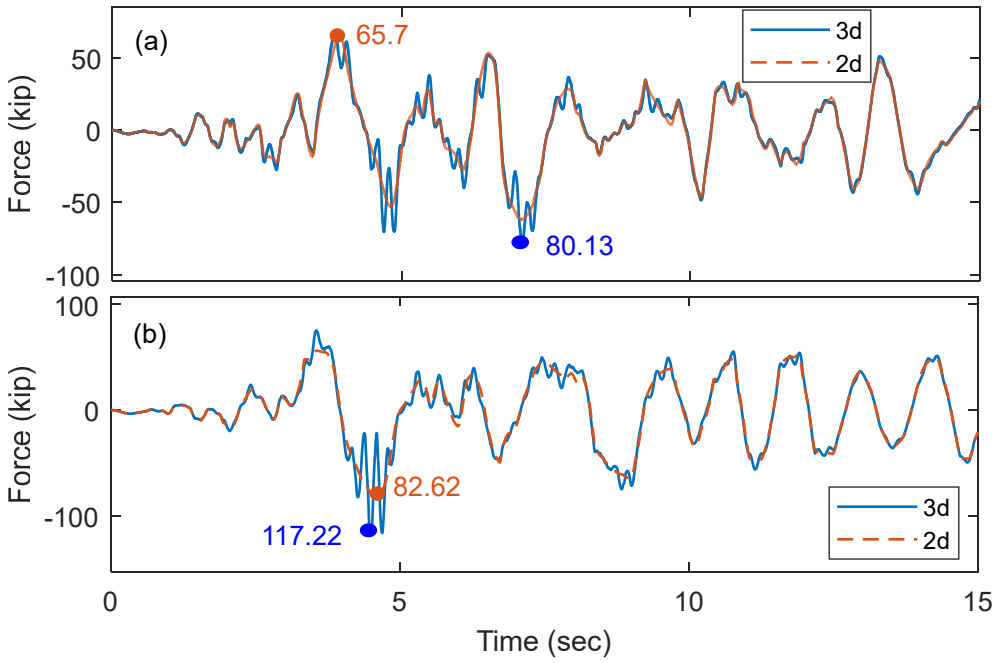

Figure 4.13 **(a) Transverse shear force history; and (b) longitudinal shear force history at Bent 1 column under IIB motion (PGA_V = 0.38g).**

Figure 4.15 depicts the displacement histories of a Bent 1 isolator due to IIG motion. The vertical component has no effect on the displacement demands of the bridge as was observed for other motions. Figure 4.16 plots the total force-displacement summed over all isolators. The displacement demands are unaffected by vertical shaking, but the base shear in both directions is increased by the presence of the vertical ground acceleration.

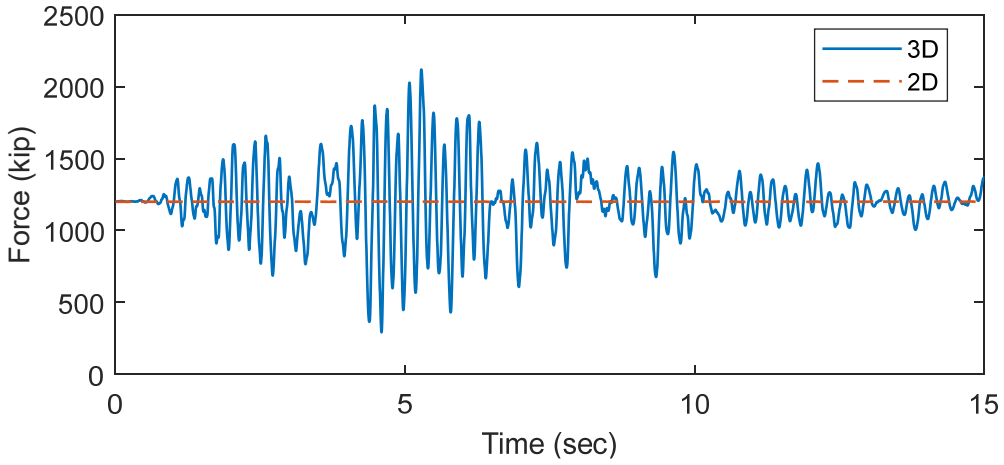

Figure 4.14 Axial force history at Bent 1 location for IIB motion (PGA_V = 0.38g).

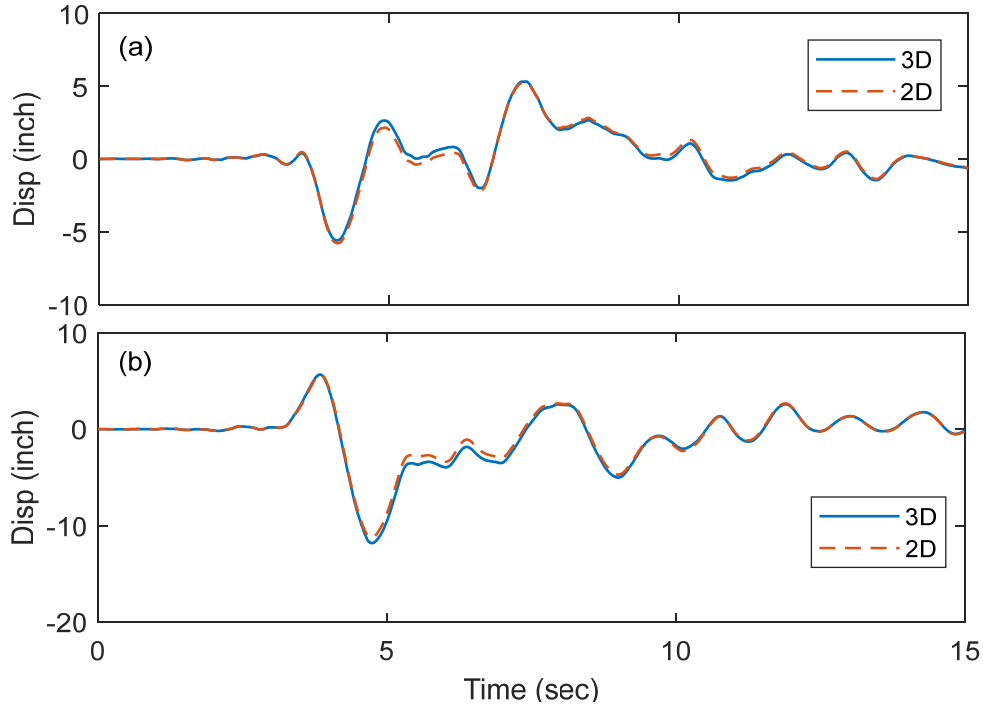

Figure 4.15 (a) Transverse displacement history; and (b) longitudinal displacement history for at Bent 1 under IIB motion (PGA_V = 0.38g).

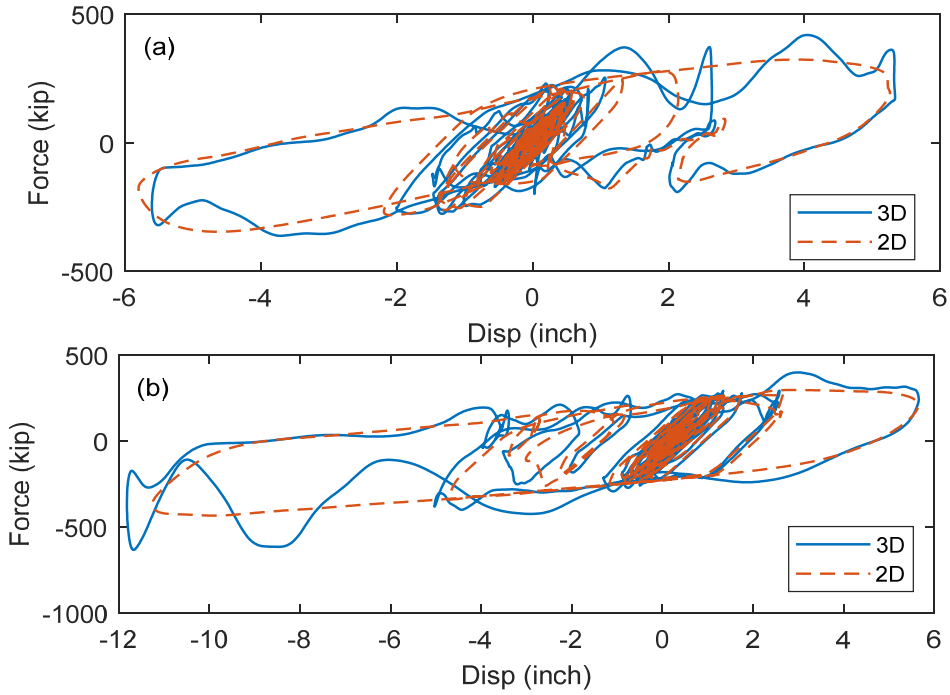

Figure 4.16 **Total force-displacement summed over all isolators in (a) transverse and (b) longitudinal direction under IIB motion (PGA_V = 0.38g).**

4.3 AMPLIFICATION FACTORS VS. GROUND-MOTION INTENSITY

This section discusses trends in peak acceleration, peak base shear, and their corresponding *AR* (Equation 4.2) for all selected motions. The differences in *AR* based on ground-motion intensity–distinguished by ground-motion group–are identified. Figure 4.17 plots the peak acceleration at Bent 1 during 2D shaking (orange dot) and 3D shaking (blue dot) for both transverse and longitudinal directions, and lists the value of the corresponding *AR*. Results are distinguished by the ground-motion group as indicated. Comparable results for base shear are presented in Figure 4.18; note that these values are for total base shear summed over all isolators, and thus some values differ slightly from those reported earlier. The *AR* for peak accelerations and total base shear are also tabulated in Table 4.2, which also shows the *AR* averaged over each ground-motion group.

Based on the presented results, the *AR* for total base shear are almost the same as for acceleration. An exception to this trend is in the transverse direction for Group 1 motions, where average *AR* for the base shear is notably higher than for acceleration. For Group 1 motions, the average acceleration *AR* are 2.55 and 1.84, and average base-shear *AR* are 2.55 and 2.02 in the transverse and longitudinal directions, respectively. Group 2 and 3 motions have similar average *ARs* for acceleration and base shear ranging from about 1.15 to 1.3. Clearly, the high vertical intensity Group 1 motions produced much higher *ARs* than the lower intensity Group 2 and 3 motions.

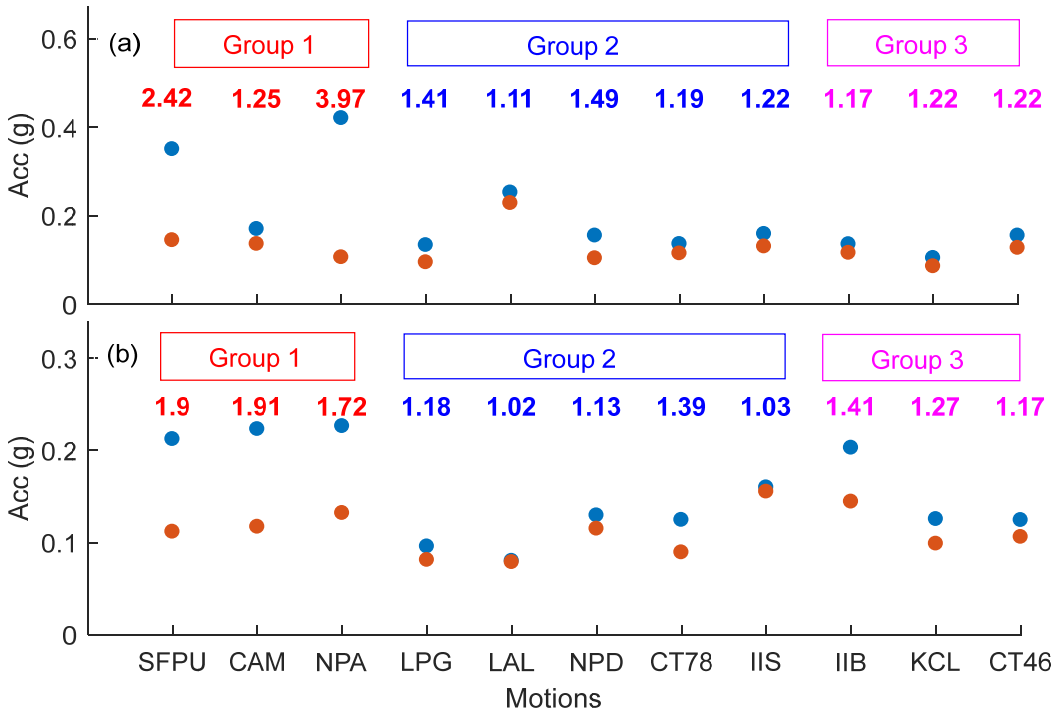

Figure 4.17 **(a) Transverse and (b) longitudinal direction peak acceleration and *AR*.**

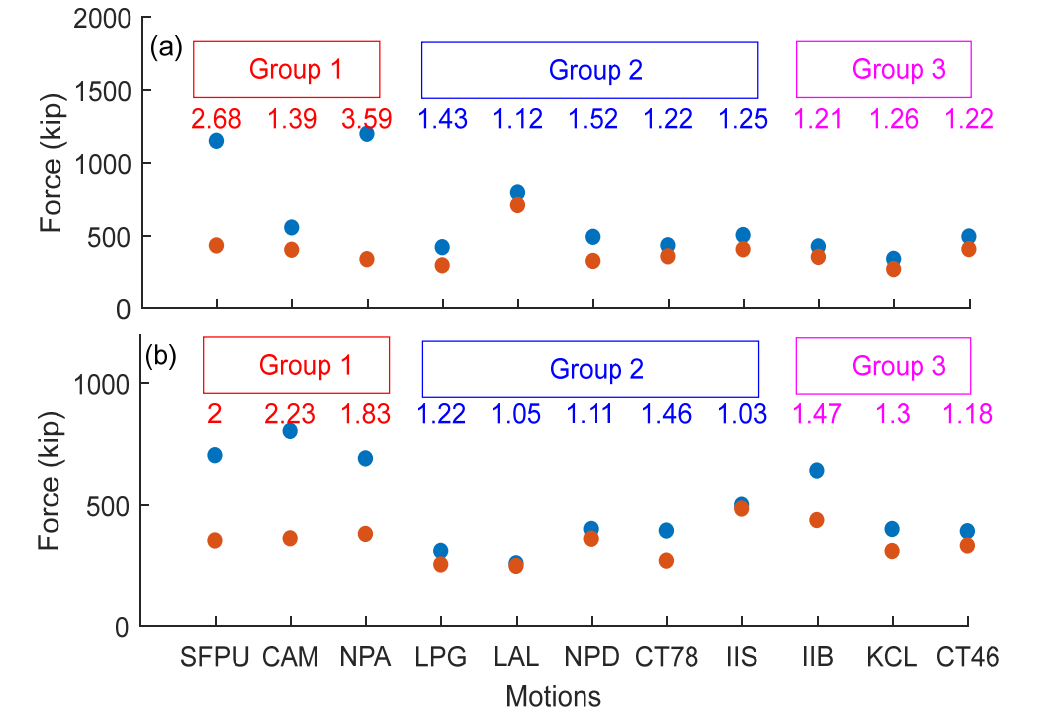

Figure 4.18 **(a) Transverse and (b) longitudinal direction peak base shear and *AR*.**

Table 4.2 *AR* for peak deck acceleration and total base shear for all motions.

Group #	Motions	Peak deck acceleration		Average peak deck acceleration		Peak base shear		Average peak base shear	
		T	*L*	*T*	*L*	*T*	*L*	*T*	*L*
1	SFPU	2.42	1.9	2.55	1.84	2.68	2	2.55	2.02
	CAM	1.25	1.91			1.39	2.23		
	NPA	3.97	1.72			3.59	1.83		
2	LPG	1.41	1.18	1.28	1.15	1.43	1.22	1.31	1.17
	LAL	1.11	1.02			1.12	1.05		
	NPD	1.49	1.13			1.52	1.11		
	CT78	1.19	1.39			1.22	1.46		
	IIS	1.22	1.03			1.25	1.03		
3	IIB	1.17	1.41	1.2	1.28	1.21	1.47	1.23	1.31
	KCL	1.22	1.27			1.26	1.3		
	CT46	1.22	1.17			1.22	1.18		

4.4 SPECTRAL RESPONSE

Acceleration response spectra of the total (absolute) deck acceleration histories as predicted by analysis in both the horizontal and vertical directions have been developed for representative motions. Peaks in these spectra are generally associated with the excited structural modes of the bridge. The spectral response for accelerations at Bent 1 in the longitudinal, transverse, and vertical directions due to the SFPU motion are plotted in Figure 4.19. These response spectra in the transverse and longitudinal direction exhibit peaks near 1.5 sec, which indicate the isolation mode in each direction. The period of these isolation modes is different from that computed in modal analysis, which utilized an effective stiffness that reflected the full displacement capacity of isolators; however, for many ground motions, the induced displacement demand is less than the capacity, resulting in a higher effective stiffness and lower effective period. For 3D relative to 2D shaking, amplification of the spectral acceleration is observed for shorter periods, which is likely controlled by the presence of a peak at about 0.2 sec for 3D shaking that is absent for 2D shaking. This peak is much stronger in the transverse direction than in the longitudinal direction. The vertical spectrum (3D motion only) exhibits grouped peaks from about 0.2 to 0.3 sec and several peaks at shorter periods. These short periods are likely associated with higher vertical modes, which have not been included in the eigenvalue analysis.

As noted above, differences in spectral response (especially in the transverse direction) are observed for 2D versus 3D shaking. To explore this further, Figure 4.21 plots the transverse direction deck spectra at three strategic locations (indicated by black dots): to the left of Bent 1,

mid-span, and to the right of Bent 2. These locations to the left and right of the bents correspond to nodes in Mode 6 (the second transverse mode in Figure 4.1), which is superimposed over the undeformed bridge (Figure 4.20). The significance of these nodal locations is that Mode 6 peaks will not be visible in the response spectra at these locations even if this mode contributes meaningfully to the response. As seen in Figure 4.20, the spectral response for 2D shaking is the same at all locations, and Mode 6 is not expressed (no peak is visible at the modal period of 0.2 sec). For 3D shaking, Mode 6 is strongly expressed at the mid-span location, with a spectral acceleration peak of 0.86g at 0.2 sec. This more than doubles the peak acceleration observed at that location compared to the 2D shaking. This peak can be conclusively associated with Mode 6 since it does not appear at the Mode-6 node locations.

To understand why the second transverse mode is expressed in 3D shaking and not 2D shaking, the vertical spectra at various locations were examined. Figure 4.21 plots the vertical deck spectra at five locations: in the middle of each span and at the two bents. One factor common among all vertical modes in Figure 4.1 (Modes 4, 5, and 7) is that the modal displacement is large at mid-span and minimal at the bent locations. This modal pattern is replicated in the deck spectra in Figure 4.21, where spectral peaks are on the order of 15g at mid-span locations and 2–3g at bent locations. The peak is observed at a period near 0.2 sec and believed to correspond to Mode 7. Although Mode 7 does not have the longest period, it is dominant among the vertical modes due to its high modal participation factor (Table 4.1) as was projected earlier.

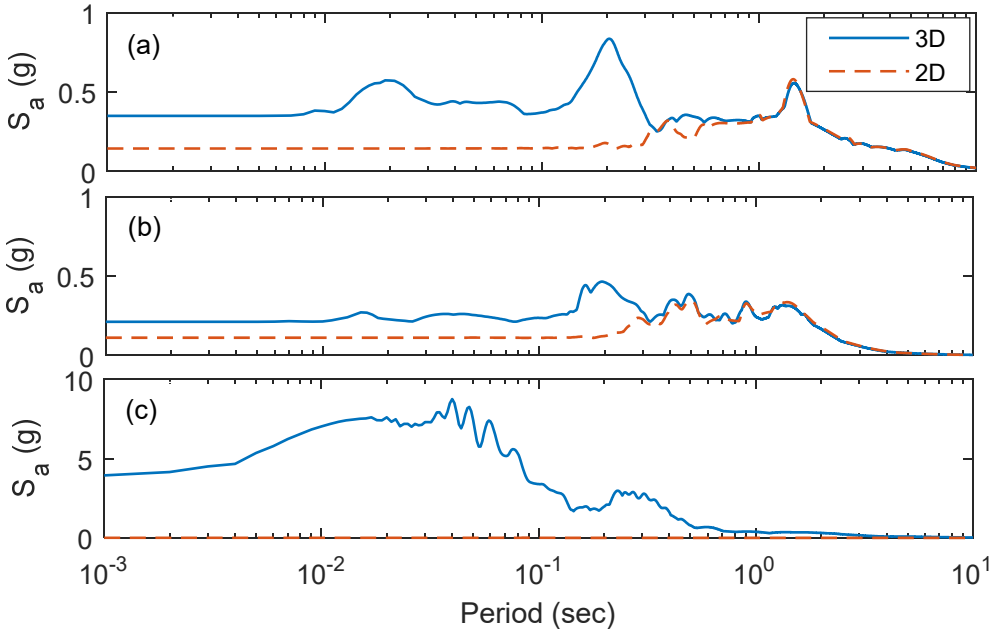

Figure 4.19 (a) Transverse, (b) longitudinal; and (c) vertical deck spectra at Bent 1.

As discussed previously, vertical ground shaking leads to high-frequency variation in the axial forces on the TPBs. Since the bearing horizontal force (based on friction) is proportional to the axial force, high-frequency oscillation is also introduced to the bearing horizontal force and overall base shear; see Figures 4.3, 4.4, 4.9, and 4.14. From the results shown in Figures 4.20 and 4.21, the higher frequency oscillation introduced to the base shear occurs at a period around 0.2 sec, which happens to be closely matched to the period of the second transverse mode (Mode 6). As a result, the second transverse mode is excited for 3D shaking only due to the coupling of the closely spaced horizontal and vertical modes. For this example, the coupling is shown to greatly increase the peak horizontal acceleration in the bridge superstructure.

As discussed in the introduction, although the horizontal–vertical (H–V) coupling phenomenon has been observed in buildings, it was assumed to be an unlikely occurrence in bridges. This has been proven false as such coupling was identified in the first bridge model examined in this study. Since bridge superstructure acceleration does not specifically correlate to damage (unlike a building with a varied assortment of acceleration-sensitive components and equipment), bridge engineers might conclude that the amplification of acceleration is unimportant. This discussion points out that such coupling is possible. The responses under such coupling can only be predicted by 3D RHA, with mass finely distributed over the superstructure spans. Bridge engineers are recommended to apply such analysis approaches when deemed necessary.

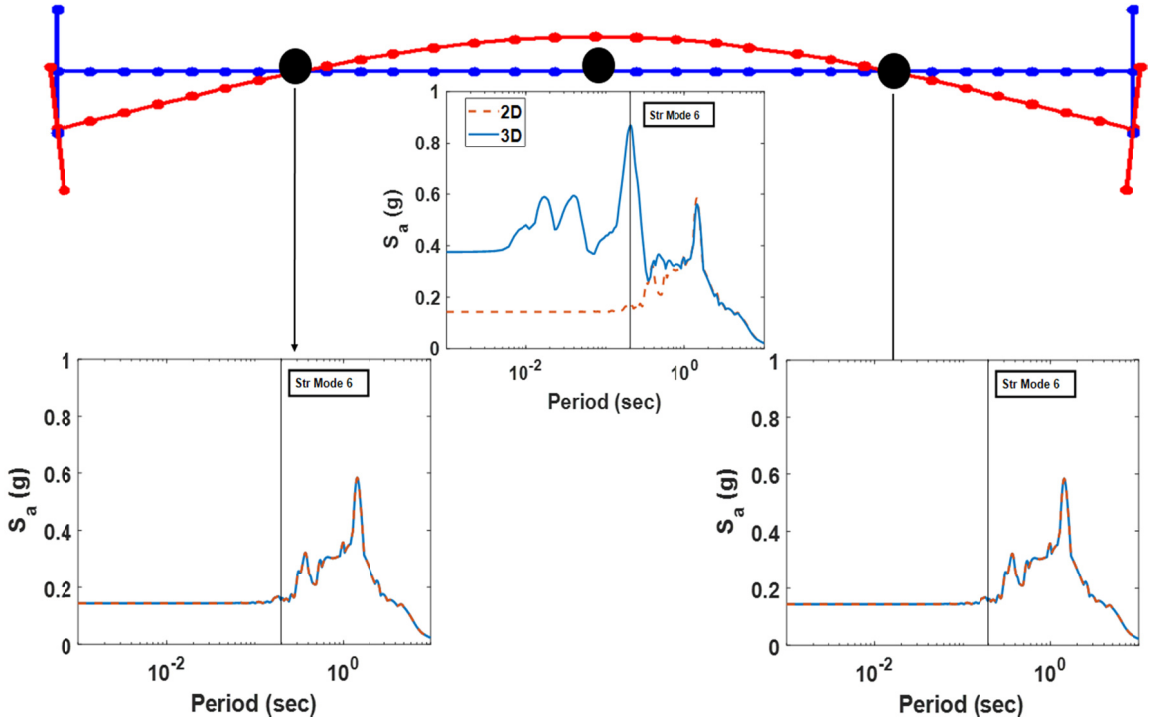

Figure 4.20 Deck spectra at dot locations and sixth mode of the base model bridge.

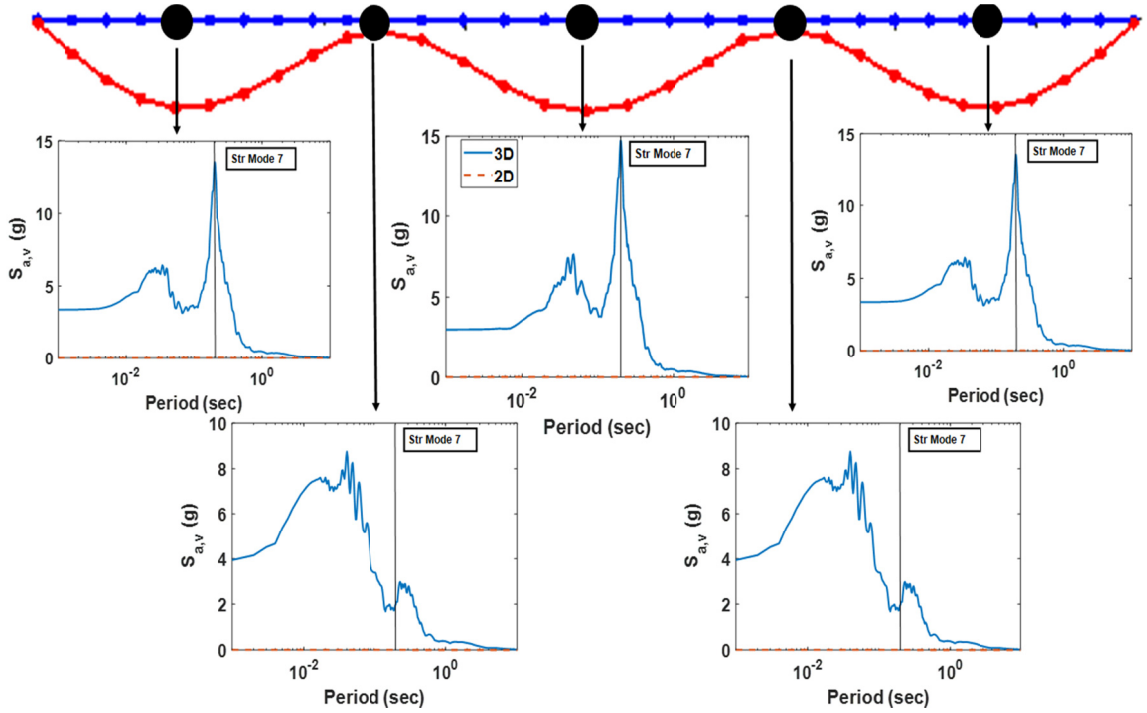

Figure 4.21 Deck spectra at dot locations and seventh mode of the base model bridge.

5 Simplified Method to Estimate Base-Shear Amplification

This chapter presents a simplified method to estimate the amplification of base shear in 3D shaking relative to 2D shaking. Section 5.1 presents a theoretical basis and proposes equations for the estimating the base-shear amplification due to vertical shaking. The theory is applicable to any spherical sliding bearing type isolation system. Two theories are proposed and followed by examples demonstrating application of those theories. Section 5.2 discusses methods to analyze the error in the estimated base shear relative to the observed base shear. Two different measures of error are developed: the amplification factor error and the base-shear normalized error. Amplified base-shear estimates and computed errors for all motions are presented and evaluated.

5.1 AMPLIFICATION THEORY

A theory is proposed here to estimate the amplification of base shear due to the vertical motion. The horizontal force of a spherical sliding bearing, based on a single pendulum mechanism, was given in Equation (1.1). This equation is a reasonable approximation of the resisting force of multi-spherical bearings when the response is dominated by the outer pendulum mechanism and represents the base shear in a system with many isolators. Thus, Equation (1.1), expressed in terms of system base shear, V_b, is repeated here for convenience:

$$V_b(u) = \frac{W}{R_{eff}}u + \mu W\left(\ \right)$$

$$AE = \left(\frac{\Delta_{\text{est}-\Delta}}{\Delta}\right)\times 100 \tag{5.1}$$

$$BSNE = \left(\frac{\frac{V_{b,3D_{est}}}{W} - \frac{V_{b,3D}}{W}}{\frac{V_{b,3D}}{W}}\right)\times 100$$

where W is the weight of the superstructure, R_{eff} is the effective radius of curvature (corresponding to the period of the dominant sliding mechanism), μ is the friction coefficient of dominant pendulum mechanism, and u is the isolator displacement. Dividing Equation (5.1) by the bridge weight, W, rearranging, and taking the peak over time, the following is obtained:

$$\frac{V_{b,2D}}{W} = \frac{u_o}{R_{eff}} + \mu \tag{5.2}$$

where $V_{b,2D}$ is the peak base shear when subjected to 2D (horizontal only) acceleration, and u_o represents the peak bearing displacement. Equation (5.2) can be applied in either the longitudinal or transverse direction.

As mentioned previously, the horizontal base shear in a spherical sliding bearing isolation system is dependent on the axial force acting on isolators. When vertical acceleration is considered, the system base shear should be determined from the instantaneous normal force, N, on the isolators rather than the static weight of the structure:

$$V_b(u) = \frac{N}{R_{eff}}u + \mu N \tag{5.3}$$

The system normal force, N, varies with time according to:

$$N = W + m\ddot{u}_z^t \tag{5.4}$$

where m is the total mass, and $\ddot{u}_z^t$ is the vertical acceleration at the isolators. Accordingly, the component of the base shear due to vertical shaking can be estimated as:

$$V_{b,V} = m\ddot{u}_{zo}^t\left(\frac{u_o}{R_{eff}} + \mu\right) \tag{5.5}$$

where $V_{b,V}$ is the horizontal force due to vertical acceleration only, and $\ddot{u}_{zo}^t$ is the peak vertical acceleration over time. Thus, an additional component of base shear arises during vertical shaking that is dependent on the vertical acceleration. Normalizing Equation (5.5) by the superstructure weight leads to:

$$\frac{V_{b,V}}{W} = \ddot{u}_{zo}^t(g)\left(\frac{u_o}{R_{eff}} + \mu\right) \tag{5.6}$$

The value of $\ddot{u}_{zo}^t$ can be estimated from the $\mathrm{PGA_V}$.

$$\ddot{u}_{zo}^t = \nu \cdot \mathrm{PGA_V} \tag{5.7}$$

where ν is an amplification factor representing the amplification of the vertical acceleration from the ground to the structure. Thus $V_{b,V}/W$ simplifies to:

$$\frac{V_{b,V}}{W} = \nu \cdot \mathrm{PGA_V}\left(\frac{u_o}{R_{eff}} + \mu\right) \tag{5.8}$$

The total base-shear coefficient can be estimated as:

$$\frac{V_{b,3D}}{W} = \frac{V_{b,2D}}{W} + \frac{V_{b,V}}{W} \tag{5.9}$$

The estimation is exact if the peak horizontal displacement and peak vertical acceleration occur at the same time. Otherwise, Equation (5.9) will give a conservative estimate of the amplified base shear.

To apply the theory, different values of the amplification factor ν are considered. Assuming $\nu = 1$ is consistent with the peak vertical acceleration at the isolators being equal to the $\mathrm{PGA_V}$, dynamic amplification is possible, wherein the vertical acceleration at the isolators is amplified compared to $\mathrm{PGA_V}$. Phase-lag effects may also occur, such that the peak lateral base shear $V_{b,2D}$ and peak vertical base shear $V_{b,V}$ do not occur at the same time. Thus, $\nu = 1$ could be justified if the dynamic amplification and phase-lag effects approximately cancel each other out. If there is no dynamic amplification and phase-lag effects are apparent, assuming a value less than 1 for ν may be appropriate. If considerable dynamic amplification is observed, and peak horizontal and vertical responses are in phase, then a value for ν considerably larger than 1 may best represent the response characteristics.

Going forward, three different values for ν represent the three conditions described above: $\nu = 0.5$, $\nu = 1$, and $\nu = S_a(T_v)/\mathrm{PGA_V}$, where $S_a(T_v)$ = spectral acceleration of the vertical ground motion at the dominant vertical period T_v of the isolated structure. The final value is predicated on the assumption that if dynamic amplification is present, the realized vertical acceleration at the isolators can be estimated from the spectral amplification of the ground motion based on the dominant vertical mode. The period T_v should be chosen independently for every bridge. For the Base Model bridge configuration, $T_v = 0.2$ sec is selected because it approximately corresponds to Mode 7, the dominant vertical mode observed in the response; see Figure 4.21.

As an example, sample calculations are tabulated for the Base Model bridge subjected to Group 1 motion SFPU. For excitation in the transverse direction, the peak isolator displacement was $u_o = 10.33$ in., and base shear for 2D shaking was $V_{b,2D}/W = 0.135$. The isolator friction coefficient $\mu = 0.08$, $R_{eff} = 120$ in. (based on $T = 3.5$ sec), $\mathrm{PGA_V} = 0.817$g, and $S_a(T_v)/\mathrm{PGA_V} = 1.98$. Calculations for each value of ν are shown in Table 5.1.

The actual base-shear coefficient for 3D shaking simulation from RHA was $V_{b,3D}/W = 0.36$. Thus, for this example, a lower amplification factor underestimates the amplification of the base shear, but including an amplification factor based on the vertical spectral response leads to a slightly conservative estimate of the base-shear amplification.

Table 5.1 Estimated base shear for SFPU motion in transverse direction by the simplified method.

v	$V_{b,V}/W$ [Equation (5.8)]	$V_{b,3D}/W$ [Equation (5.9)]	AE %	BSNE %
0.5	0.5(0.817)(10.33/120+0.08) = 0.068	0.135+0.068 = 0.203	-69.8	-43.8
1.0	1.0(0.817)(10.33/120+0.08) = 0.136	0.135+0.136 = 0.271	-39.7	-25.0
1.98	1.98(0.817)(10.33/120+0.08)= 0.269	0.135+0.269 = 0.404	19.4	11.8

Figures 5.1 and 5.2 present the simulated base-shear coefficients for 2D and 3D motions, along with base-shear coefficient for 3D motions estimated with different amplification factors in the transverse and longitudinal directions, respectively. In the transverse direction, the estimated base-shear values are conservative for almost all motions, except for two Group 1 motions. These motions have high vertical acceleration intensity, which for SFPU was shown to lead to uplift and subsequent pounding on the isolators (Figure 4.4) that greatly increased the realized vertical acceleration and subsequent base shear. In such cases, the proposed approximations underestimated the base-shear coefficient for 3D shaking. For many motions, $v = 0.5$ gives a very good estimate, while increasing the amplification factor leads to a more conservative estimate. In the longitudinal direction, the base shear is not as strongly affected by the vertical acceleration spikes, and the base-shear estimates are a little more conservative than in the transverse direction. Again, $v = 0.5$ is often adequate, and $v = 1$ is conservative for almost every ground motion in the longitudinal direction.

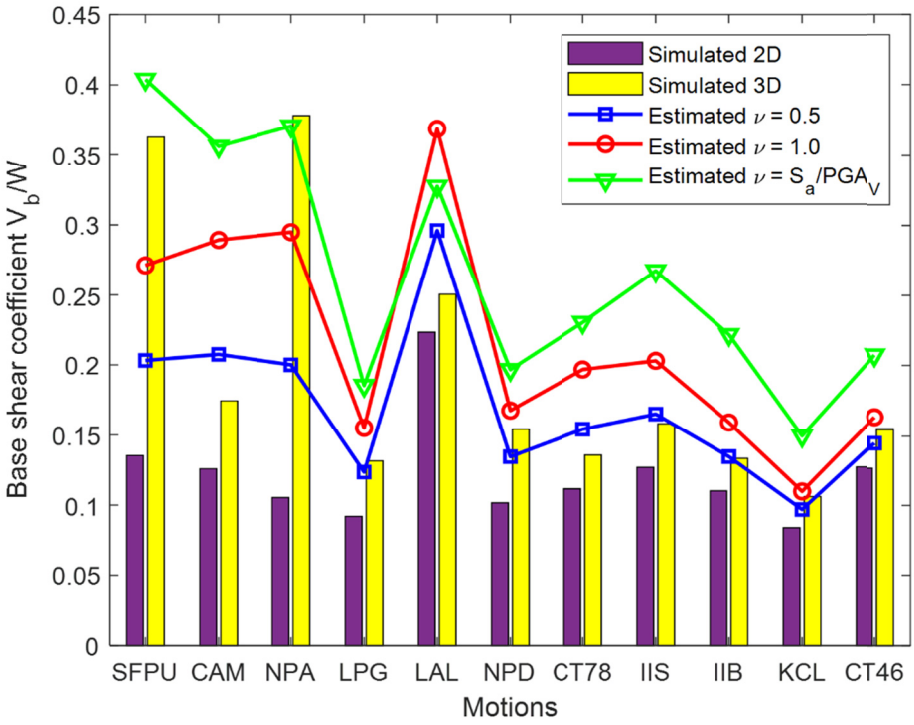

Figure 5.1 **Simulated and estimated base shear of the Base Model bridge in transverse direction for all motions.**

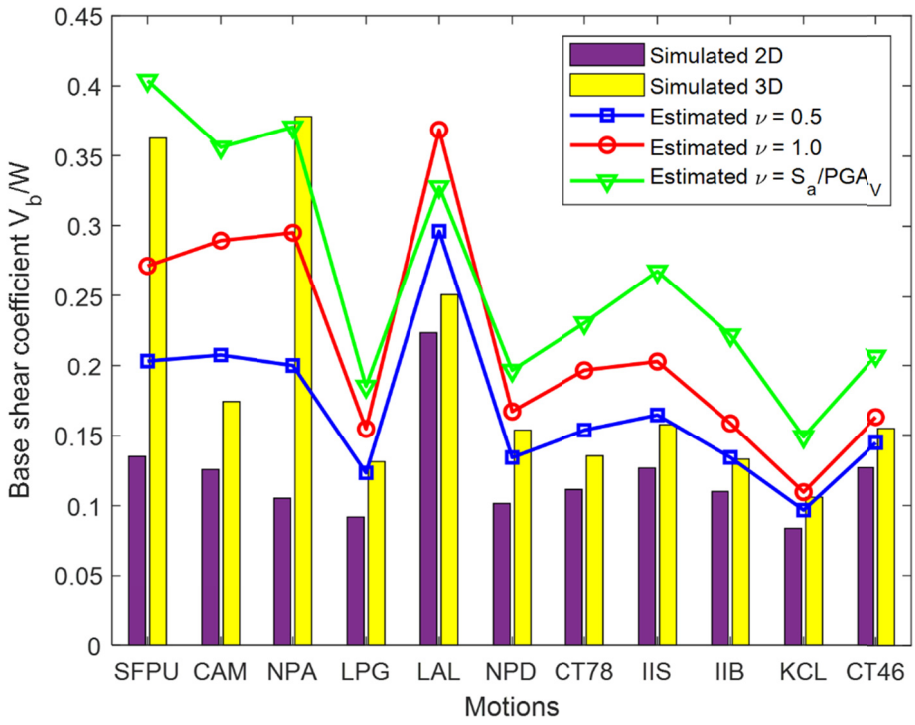

Figure 5.2 **Simulated and estimated base shear of the Base Model bridge in longitudinal direction for all motions.**

5.2 ERROR ESTIMATION

To evaluate the overall applicability of either proposed method to estimate the increase in base shear due to vertical shaking, a meaningful quantification of error is necessary. The methods presented in Section 5.1 attempted to estimate directly the increase or amplification in base shear for 3D shaking relative to 2D shaking. Therefore, a logical approach is to quantify directly the error in this estimated base-shear amplification relative to the actual base-shear amplification. Thus, an amplification error or *AE*, is proposed as:

$$AE = \left(\frac{\Delta_{\text{est}-\Delta}}{\Delta} \right) \times 100 \tag{5.10}$$

where $\Delta_{\text{est}} = V_{b,3D_{\text{est}}} / W - V_{b,2D} / W$ is the estimated base-shear amplification, and $\Delta = V_{b,3D_{\text{est}}} / W - V_{b,2D} / W$ is the actual (simulated) base-shear amplification.

Using the calculations for the Base Model bridge subjected to the SFPU motion in the transverse direction and assuming $v = 1$ (see Table 5.1), $V_{b,2D} / W = 0.133$, $V_{b,3D} / W = 0.36$, and $V_{b,3D_{\text{est}}} / W = 0.271$ by Equations (5.8) and (5.9). Substituting theses values into Equation (5.10), $\Delta_{\text{est}} = 0.271 - 0.135 - 0.135$, $\Delta = 0.36 - 0.135 = 0.225$, and $AE = -39.7\%$. The negative sign indicates that the base shear is underestimated. Values of *AE* for all three considered values of *v* for this example are tabulated in Table 5.1.

Figures 5.3 and 5.4 present *AE* for all motions in the transverse and longitudinal directions, respectively, for all three values of amplification factor *v*. The value of *AE* is generally positive for moderate- and low-intensity vertical motions except for *v* = 0.5 for some ground motions. The value of *AE* is most likely to be negative for high-intensity vertical motions as the amplification estimate is unconservative. Using an amplification factor *v* = 0.5 seems to produce an average *AE* closest to 0 (i.e., it minimizes the average error), but increases the likelihood that the estimate may be unconservative. All amplification estimates are conservative on average. Incorporating the spectral acceleration in the amplification factor increases the likelihood that the estimated base shear is very conservative.

Figure 5.4 illustrates instances of *AE* reaching more than 1000%, which would seem to imply that the proposed base-shear estimates are worthless; however, the *AE* measures the error only relative to the observed base-shear amplification, which may not give reasonable values when amplification of base shear due to vertical shaking is small. Evidence of this phenomenon is shown in Figure 5.2 for the LAL and IIS motions. The actual base-shear amplification from 2D to 3D motion [Δ in Equation (5.10)] is 0.0035 for the LAL motion and 0.005 for the IIS motion. Since the quantity to be estimated is near 0, the apparent *AE* is very large. This does not necessarily mean that the overall estimate of base-shear coefficient is unreasonable or unacceptable.

Another error estimation method is presented hereafter to avoid penalizing observations where the amplification in the base shear is low. The proposed base-shear normalized error or *BSNE*, directly quantifies the error in the total 3D estimated base-shear coefficient estimate relative to the base-shear coefficient determined from the simulations:

$$BSNE = \left(\frac{\frac{V_{b,3D_{\text{est}}}}{W} - \frac{V_{b,3D}}{W}}{\frac{V_{b,3D}}{W}} \right) \times 100 \tag{5.11}$$

where $V_{b,3D_{\text{est}}}/W$ and $V_{b,3D}/W$ are as defined earlier.

Using the values presented earlier for the SFPU ground motion in transverse direction ($V_{b,3D}/W$ = 0.36 and $V_{b,3Dest}/W$ = 0.271 when v = 1), *BSNE* = -25.0%. The *BSNEs* for all values of v are listed in Table 5.1. The signs and their interpretations (negative = underestimated, positive = overestimated) are consistent with *AE*, but the magnitude of the error has decreased relative to *AE* as *BSNE* represents an error in the full base-shear coefficient, rather than just the amplification term.

Figures 5.5 and 5.6 compare *BSNE* for the base-shear estimates in the transverse and longitudinal directions, respectively, for different values of the amplification factor v. The trends are similar as those observed for *AE*, except that the error magnitudes are smaller. The average *BSNE* is around 0 for v = 0.5, while the average increases (implying that the estimated base shear is more conservative) for v = 1.0 and for v computed by spectral acceleration. The potential for a large negative *BSNE* appears to exist only for the high-intensity motions and when v is taken to be 0.5. A sufficiently conservative estimate is achieved, on the other hand, by using v with the spectral acceleration amplification factor.

Based on results from both error estimation methods, *BSNE* is concluded to be a more meaningful error estimate than *AE*. Going forward, results from other parametric variations will be evaluated using *BSNE* alone. For moderate- to low-intensity vertical intense shaking, v = 0.5 generally gives an adequate estimate of the base shear. For high-intensity vertical motions, the v based on spectral amplification is, while more conservative, a better option to predict with base shear accurately. In the transverse direction, where coupling was observed between the transverse horizontal and vertical modes, the largest amplification factor can still underestimate the base shear for high-intensity vertical motions. Going forward, all amplification factors will be more comprehensively evaluated for a wider range of parameters.

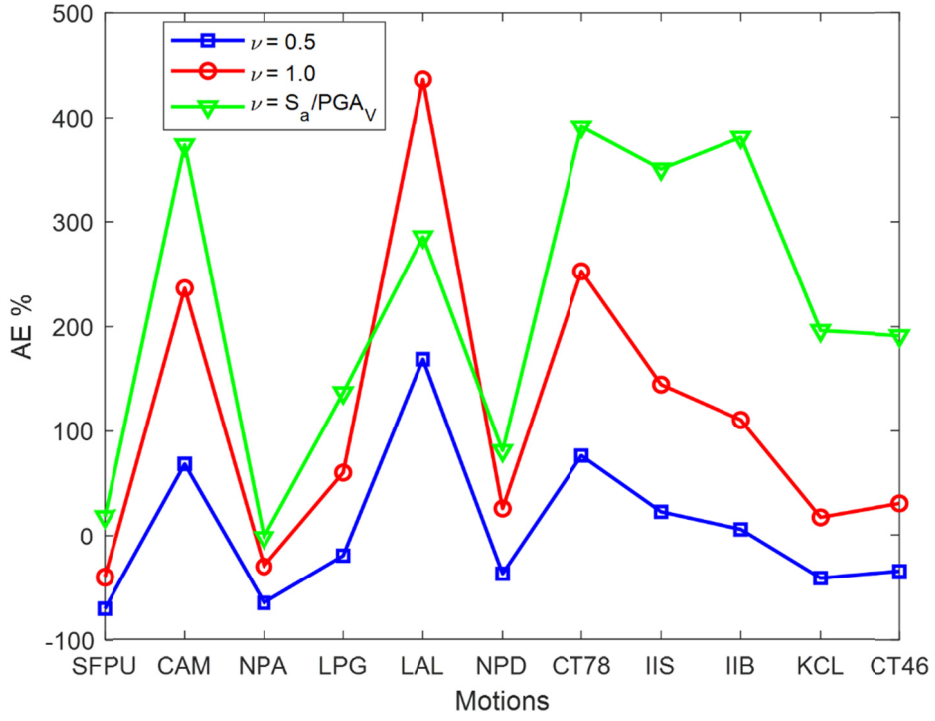

Figure 5.3 **The *AE* in the transverse direction for different amplification factors.**

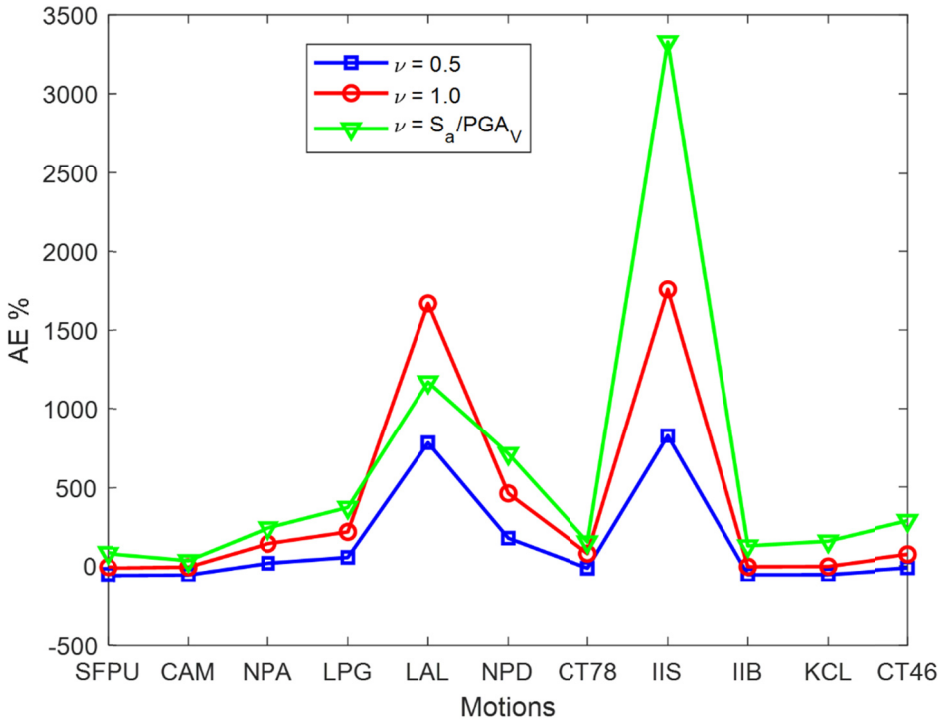

Figure 5.4 **The *AE* in the longitudinal direction for different amplification factors.**

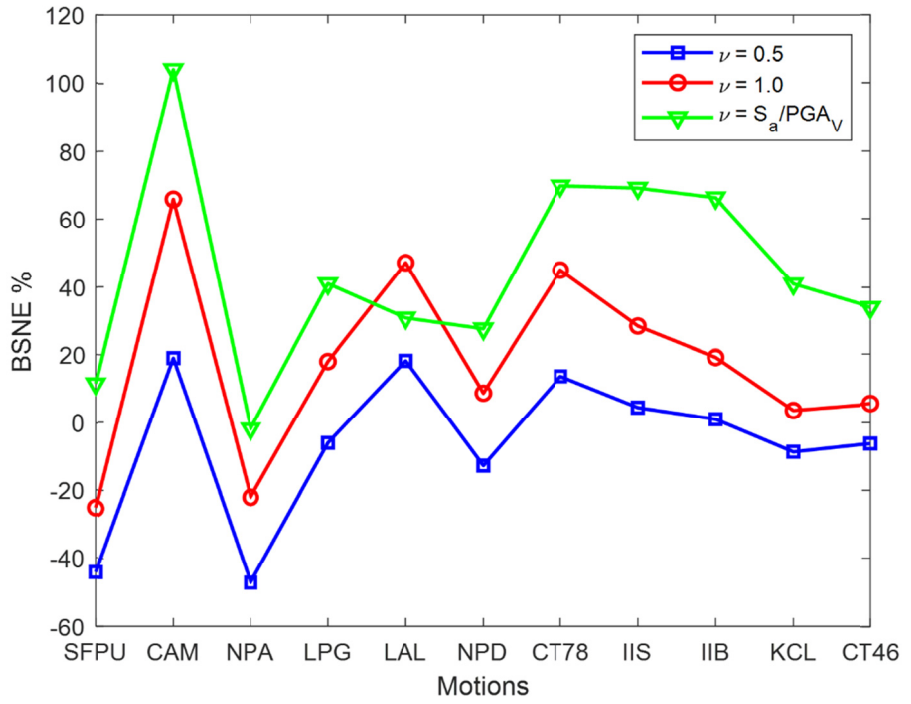

Figure 5.5 The ***BSNE*** **in the transverse direction for different amplification factors.**

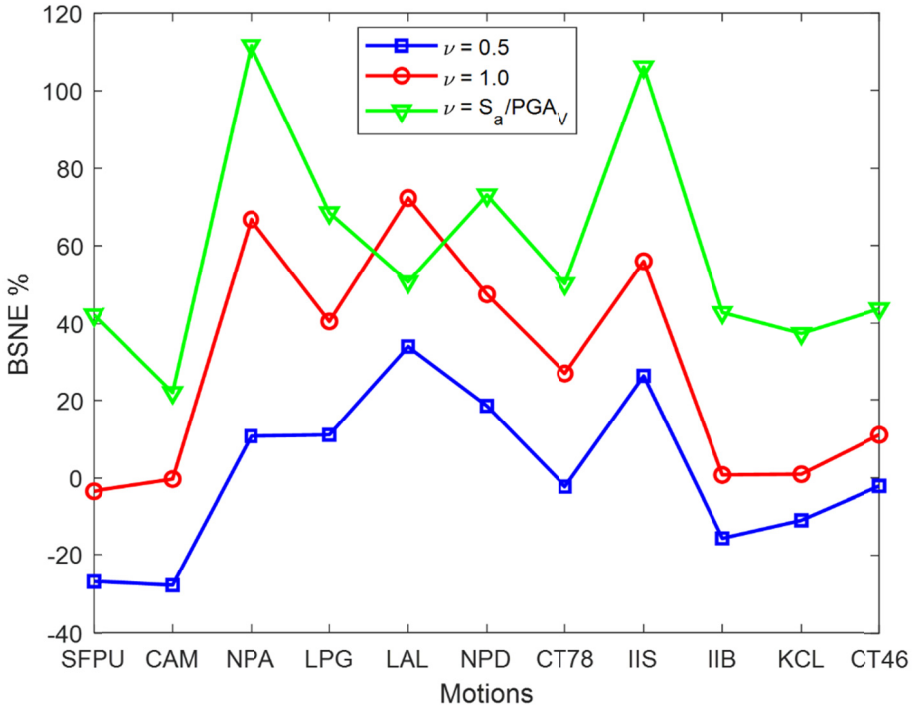

Figure 5.6 The ***BSNE*** **in the longitudinal direction for different amplification factors.**

6 Bridge Parameter Study

This chapter describes parametric variations implemented on the Base Model bridge to evaluate the validity and accuracy of the proposed simplified method to predict amplified base shear under 3D motions. Section 6.1 considers isolation parameter variations applied to the Base Model bridge. Section 6.2 considers bridge parameters varied relative to the Base Model bridge. In both sections, the base-shear coefficients from RHA simulations are compared with the estimated base-shear coefficients obtained from simplified theory; analysis of the errors is presented. The validity of the proposed simplified method is further evaluated.

6.1 INFLUENCE OF ISOLATION SYSTEM PARAMETERS

The Base Model bridge was modified to create nine different models by changing only the isolation properties (friction coefficients and pendulum lengths that determine the period associated with each portion of the normalized backbone curve); all other parameters remained the same. The objective was to evaluate the accuracy of the proposed base-shear estimation methods and amplification factors across a range of isolation periods and friction coefficients. The isolation parameter variations listed in Table 3.3 were applied. Recall that μ_2 is the friction coefficient and T_2 is the period associated with the second slope of the normalized backbone curve (or sliding on the outer pendulum surfaces). All combinations of $\mu_2 = 0.04$, 0.06, and 0.08, and $T_2 = 2$, 3.5, and 5 sec were considered. For each case, $T_1 = T_2/4$ and $\mu_1 = \mu_2/4$.

Simulated and estimated base-shear coefficients under 2D and 3D input to the SFPU motion (Group 1), LPG motion (Group 2), and IIB motion (Group 3) are shown in Figure 6.1 for all isolation system parameter variations. The general trend in base-shear coefficient for each motion and longitudinal or transverse direction is easily explained. The isolation period T_2 = 2 sec for System Nos. 1–3, 3.5 sec for System Nos. 4–6, and 5 sec for System Nos. 7–9. Therefore, the actual base-shear coefficient decreases for each subgroup as the period increases. The base-shear coefficient also increases slightly over each subgroup as the friction coefficient increases (e.g., μ_2 increases from 0.04 to 0.08 over System Nos. 1–3). The general trend observed in the figure is that the amplification of base shear (the increase from 2D to 3D) tends to be proportional to the intensity of the base shear. Therefore, the shorter period systems with higher base-shear coefficients also see greater amplification of base shear. For the high-intensity motion

SFPU, amplification of the base-shear coefficient from 2D to 3D is significant for all isolation system parameters; see Figure 6.1(a)-(b). For the moderate- and low-intensity motions (LPG and IIB), the base-shear amplification is noticeable for the short-period $T_2 = 2$ sec Systems 1–3, but is relatively small for other periods; see Figure 6.1(c)-(f).

A key observation is that the base-shear coefficient estimates follow the trends observed in the simulated base-shear coefficients. In other words, these estimated base-shear coefficients vary with T_2 and μ_2 in a manner consistent with the simulated base-shear coefficients shown in Figure 6.1. Recall that the dependence of base-shear amplification on these isolation system parameters is inherently captured through Equation (5.8). Increasing the amplification factor offers an increasing level of conservatism in the estimate.

For each pair of isolation parameters, the base-shear amplification and *BSNE* were evaluated for all motions, In addition, the average *BSNE* over the 11 motions was evaluated. Figure 6.2 compares average *BSNE* estimated for all amplification factors v in the longitudinal direction [Figure 6.2(a)] and transverse direction [Figure 6.2(b)]. In general, the average *BSNE* is approximately constant with respect to isolation parameter variations, which confirms the observation that the base-shear estimates follow the trends shown in the simulations. In the longitudinal direction, the average *BSNE* increases slightly over the subgroups, which is correlated to increasing conservatism in the base-shear amplification estimate as the friction coefficient increases. The reason why is unclear, but the effect is slight, and the same trend is not apparent in the longitudinal direction.

The average *BSNE* provides insight as to which amplification factor might be most appropriate. For $v = 0.5$, the average *BSNE* oscillates near 0 but tends to be slightly negative. The range of the average *BSNE* is -5% to 2% in the longitudinal direction and -9% to -3% in the longitudinal direction. Thus, although the average *BSNE* is small, this lower amplification factor is likely to underestimate the base-shear coefficient, and a more conservative estimate may be preferred. The average *BSNE* for $v = 1.0$ varies from 20% to 30% in the longitudinal direction and 14% to 21% in the transverse direction. This appears to be a good choice for the amplification factor leading to sufficiently conservative, but not overly conservative estimates. Applying the vertical spectral acceleration to the amplification factor further increases conservatism so that average *BSNE* is in the 40% to 60% range. Thus, consistent with observations noted in Chapter 5, using the spectral acceleration of the vertical motion to represent the dynamic amplification effect does not appear to be necessary.

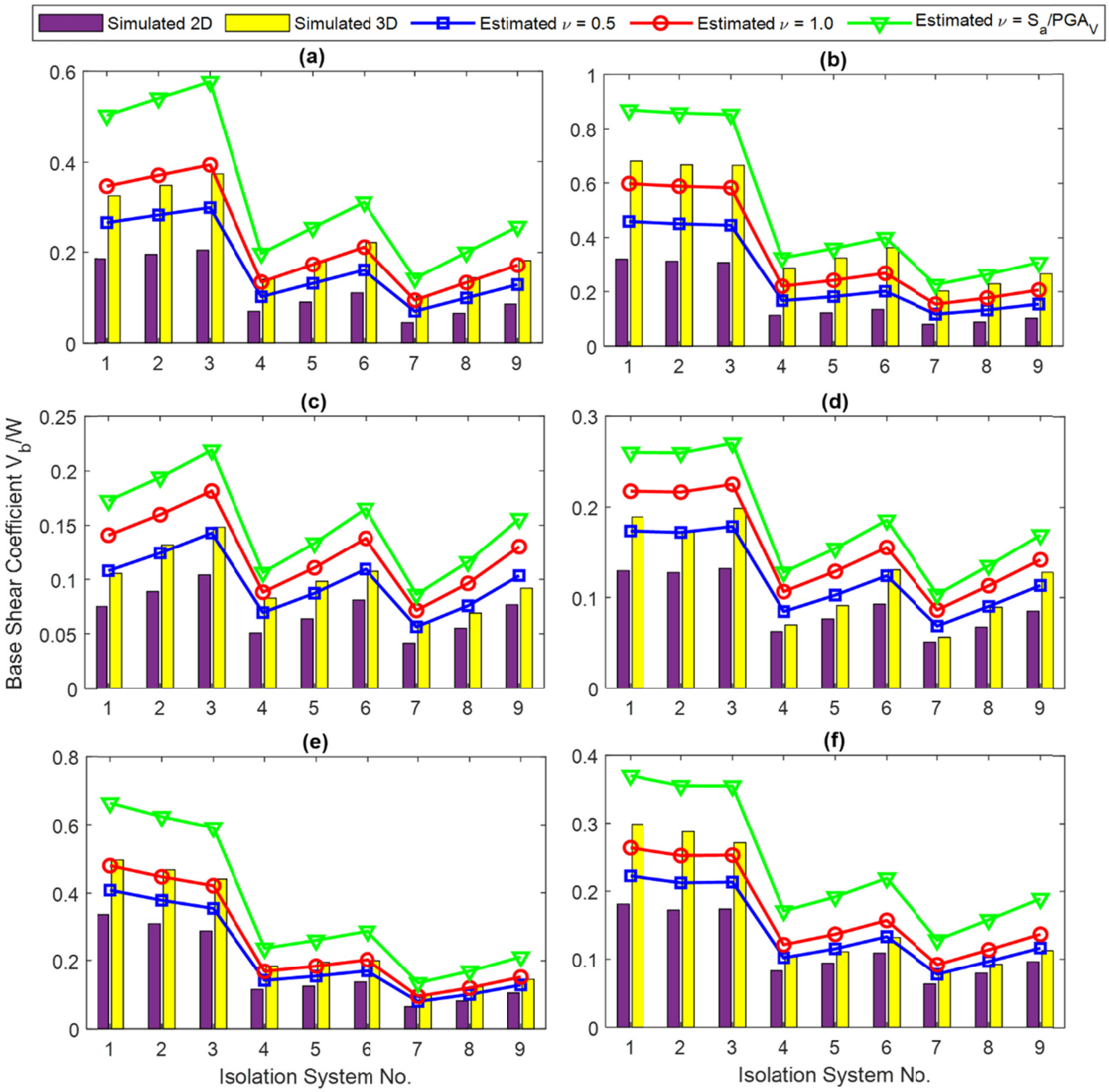

Figure 6.1 **Simulated and estimated base shear of the Base Model bridge with isolation parameter variations: SFPU motion (a) longitudinal, (b) transverse; LPG motion (c) longitudinal, (d) transverse; IIB motion (e) longitudinal, and (f) transverse.**

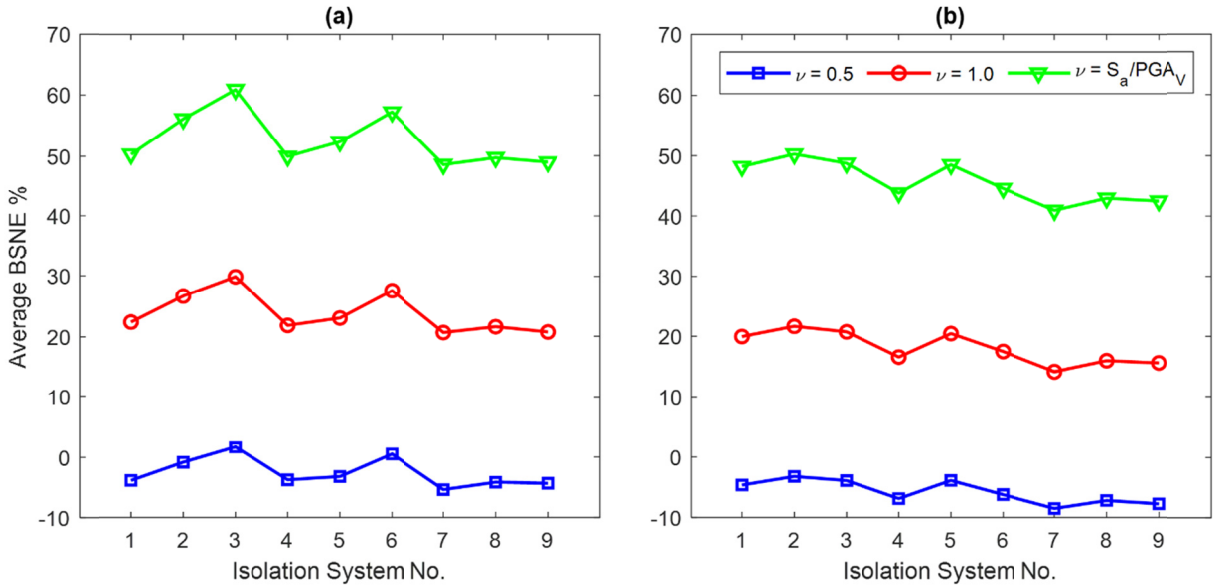

Figure 6.2 **Average *BSNE* for all isolation system parameter variations on Base Model bridge: (a) longitudinal direction and (b) transverse direction.**

Figure 6.3 presents the same average *BSNE* as shown in Figure 6.2, but superimposed over scatter plots that depict *BSNE* for individual ground motions. The various amplification factors are represented in the different subfigures; v = 0.5 in Figure 6.3(a) and (b), v = 1.0 in Figure 6.3(c) and (d), and $v = S_a(T_v)/\text{PGA}_\text{V}$ in Figure 6.3(e) and (f). The average *BSNE* is depicted as a thick line with circle marker, while *BSNE* for individual ground motions are depicted by *.

The data in Figure 6.3 highlight the significant dispersion in the accuracy of the base-shear coefficient over the ground-motion suite. This suggests that for individual ground motions, the simplified method cannot estimate the base-shear amplification with high confidence. If the amplification factor is selected as v = 0.5, even though average *BSNE* is near 0, there is a possibility that base shear is underestimated by as much as 20 to 40%. Although choosing v = 1.0 significantly reduces the possibility that the base-shear estimate is grossly unconservative, it cannot eliminate the possibility of a negative error. Finally, applying the amplification factor $v = S_a(T_v)/\text{PGA}_\text{V}$ can almost eliminate the possibility of a negative error for individual motions, but as mentioned before, it is quite conservative on average.

In summary, the amplification factor v = 1.0 appears to lend itself to the most appropriately conservative base-shear estimates that account for the amplification from 2D to 3D shaking. Recalling the effect of ground-motion intensity (Figures 5.1 and 5.2), the motions that appear as negative outliers in Figure 6.3 are likely associated with high-intensity motions, suggesting a limit on the applicability of the simplified method to estimate base-shear amplification.

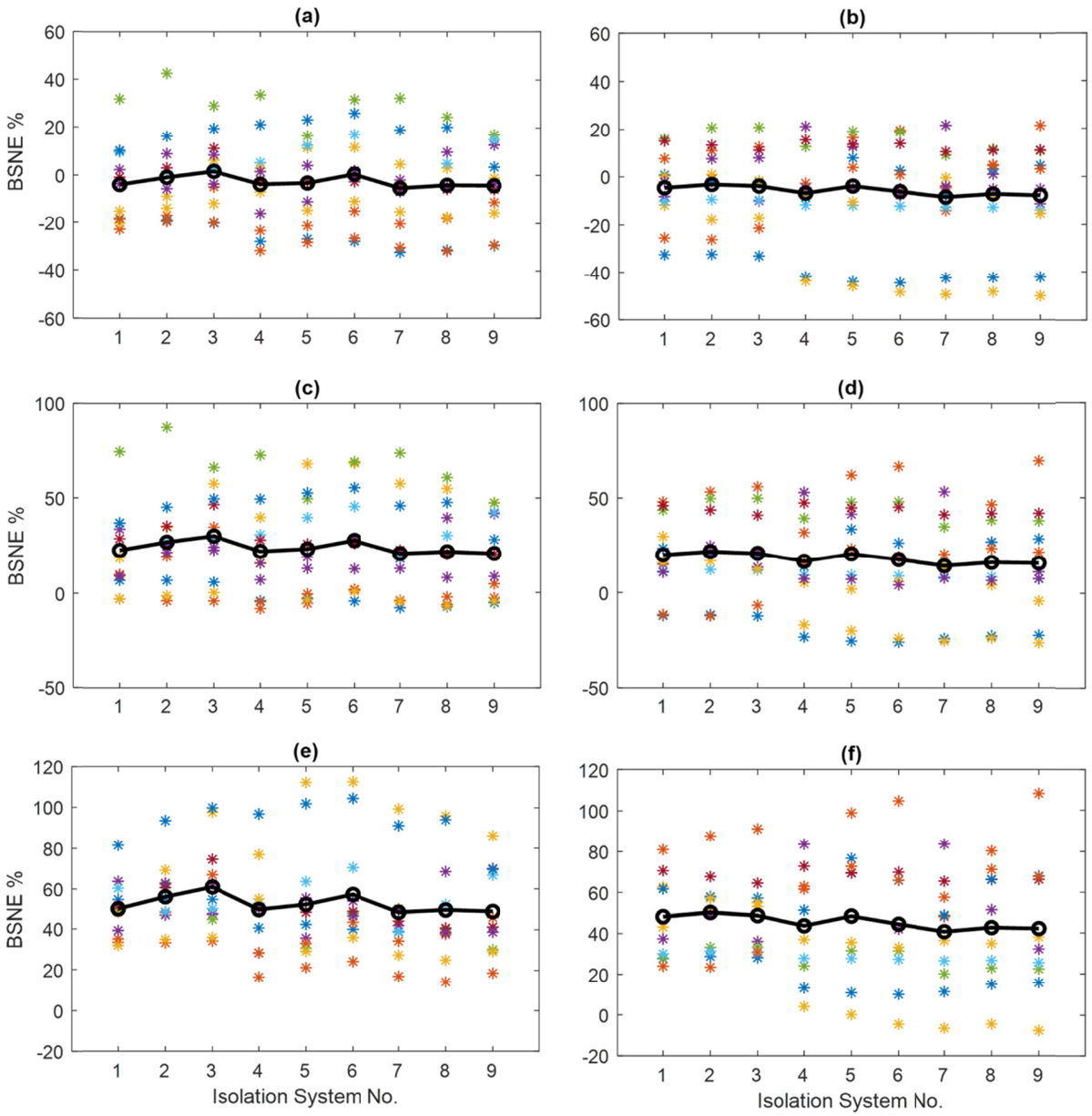

Figure 6.3 **Average *BSNE* and *BSNE* for individual motions for all isolation system parameter variations on Base Model bridge: ν = 0.5 (a) longitudinal, (b) transverse; ν = 1.0 (c) longitudinal; (d) transverse, $\nu = S_a(T_V)/PGA_V$ (e) longitudinal, and (f) transverse.**

6.2 INFLUENCE OF BRIDGE PARAMETERS

A bridge parameter study was performed to validate the accuracy of the proposed simplified methods to estimate base shear over a wide range of bridge parameters compared to the response of the Base Model bridge. The bridge parameter variations were presented in Table 3.2. Modal analysis was performed for all the various bridge models, and the first ten modes and associated

periods for each bridge are tabulated below in Table 6.1. Again, for all bridge models, the isolator model was changed to a linear spring for modal analysis, corresponding to an isolation period of 3 sec.

Figure 6.4 plots some common mode shapes of the bridge models. The first three modes in all bridge models are the isolation modes: the first mode is the longitudinal isolation mode, the second mode is the transverse isolation mode, and the third mode is the torsional isolation mode. These first two modes in all bridges have periods greater than 3 sec, and the third mode has a period a bit less than 3 sec. All bridge models have a vertical C-shape mode with all span movement in the same direction, which tends to lead to very high mass participation of that mode in the vertical direction. Most bridges have more than one vertical S-shape mode wherein individual spans move in different directions. A transverse C-shape mode causes in-plane bending of the deck in one direction. A deck torsional mode is characterized by rotation of the deck in two different directions from each end such that deck is in torsion. In contrast, a deck rotational mode represents rotation of the deck in one direction.

The vertical mode with the 2C/3C/4C shape tends to be dominant and always shows up in the deck spectra, even if its period is higher than other modes. In this mode, the mass participation in vertical direction tends to be high—around 80%. Bridges 4, 5, and 8 have similar dynamic and modal properties as the Base Model (Bridge 1), and only the periods vary slightly according to the flexibility of each bridge. The close spacing of the vertical C-shape mode and transverse C-shape mode identified in the Base Model bridge (Figures 4.21 and 4.22) that led to modal coupling is also present in Bridges 4, 5, 7, and 8. Thus, transverse–vertical coupling would also be expected in Bridge 4, 5, 7, and 8. Bridges 2, 3, and 6 would not be expected to exhibit this coupling. In fact, for Bridge 6 the transverse mode does not appear in the first ten modes because the deck is very stiff in the transverse direction. In Bridge 3, the transverse mode and the vertical C-shape mode are not near each other, while in Bridge 2 the transverse mode and vertical C-shape modes are adjacent but the periods are far from each other.

Table 6.1 Modes and periods of bridge models.

Mode#	Bridge 1 (Base model)	Bridge 2	Bridge 3	Bridge 4	Bridge 5	Bridge 6	Bridge 7	Bridge 8
1	ISO Long. mode (3.02 sec)	ISO Long. mode (3.06 sec)	ISO Long. mode (3.01 sec)	ISO Long. mode (3.02 sec)	ISO Long. mode (3.03 sec)	ISO Long. mode (3.03 sec)	ISO Long. mode (3.02 sec)	ISO Long. mode (3.01 sec)
2	ISO Trans. mode (3.01 sec)	ISO Trans. mode (3.04 sec)	ISO Trans. mode (3.0 sec)	ISO Trans. mode (3.01 sec)	ISO Trans. mode (3.01 sec)	ISO Trans. mode (3.01 sec)	ISO Trans. mode (3.01 sec)	ISO Trans. mode (3.0 sec)
3	ISO torsional mode (2.69 sec)	ISO torsional mode (2.82 sec)	ISO torsional mode (2.43 sec)	ISO torsional mode (2.69 sec)	ISO torsional mode (2.7 sec)	ISO torsional mode (2.61 sec)	ISO torsional mode (2.69 sec)	ISO torsional mode (2.69 sec)
4	1st vertical mode (0.35 sec)	Deck transverse mode – *C shape* (0.39 sec)	1st vertical mode – *S shape* (0.43 sec)	1st vertical mode (0.44 sec)	1st vertical mode (0.64 sec)	1st vertical mode (0.35 sec)	1st vertical mode (0.35 sec)	1st Vertical mode (0.35 sec)
5	2nd vertical mode (0.25 sec)	1st vertical mode (0.38 sec)	2nd vertical mode – *2C shape* (0.28 sec)	2nd vertical mode (0.29 sec)	2nd vertical mode (0.44 sec)	Deck Rotational mode (0.25 sec)	Deck transverse mode – *C shape* (0.25 sec)	2nd vertical mode (0.24 sec)
6	Deck transverse mode – *C shape* (0.20 sec)	2nd vertical mode (0.29 sec)	Deck rotational mode (0.13 sec)	Deck transverse mode – *C shape* (0.25 sec)	3rd vertical mode – *3C shape* (0.35 sec)	2nd vertical mode (0.24 sec)	2nd vertical mode (0.24 sec)	Deck transverse mode – *C shape* (0.20 sec)
7	3rd vertical mode – *3C shape* (0.20 sec)	3rd vertical mode (0.22 sec)	Deck torsional mode (0.12 sec)	3rd vertical mode – *3C shape* (0.24 sec)	Deck transverse mode – *C shape* (0.35 sec)	Deck torsional (0.21 sec)	3rd vertical mode – *3C shape* (0.24 sec)	3rd vertical mode – *3C shape* (0.19 sec)
8	Deck Rotational mode (0.14 sec)	4th vertical mode – *4C shape* (0.19 sec)	Deck transverse mode – *C shape* (0.11 sec)	Deck Rotational mode (0.15 sec)	4th vertical mode (0.17 sec)	Deck Rotational mode (0.21 sec)	Deck Rotational mode (0.18 sec)	Deck Rotational mode (0.13 sec)
9	Deck torsional mode (0.11 sec)	2nd Deck transverse mode (0.14 sec)	3rd vertical mode (0.11 sec)	Deck torsional mode (0.12 sec)	Deck Rotational mode (0.15 sec)	3rd vertical mode – *3C shape* (0.19 sec)	Deck torsional mode (0.11 sec)	Deck torsional mode (0.11 sec)
10	Deck Rotational mode (0.11 sec)	Deck Rotational mode (0.13 sec)	4th vertical mode (0.09 sec)	Deck Rotation-al mode (0.12 sec)	2nd deck transverse mode (0.12 sec)	Deck torsional mode (0.12 sec)	4th vertical mode (0.09 sec)	Deck Rotational mode (0.11 sec)

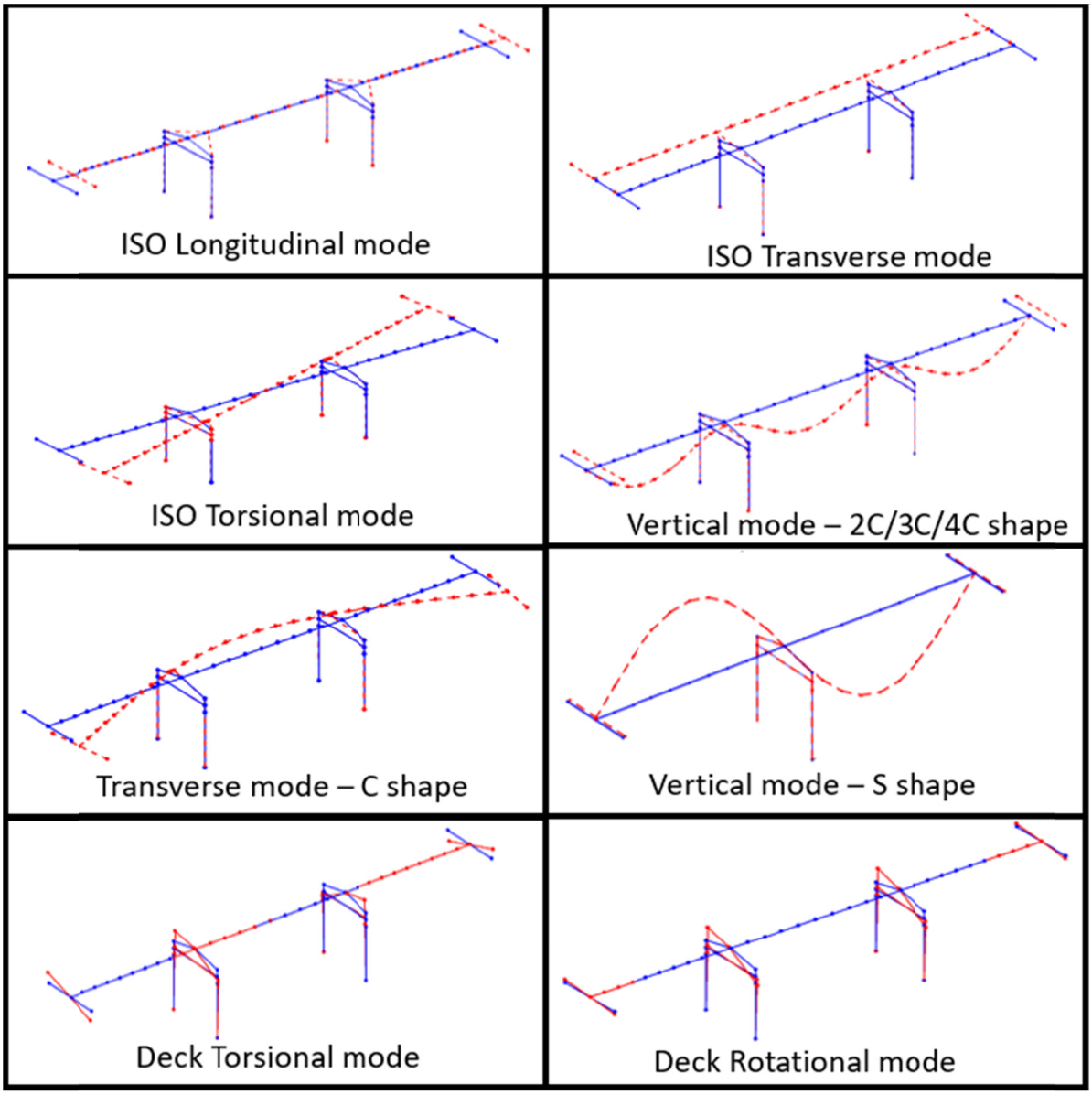

Figure 6.4 Common mode shapes identified.

Figure 6.5 compares simulated and estimated base-shear coefficients under 2D and 3D input for the different bridge model parameter variations for the representative motions SFPU (Group1), LPG (Group 2), and IIB (Group 3) for all bridge models. "BaseM" refers to the Base Model, while Bridge Nos. 2–8 represent the individual parameter variations referred to in Table 3.2. The estimated base-shear coefficients are shown for all three different amplification factors.

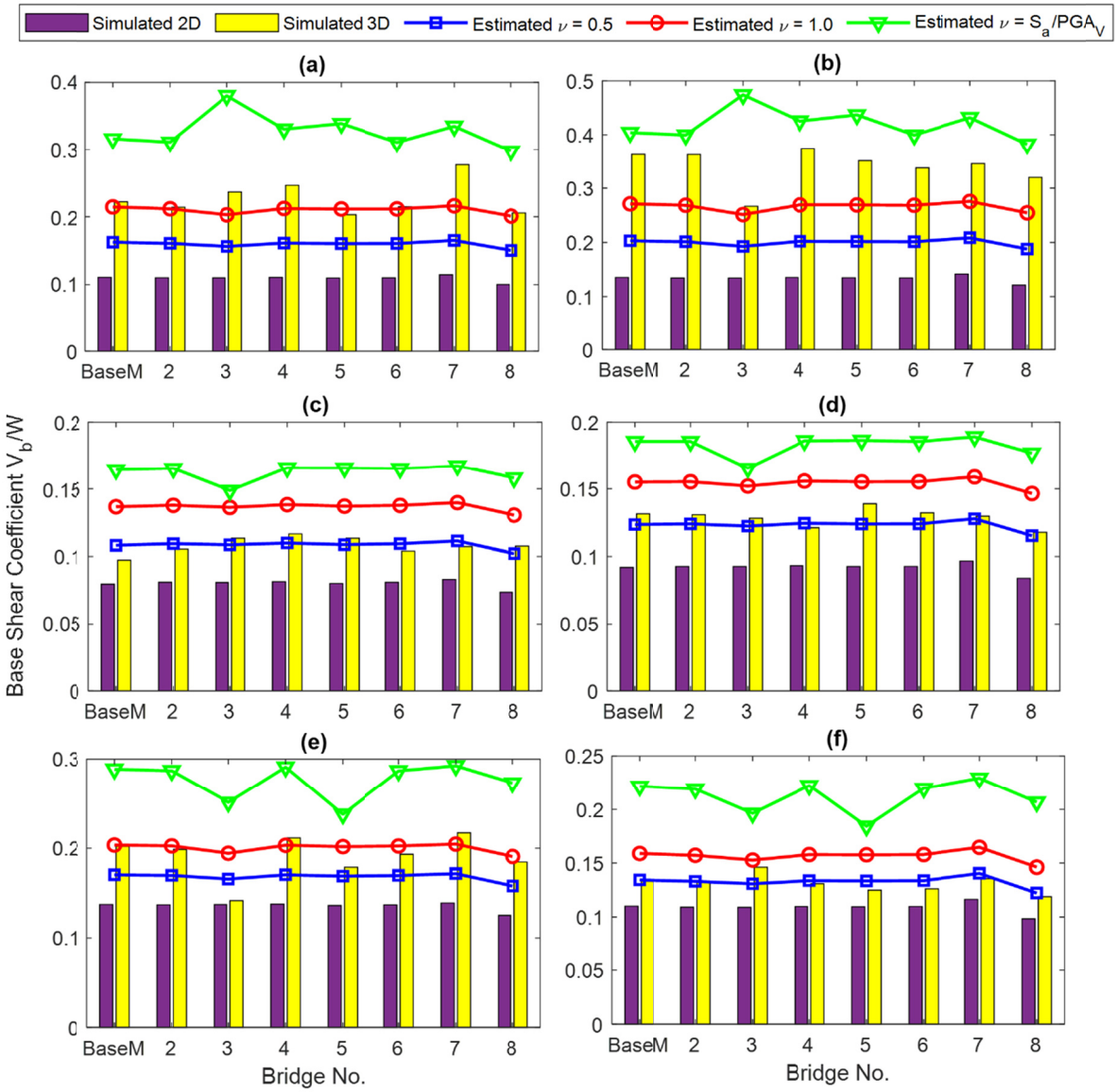

Figure 6.5 **Simulated and estimated base shear for all bridge models: SFPU motion (a) longitudinal, (b) transverse; LPG motion (c) longitudinal, (d) transverse; IIB motion (e) longitudinal, and (f) transverse.**

A key observation is that differences in base-shear amplification on bridge models incorporating various bridge parameter variations—see Table 3.2—are very minor. Because the bridges are seismically isolated, the deck (regardless of its properties) moves essentially as a rigid mass on the sliding bearings. The differences in the estimated base-shear amplifications among the bridge parameter variations are also minor. Hence, the accuracy of the simplified method does not vary much among the bridge models. In particular, amplification factors $v = 0.5$ and $v = 1.0$ predict the same base-shear amplification for all bridge models as the amplification (Equation 5.8) is independent of bridge superstructure or substructure parameters. For v =

$S_a(T_v)/\text{PGA}_V$, the estimated base-shear amplification differs for different bridge models only due to changes in the period of the dominant vertical mode.

Under the Group 1 motion SFPU, the base-shear amplification is high for all bridge models in both longitudinal and transverse directions [Figure 6.5(a) and (b)]. Of the three motions considered, SFPU produces the greatest variation in base-shear amplification for different models. Increased randomness in the response is expected as the vertical shaking intensity increases, as well as a susceptibility to uplift and the impact of dynamic effects. Note: there is no correlation between base-shear amplification and the bridge models that were expected to be most susceptible to transverse–vertical coupling (Bridges 4, 5, 7, and 8). Only the spectral acceleration amplification factor, $v = S_a(T_v)/\text{PGA}_V$, provides a conservative estimate of the base-shear amplification for this motion. Differences in spectral amplification due to vertical period shifts that affect the estimated base-shear coefficients are not consistent with simulated response.

The base-shear coefficient and its amplification due to vertical shaking is least sensitive to bridge modeling parameters for the Group 2 moderate-intensity motion LGP [Figure 6.5(c) and (d)]. The amplification factor $v = 0.5$ is quite accurate for this motion. For the Group 3 low-intensity motion IIB, the simulated base-shear coefficient again shows some variation over bridge models (e.g., almost no amplification is observed for Bridge 3—a two-span bridge—in the longitudinal direction, while all other bridge models experience some amplification.) This result is a consequence of phase variation in the vertical and longitudinal response. Although it does not capture any variations in amplification over the bridge models, the amplification factor $v = 1.0$ leads to accurate estimates for this motion.

The base-shear amplification and *BSNE* for each bridge model were evaluated for all motions. In addition, the average *BSNE* over the 11 motions was evaluated. Figure 6.6 compares the average *BSNE* estimated for all amplification factors v in the longitudinal direction [Figure 6.6(a)] and transverse direction [Figure 6.6(b)]. The error trends with respect to bridge model variation are very similar to those found for isolation system parameter variation. That is, for each amplification factor, the *BSNE* is approximately constant—or varies within a narrow range—with the bridge parameter variation. The average *BSNE* is a little higher in the longitudinal direction (meaning the estimated base shear is more conservative) than in the transverse direction, which is likely due to the complexities associated with transverse–vertical coupling as mentioned previously. The average *BSNE* ranges are: -5% to 2% in the longitudinal direction and -7% to 1% in the transverse direction for $v = 0.5$; 21% to 30% in the longitudinal direction and 15% to 27% in the transverse direction for $v = 1.0$; and 40% to 61% in the longitudinal direction and 40% to 52% in the transverse direction for $v = S_a(T_v)/\text{PGA}_V$.

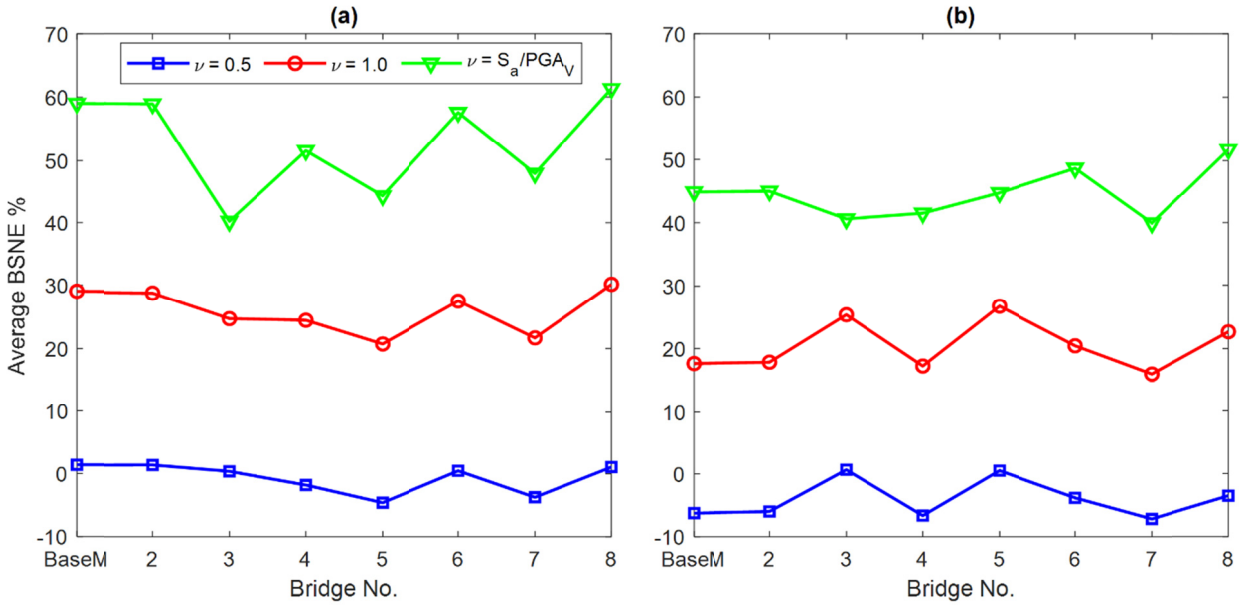

Figure 6.6 **Average *BSNE* for all bridge models: (a) longitudinal direction and (b) transverse direction.**

Figure 6.7 superimposes the average *BSNE* on scatter plots of *BSNE* for individual ground motions to show the dispersion in the error estimates. Subfigures represent the various amplification factors in the longitudinal and transverse directions: $v = 0.5$ [Figure 6.7(a) and (b)], $v = 1.0$ [Figure 6.7(c) and (d)], and $v = Sa(T_v)/\text{PGA}_\text{V}$ [Figure 6.7(e) and (f)]. The average *BSNE* is depicted as a thick line with circle marker, while *BSNE* for individual ground motions are depicted by *. Again, significant dispersion in the accuracy of the base-shear coefficient over the ground-motion suite is observed, meaning that the simplified method cannot estimate the base-shear amplification for individual motions with high confidence. The average *BSNE* is closest to 0; thus the estimate is the most accurate on average when the amplification factor v is taken to be 0.5. However, at this time the amplification factor $v = 0.5$ is not recommended for application because it lacks sufficient conservatism.

In summary, for the different isolation parameter variations and bridge model variations studied, the proposed method to estimate base shear for 3D shaking captures well the observed trends in base-shear coefficient. The three different amplification factors considered led to increasingly conservative estimates. While an amplification factor $v = 0.5$ leads to the lowest average *BSNE*, it raises the possibility of significantly under-predicting the base-shear coefficient for individual ground motions. The amplification factor $v = 1.0$ is recommended for predictions that are sufficient but not overly conservative. Statistical analysis over many ground motions and model variations is advisable to determine a "best fit" value of the amplification factor. Because of the complexities associated with high-intensity PGA_V, determination of a threshold PGA_V is envisioned above which the simplified method cannot reliably be applied, and 3D RHA

procedures are recommended. Implementation of a PGA_V limit may improve the reliability of the estimation method in the applicable range of ground-motion intensity.

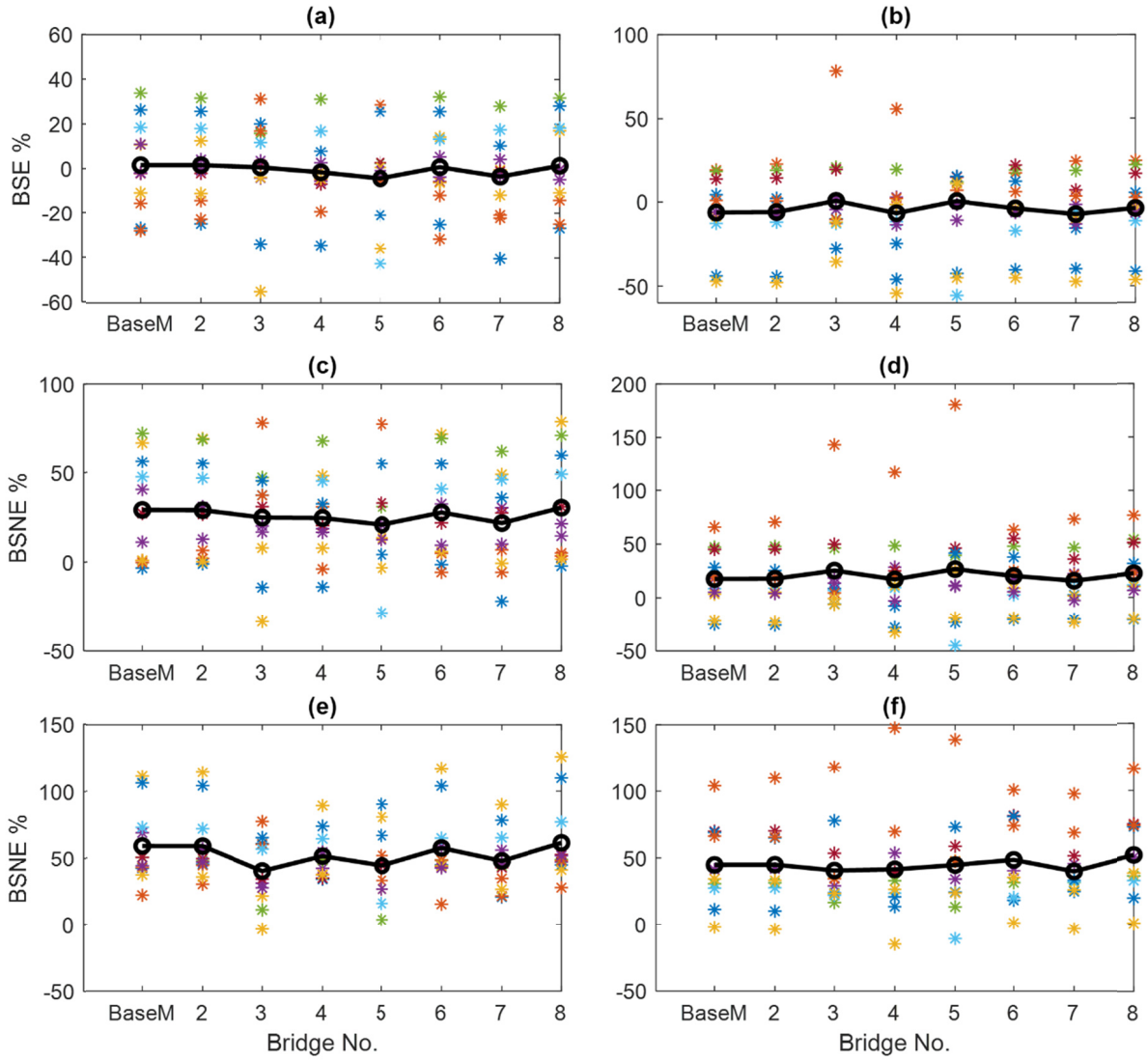

Figure 6.7 **Average *BSNE* and *BSNE* for individual motions for all bridge models: ν = 0.5 (a) longitudinal, (b) transverse; ν = 1.0 (c) longitudinal; (d) transverse, $\nu = S_a(T)/PGA_V$; (e) longitudinal; and (f) transverse.**

7 Summary and Conclusions

In this study, a series of ground motions with a wide range of vertical shaking intensity were applied to three-dimensional models of bridges isolated with triple pendulum bearings (TPBs) that both excluded the vertical component (2D shaking) and included the vertical component (3D motion). Bridge response under 2D and 3D shaking was then compared to investigate the direct effect of vertical shaking. The objective of this work was to evaluate the amplification of base shear under 3D motion, and to develop a simplified method to predict base-shear amplification.

An existing ground-motion suite was selected that had been fitted to a target horizontal spectrum, and vertical components were scaled individually to fit a target vertical spectrum that corresponded to the target horizontal spectrum. The target vertical spectrum was created based on NEHRP recommended seismic provisions [FEMA 2009b]. Ground motions were divided into three groups based on peak vertical ground acceleration (PGA_V). The PGA_V intensity ranges were: Group 1 = 0.8g and above (High Intensity), Group 2 = 0.5g to 0.7g (Moderate Intensity), and Group 3 = 0.2g to 0.4g (Low Intensity).

Multi-span concrete box girder bridges were selected for this study as they are a prominent bridge type in California and are suitable for seismic isolation. A three-span, 45-ft wide, multi-column bent bridge was established as the Base Model bridge. The isolation system friction coefficients were $\mu_1 = 0.02$ and $\mu_2 = 0.08$, and isolation periods were $T_1 = 1$ sec and $T_2 = 3.5$ sec for sliding on first and second slope of the backbone curve, respectively. A bridge parameter variation was implemented to evaluate the effect of various parameter variations on the amplification of base shear. Also, isolation system parameter variations were applied to the Base Model bridge. The Base Model bridge and all variations were modeled in OpenSees using the spine-modeling approach, and TPBs were modeled using the *TripleFrictionPendulum* element.

Response histories were compared for a representative motion from each ground-motion group under 2D and 3D shaking. Peak responses were compared under 2D and 3D shaking for all motions. Modal and spectral analyses were also conducted to understand dynamic properties and behavior of the bridges under vertical motion. Deck acceleration spectral response at different locations revealed that higher modes were excited.

A simplified theory was also proposed, leading to a method to predict the amplified base-shear coefficient for 3D shaking from the base-shear coefficient for 2D shaking. Thus, the method is applicable for bridge design based on equivalent static analysis. The theory predicts that the amplification of base shear is proportional to $(u_o/R_{eff} + \mu)$, where u_o is peak isolator displacement, R_{eff} is the radius and μ the friction coefficient of the effective pendulum mechanism, as well as PGA_V, thus accounting for any variation of isolation system parameters in the estimate. Three different amplification factors, v, were considered: $v = 0.5$, $v = 1.0$, and $v = S_a(T_v)/PGA_V$. The last, $v = S_a(T_v)/PGA_V$, can be interpreted as the effective or realized vertical acceleration at the isolators and is the spectral acceleration at the period of the dominant vertical mode.

The proposed method with different amplification factors was evaluated using two different error estimates: the amplification error or *AE*, and the base-shear normalized error or *BSNE*. The simplified method with a different amplification factor was assessed over a range of isolation parameters and bridge parameter variations. Key conclusions from this work are as follows.

1. Response history analysis over the suite of motions demonstrated that the horizontal response of the bridge was amplified when vertical motion was included. The transverse-direction base shear in the Base Model bridge was amplified by factors ranging from 1.39 to 3.59 for the Group 1 motions, 1.12 to 1.52 for the Group 2 motions, and 1.21 to 1.26 in Group 3 motions. The longitudinal-direction base shear in the Base Model bridge was amplified by factors ranging from 1.83 to 2.23 for the Group 1 motions, 1.03 to 1.46 for the Group 2 motions, and 1.18 to 1.47 for Group 3 motions. These amplification factors imply that exclusion of the vertical component of shaking could lead to underestimation of demand shear forces on bridge piers. Base shear was amplified more in the transverse direction than in longitudinal direction, which is believed to be due, in part, to excited horizontal–vertical coupled modes.
2. A transverse–vertical modal coupling was observed in the Base Model bridge by examining spectral responses at various locations on the bridge. Mode 7, the vertical mode with the highest mass participation, was excited under 3D shaking. The vertical motion introduced a high-frequency axial force variation to the isolators, which was transferred to the isolator horizontal forces since the horizontal friction force is proportional to the axial force. It was determined that high-frequency oscillation affected the base shear at a period of around 0.2 sec, which is the period of the second transverse mode and, consequently, excited the second transverse mode under 3D motion only. This type of coupling has been observed in multi-story buildings, and the analysis here shows that such coupling is also possible in bridges.
3. Modal analysis of the various bridge models in the parameter study showed that all bridges have a 2C/3C/4C-shape vertical mode with high modal-mass participation that is expected to be the dominant vertical mode. In many of the bridge models, the vertical

mode was closely spaced to a second transverse mode. Spectral responses were not examined in detail for these bridges, but modal coupling is expected for those models with closely spaced coupled horizontal–vertical modes. This type of transverse–vertical modal coupling should be evaluated on a case-by-case basis for bridges with the potential for being subjected to high-intensity vertical ground shaking. Because the effects of such coupling were not evident from analysis of the base-shear coefficient alone, the greatest impact of the coupling is expected to be amplification of mid-span accelerations, which may not be that significant for bridges.

4. Regarding error estimates, the *AE* was found to be unreasonably large when amplification of the base shear from 2D to 3D is close to 0. Thus, the *AE* was not found to be a meaningful measure of the accuracy of the simplified method, whereas the *BSNE* evaluated directly the error in the total base-shear estimate relative to the simulated base shear. The *BSNE* was found to be a reasonable error measure and is recommended to evaluate the accuracy of the simplified method.

5. Amplification of base shear decreased with the increase of effective period (or radius R_{eff} of the effective pendulum mechanism) and increased with an increasing friction coefficient μ. The proposed method to estimate base shear for 3D shaking well captures these observed trends in the base-shear coefficient vs isolation system parameters. The average *BSNE* was essentially independent of the variation in isolation system parameters. Differences in base-shear amplification for bridge superstructure parameter variations were insignificant, and the simplified method also estimated base shear for 3D shaking accurately across the range of bridge model variations.

6. Large dispersion of the *BSNE* was observed over the suite of ground motions. While the amplification factor $v = 0.5$ led to the lowest average *BSNE*, using this amplification factor could lead to the possibility of significantly under-predicting the base-shear coefficient for an individual ground motion. On average, using an amplification factor $v = 1.0$ overestimated the base-shear coefficient by 15–30% (i.e., the average *BSNE* ranged between 15–30%). Application of the simplified method with $v = 1.0$ is recommended for estimates of response that are sufficient but not overly conservative. Applying an amplification factor consistent with the vertical spectral acceleration of the dominant vertical mode of the bridge was unnecessarily conservative for most motions. In other words, dynamic amplification of the ground motion was not generally observed.

7. Future work is advisable to fine tune the estimation method for implementation in bridge design codes. Analysis with a statistically significant number of ground motions and range of shaking intensities, along with model variations. should be used to determine a "best fit" value of the amplification factor. Because of the complexities associated with high-intensity shaking, determination of a threshold PGA_V is envisioned above which the simplified method cannot reliably be applied, and 3D RHA procedures are recommended.

Implementation of a PGA_V limit may improve the accuracy of the estimation method in the applicable range of ground-motion intensity.

REFERENCES

AASHTO (2010). *Guide Specifications for Seismic Isolation Design*, American Association of State Highway and Transportation Officials, Washington, DC.

Abrahamson N., Silva W. (2008). Summary of the Abrahamson & Silva NGA ground-motion relations, *Earthq. Spectra*, 24(1): 67–97.

ASCE (2017). Seismic design requirements for seismically isolated structures. Chapter 17, *ASCE 7-16: Minimum design loads for buildings and other structures*. American Society of Civil Engineers, Reston, VA.

Aviram A., Mackie K.R., Stojandinovic B. (2008). Guidelines for nonlinear analysis of bridge structures in California, *PEER Report No. 2008/03*, Pacific Earthquake Engineering Research Center, University of California, Berkeley, CA.

Baker J.W., Lin T., Shahi S.K., Jayaram N. (2011). New ground motion selection procedures and selected motions for the PEER transportation research program, *PEER Report No. 2011/03*, Pacific Earthquake Engineering Research Center, University of California, Berkeley, CA.

Boore D.M., Atkinson G.M. (2008). Ground-motion prediction equations for the average horizontal component of PGA, PGV, and 5%-damped PSA at spectral periods between 0.01 s and 10.0 s, *Earthq. Spectra*, 24(1): 99–138.

Buckle I.G., Constantinou M.C., Diceli M., Ghasemi H. (2006). Seismic isolation of highway bridges, *Special Report No. MCEER-06-SP07*, Department of Civil and Environmental Engineering, SUNY Buffalo, Buffalo, NY.

Calvi G.M., Ceresa P., Casarotti C., Bolognini D., Auricchio F. (2004). Effects of axial force variation in the seismic response of bridges isolated with friction pendulum systems, *J. Earthq. Eng.*, 8(spec01), 187–224.

Caltrans (2004). *Seismic Design Criteria Version 1.3*, California Department of Transportation, Sacramento, CA.

Campbell K.W., Bozorgnia Y. (2008). NGA ground motion model for the geometric mean horizontal component of PGA, PGV, PGD and 5% damped linear elastic response spectra for periods ranging from 0.01 to 10 s, *Earthq. Spectra*, 24(1): 139–171.

Carlton B. (2014). *An Improved Description of the Seismic Response of Sites with High Plasticity Soils, Organic Clays, and Deep Soft Soil Deposits*, Ph.D. thesis, Department of Civil and Environmental Engineering, University of California, Berkeley, CA.

Chiou B.-S.J., Youngs R.R. (2008). An NGA model for the average horizontal component of peak ground motion and response spectra, *Earthq. Spectra*, 24(1): 173–215.

Choi E. (2002). *Seismic Analysis and Retrofit of Mid-America Bridges*, Ph.D. thesis, School of Civil and Environmental Engineering, Georgia Institute of Technology, Atlanta, GA.

Cilsalar H., Constantinou M.C. (2017). Effect of vertical ground motion on the response of structures isolated with friction pendulum isolators, *Inter. J. Earthq. Impact Eng.*, 2(2): 135–157.

CSI (2017). *SAP2000 Version 20.0.0*, Computers and Structures, Inc., Walnut Creek, CA.

Dao N.D., Ryan K.L., Sato E., Sasaki T. (2013). Predicting the displacement of triple pendulum bearings in a full scale shake table experiment using a three-dimensional element, *Earthq. Eng. Struct. Dyn.*, 42(11): 1677–1695.

Dao N.D., Ryan K.L. (2015). Seismic response of a full-scale 5-story steel frame building isolated by triple pendulum bearings under 3D excitations, *Report No. CCEER 15-01*, Center for Civil Engineering Earthquake Research, University of Nevada, Reno, NV.

Earthquake Protection Systems. Retrieved from https://earthquakeprotection.com/triple-pendulum.

Eroz M. (2007). *Advanced Models for Sliding Seismic Isolation and Applications for Typical Multi-Span Highway Bridges*, Ph.D. thesis, School of Civil and Environmental Engineering, Georgia Institute of Technology, Atlanta, GA.

FEMA (2009a). *Quantification of building seismic performance factors and commentary for the seismic rehabilitation of buildings. FEMA P-695*, National Earthquake Hazards Reduction Program, Federal Emergency Management Agency, Washington, D.C.

FEMA (2009b). *Recommended seismic provisions for new buildings and other structures. FEMA P-750*, National Earthquake Hazards Reduction Program, Federal Emergency Management Agency, Washington, D.C.

Fenz D.M., Constantinou M.C. (2008). Development, implementation and verification of dynamic analysis models for multi-spherical sliding bearings, *Technical Report MCEER-08-0018*, Multidisciplinary Center for Earthquake Engineering Research, SUNY Buffalo, Buffalo, NY.

Idriss I.M. (2008). An NGA empirical model for estimating the horizontal spectral values generated by shallow crustal earthquakes, *Earthq. Spectra*, 24(1): 21–242.

Iemura H., Taghikhany T., Takahashi Y., Jain S.K. (2005). Effect of variation of normal force on seismic performance of resilient sliding isolation systems in highway bridges, *Earthq. Eng. Struct. Dyn.*, 34(15): 1777–1797.

IICGE (2019). Retrieved from International Information Center for Geotechnical Engineers, https://www.geoengineer.org/software/sigmaspectra (accessed 7/1/2019).

Kartoum A. (2018). *Personal Communication*.

Kottke A., Rathje E. (2008). A semi-automated procedure for selecting and scaling recorded earthquake motions for dynamic analysis, *Earthq. Spectra*, 24(4): 911–932.

Lin B.C., Tadjbakhsh I. (1986). Effect of vertical motion on friction-driven isolation systems, *Earthq. Eng. Struct. Dyn*., 14(4): 609–622.

Mangalathu Sivasubramanian Pillai, S. (2017). *Performance Based Grouping and Fragility Analysis of Box-Girder Bridges in California,* Ph.D. thesis, School of Civil and Environmental Engineering, Georgia Institute of Technology, Atlanta, GA

Morgan T.A., Mahin S.A. (2011). The use of innovative base isolation systems to achieve complex seismic performance objectives, *PEER Report No. 2011/06*, Pacific Earthquake Engineering Research Center, University of California, Berkeley, CA.

Mosqueda G., Whittaker A.S., Fenves G.L. (2004). Characterization and modeling of friction pendulum bearings subjected to multiple components of excitation, ASCE, *J. Struct. Eng.*, 130(3): 433–442.

NBI (2010). *National Bridge Inventory Data*, U.S. Department of Transportation, Federal Highway Administration, Washington, DC, available at: http://www.fhwa.dot.gov/bridge/nbi/ascii.cfm (accessed 10/01/2019).

OpenSees (2019). Open System for Earthquake Engineering Simulation. http://opensees.berkeley.edu (accessed 10/1/2019).

Politopoulos I., Moussallam N. (2012). Horizontal floor response spectra of base-isolated buildings due to vertical excitation, *Earthq. Eng. Struct. Dyn.*, 41(3): 587–592.

Rabiei M., Khoshnoudian F. (2011). Response of multistory friction pendulum base-isolated buildings including the vertical component of earthquakes, *Can. J. Civ. Eng.*, 38(10): 1045–1059.

Ramanathan K.N. (2012). *Next Generation Seismic Fragility Curves for California Bridges Incorporating the Evolution in Seismic Design Philosophy*. Ph.D. thesis, School of Civil and Environmental Engineering, Georgia Institute of Technology, Atlanta, GA.

Ryan K.L., Dao N.D. (2015). Influence of vertical ground shaking on horizontal response of seismically isolated buildings with friction bearings, ASCE, *J. Struct. Eng.*, 142(1), 04015089.

Shakib H., Fuladgar A. (2003). Effect of vertical component of earthquake on the response of pure-friction base-isolated asymmetric buildings, *Eng. Struct*., 25(14): 1841–1850.

Soroushian S., Maragakis E.M., Ryan K.L., Sato E., Sasaki T., Okazaki T., Mosqueda, G. (2015). Seismic simulation of an integrated ceiling-partition wall-piping system at E-Defense. II: Evaluation of nonstructural damage and fragilities, ASCE, *J. Struct. Eng.*, 142(2): 04015131.

Zayas V.A., Low S.S., Mahin S.A. (1987). The FPS earthquake resisting system, *Report No. UCB/EERC-87/01*, Earthquake Engineering Research Center, University of California, Berkeley, CA.

PEER REPORTS

PEER reports are available as a free PDF download from https://peer.berkeley.edu/peer-reports. In addition, printed hard copies of PEER reports can be ordered directly from our printer by following the instructions at https://peer.berkeley.edu/peer-reports. For other related questions about the PEER Report Series, contact the Pacific Earthquake Engineering Research Center, 325 Davis Hall, Mail Code 1792, Berkeley, CA 94720. Tel.: (510) 642-3437; and Email: peer_center@berkeley.edu.

PEER 2019/07 *PEER Hub ImageNet* (*ϕ*-Net): *A Large-Scale Multi-Attribute Benchmark Dataset of Structural Images*. Yuqing Gao, and Khalid. M. Mosalam. November 2019.

PEER 2019/06 *Fluid-Structure Interaction and Python-Scripting Capabilities in OpenSees*. Minjie Zhu and Michael H. Scott. August 2019.

PEER 2019/05 *Expected Earthquake Performance of Buildings Designed to the California Building Code (California Alfred E. Alquist Seismic Safety Publication 19-01).* Grace S. Kang, Sifat Muin, Jorge Archbold, Bitanoosh Woods, and Khalid Mosalam. July 2019.

PEER 2019/04 *Aftershock Seismic Vulnerability and Time-Dependent Risk Assessment of Bridges*. Sujith Mangalathu, Mehrdad Shokrabadi, and Henry V. Burton. May 2019.

PEER 2019/03 *Ground-Motion Directivity Modeling for Seismic Hazard Applications.* Jennifer L. Donahue, Jonathan P. Stewart, Nicolas Gregor, and Yousef Bozorgnia. Review Panel: Jonathan D. Bray, Stephen A. Mahin, I. M. Idriss, Robert W. Graves, and Tom Shantz. May 2019.

PEER 2019/02 *Direct-Finite-Element Method for Nonlinear Earthquake Analysis of Concrete Dams Including Dam–Water–Foundation Rock Interaction.* Arnkjell Løkke and Anil K. Chopra. March 2019.

PEER 2019/01 *Flow-Failure Case History of the Las Palmas, Chile, Tailings Dam.* R. E. S. Moss, T. R. Gebhart, D. J. Frost, and C. Ledezma. January 2019.

PEER 2018/08 *Central and Eastern North America Ground-Motion Characterization: NGA-East Final Report*. Christine Goulet, Yousef Bozorgnia, Norman Abrahamson, Nicolas Kuehn, Linda Al Atik, Robert Youngs, Robert Graves, and Gail Atkinson. December 2018.

PEER 2018/07 *An Empirical Model for Fourier Amplitude Spectra using the NGA-West2 Database*. Jeff Bayless, and Norman A. Abrahamson. December 2018.

PEER 2018/06 *Estimation of Shear Demands on Rock-Socketed Drilled Shafts subjected to Lateral Loading*. Pedro Arduino, Long Chen, and Christopher R. McGann. December 2018.

PEER 2018/05 *Selection of Random Vibration Procedures for the NGA-East Project*. Albert Kottke, Norman A. Abrahamson, David M. Boore, Yousef Bozorgnia, Christine Goulet, Justin Hollenback, Tadahiro Kishida, Armen Der Kiureghian, Olga-Joan Ktenidou, Nicolas Kuehn, Ellen M. Rathje, Walter J. Silva, Eric Thompson, and Xiaoyue Wang. December 2018.

PEER 2018/04 *Capturing Directivity Effects in the Mean and Aleatory Variability of the NGA-West 2 Ground Motion Prediction Equations.* Jennie A. Watson-Lamprey. November 2018.

PEER 2018/03 *Probabilistic Seismic Hazard Analysis Code Verification*. Christie Hale, Norman Abrahamson, and Yousef Bozorgnia. July 2018.

PEER 2018/02 *Update of the BCHydro Subduction Ground-Motion Model using the NGA-Subduction Dataset.* Norman Abrahamson, Nicolas Kuehn, Zeynep Gulerce, Nicholas Gregor, Yousef Bozorgnia, Grace Parker, Jonathan Stewart, Brian Chiou, I. M. Idriss, Kenneth Campbell, and Robert Youngs. June 2018.

PEER 2018/01 *PEER Annual Report 2017–2018*. Khalid Mosalam, Amarnath Kasalanati, and Selim Günay. June 2018.

PEER 2017/12 *Experimental Investigation of the Behavior of Vintage and Retrofit Concentrically Braced Steel Frames under Cyclic Loading*. Barbara G. Simpson, Stephen A. Mahin, and Jiun-Wei Lai, December 2017.

PEER 2017/11 *Preliminary Studies on the Dynamic Response of a Seismically Isolated Prototype Gen-IV Sodium-Cooled Fast Reactor* (*PGSFR*). Benshun Shao, Andreas H. Schellenberg, Matthew J. Schoettler, and Stephen A. Mahin. December 2017.

PEER 2017/10 *Development of Time Histories for IEEE693 Testing and Analysis (including Seismically Isolated Equipment).* Shakhzod M. Takhirov, Eric Fujisaki, Leon Kempner, Michael Riley, and Brian Low. December 2017.

PEER 2017/09 *""R" Package for Computation of Earthquake Ground-Motion Response Spectra.* Pengfei Wang, Jonathan P. Stewart, Yousef Bozorgnia, David M. Boore, and Tadahiro Kishida. December 2017.

PEER 2017/08 *Influence of Kinematic SSI on Foundation Input Motions for Bridges on Deep Foundations*. Benjamin J. Turner, Scott J. Brandenberg, and Jonathan P. Stewart. November 2017.

PEER 2017/07 *A Nonlinear Kinetic Model for Multi-Stage Friction Pendulum Systems*. Paul L. Drazin and Sanjay Govindjee. September 2017.

PEER 2017/06 *Guidelines for Performance-Based Seismic Design of Tall Buildings, Version 2.02*. TBI Working Group led by co-chairs Ron Hamburger and Jack Moehle: Jack Baker, Jonathan Bray, C.B. Crouse, Greg Deierlein, John Hooper, Marshall Lew, Joe Maffei, Stephen Mahin, James Malley, Farzad Naeim, Jonathan Stewart, and John Wallace. May 2017.

PEER 2017/05 *Recommendations for Ergodic Nonlinear Site Amplification in Central and Eastern North America*. Youssef M.A. Hashash, Joseph A. Harmon, Okan Ilhan, Grace A. Parker, and Jonathan P. Stewart. March 2017.

PEER 2017/04 *Expert Panel Recommendations for Ergodic Site Amplification in Central and Eastern North America*. Jonathan P. Stewart, Grace A. Parker, Joseph P. Harmon, Gail M. Atkinson, David M. Boore, Robert B. Darragh, Walter J. Silva, and Youssef M.A. Hashash. March 2017.

PEER 2017/03 *NGA-East Ground-Motion Models for the U.S. Geological Survey National Seismic Hazard Maps*. Christine A. Goulet, Yousef Bozorgnia, Nicolas Kuehn, Linda Al Atik, Robert R. Youngs, Robert W. Graves, and Gail M. Atkinson. March 2017.

PEER 2017/02 *U.S.–New Zealand–Japan Workshop: Liquefaction-Induced Ground Movements Effects, University of California, Berkeley, California, 2–4 November 2016.* Jonathan D. Bray, Ross W. Boulanger, Misko Cubrinovski, Kohji Tokimatsu, Steven L. Kramer, Thomas O'Rourke, Ellen Rathje, Russell A. Green, Peter K. Robinson, and Christine Z. Beyzaei. March 2017.

PEER 2017/01 *2016 PEER Annual Report*. Khalid M. Mosalam, Amarnath Kasalanati, and Grace Kang. March 2017.

PEER 2016/10 *Performance-Based Robust Nonlinear Seismic Analysis with Application to Reinforced Concrete Bridge Systems*. Xiao Ling and Khalid M. Mosalam. December 2016.

PEER 2017/09 *Detailing Requirements for Column Plastic Hinges subjected to Combined Flexural, Axial, and Torsional Seismic Loading.* Gabriel Hurtado and Jack P. Moehle. December 2016.

PEER 2016/08 *Resilience of Critical Structures, Infrastructure, and Communities*. Gian Paolo Cimellaro, Ali Zamani-Noori, Omar Kamouh, Vesna Terzic, and Stephen A. Mahin. December 2016.

PEER 2016/07 *Hybrid Simulation Theory for a Classical Nonlinear Dynamical System*. Paul L. Drazin and Sanjay Govindjee. September 2016.

PEER 2016/06 *California Earthquake Early Warning System Benefit Study*. Laurie A. Johnson, Sharyl Rabinovici, Grace S. Kang, and Stephen A. Mahin. July 2006.

PEER 2016/05 *Ground-Motion Prediction Equations for Arias Intensity Consistent with the NGA-West2 Ground-Motion Models.* Charlotte Abrahamson, Hao-Jun Michael Shi, and Brian Yang. July 2016.

PEER 2016/04 *The M_W 6.0 South Napa Earthquake of August 24, 2014: A Wake-Up Call for Renewed Investment in Seismic Resilience Across California.* Prepared for the California Seismic Safety Commission, Laurie A. Johnson and Stephen A. Mahin. May 2016.

PEER 2016/03 *Simulation Confidence in Tsunami-Driven Overland Flow.* Patrick Lynett. May 2016.

PEER 2016/02 *Semi-Automated Procedure for Windowing time Series and Computing Fourier Amplitude Spectra for the NGA-West2 Database.* Tadahiro Kishida, Olga-Joan Ktenidou, Robert B. Darragh, and Walter J. Silva. May 2016.

PEER 2016/01 *A Methodology for the Estimation of Kappa (κ) from Large Datasets: Example Application to Rock Sites in the NGA-East Database and Implications on Design Motions.* Olga-Joan Ktenidou, Norman A. Abrahamson, Robert B. Darragh, and Walter J. Silva. April 2016.

PEER 2015/13 *Self-Centering Precast Concrete Dual-Steel-Shell Columns for Accelerated Bridge Construction: Seismic Performance, Analysis, and Design*. Gabriele Guerrini, José I. Restrepo, Athanassios Vervelidis, and Milena Massari. December 2015.

PEER 2015/12 *Shear-Flexure Interaction Modeling for Reinforced Concrete Structural Walls and Columns under Reversed Cyclic Loading*. Kristijan Kolozvari, Kutay Orakcal, and John Wallace. December 2015.

PEER 2015/11 *Selection and Scaling of Ground Motions for Nonlinear Response History Analysis of Buildings in Performance-Based Earthquake Engineering*. N. Simon Kwong and Anil K. Chopra. December 2015.

PEER 2015/10 *Structural Behavior of Column-Bent Cap Beam-Box Girder Systems in Reinforced Concrete Bridges Subjected to Gravity and Seismic Loads. Part II: Hybrid Simulation and Post-Test Analysis*. Mohamed A. Moustafa and Khalid M. Mosalam. November 2015.

PEER 2015/09 *Structural Behavior of Column-Bent Cap Beam-Box Girder Systems in Reinforced Concrete Bridges Subjected to Gravity and Seismic Loads. Part I: Pre-Test Analysis and Quasi-Static Experiments*. Mohamed A. Moustafa and Khalid M. Mosalam. September 2015.

PEER 2015/08 *NGA-East: Adjustments to Median Ground-Motion Models for Center and Eastern North America*. August 2015.

PEER 2015/07 *NGA-East: Ground-Motion Standard-Deviation Models for Central and Eastern North America*. Linda Al Atik. June 2015.

PEER 2015/06 *Adjusting Ground-Motion Intensity Measures to a Reference Site for which V_{S30} = 3000 m/sec*. David M. Boore. May 2015.

PEER 2015/05 *Hybrid Simulation of Seismic Isolation Systems Applied to an APR-1400 Nuclear Power Plant.* Andreas H. Schellenberg, Alireza Sarebanha, Matthew J. Schoettler, Gilberto Mosqueda, Gianmario Benzoni, and Stephen A. Mahin. April 2015.

PEER 2015/04 *NGA-East: Median Ground-Motion Models for the Central and Eastern North America Region*. April 2015.

PEER 2015/03 *Single Series Solution for the Rectangular Fiber-Reinforced Elastomeric Isolator Compression Modulus*. James M. Kelly and Niel C. Van Engelen. March 2015.

PEER 2015/02 *A Full-Scale, Single-Column Bridge Bent Tested by Shake-Table Excitation.* Matthew J. Schoettler, José I. Restrepo, Gabriele Guerrini, David E. Duck, and Francesco Carrea. March 2015.

PEER 2015/01 *Concrete Column Blind Prediction Contest 2010: Outcomes and Observations.* Vesna Terzic, Matthew J. Schoettler, José I. Restrepo, and Stephen A Mahin. March 2015.

PEER 2014/20 *Stochastic Modeling and Simulation of Near-Fault Ground Motions for Performance-Based Earthquake Engineering*. Mayssa Dabaghi and Armen Der Kiureghian. December 2014.

PEER 2014/19 *Seismic Response of a Hybrid Fiber-Reinforced Concrete Bridge Column Detailed for Accelerated Bridge Construction*. Wilson Nguyen, William Trono, Marios Panagiotou, and Claudia P. Ostertag. December 2014.

PEER 2014/18 *Three-Dimensional Beam-Truss Model for Reinforced Concrete Walls and Slabs Subjected to Cyclic Static or Dynamic Loading*. Yuan Lu, Marios Panagiotou, and Ioannis Koutromanos. December 2014.

PEER 2014/17 *PEER NGA-East Database.* Christine A. Goulet, Tadahiro Kishida, Timothy D. Ancheta, Chris H. Cramer, Robert B. Darragh, Walter J. Silva, Youssef M.A. Hashash, Joseph Harmon, Jonathan P. Stewart, Katie E. Wooddell, and Robert R. Youngs. October 2014.

PEER 2014/16 *Guidelines for Performing Hazard-Consistent One-Dimensional Ground Response Analysis for Ground Motion Prediction*. Jonathan P. Stewart, Kioumars Afshari, and Youssef M.A. Hashash. October 2014.

PEER 2014/15 *NGA-East Regionalization Report: Comparison of Four Crustal Regions within Central and Eastern North America using Waveform Modeling and 5%-Damped Pseudo-Spectral Acceleration Response*. Jennifer Dreiling, Marius P. Isken, Walter D. Mooney, Martin C. Chapman, and Richard W. Godbee. October 2014.

PEER 2014/14 *Scaling Relations between Seismic Moment and Rupture Area of Earthquakes in Stable Continental Regions*. Paul Somerville. August 2014.

PEER 2014/13 *PEER Preliminary Notes and Observations on the August 24, 2014, South Napa Earthquake*. Grace S. Kang and Stephen A. Mahin, Editors. September 2014.

PEER 2014/12 *Reference-Rock Site Conditions for Central and Eastern North America: Part II – Attenuation (Kappa) Definition*. Kenneth W. Campbell, Youssef M.A. Hashash, Byungmin Kim, Albert R. Kottke, Ellen M. Rathje, Walter J. Silva, and Jonathan P. Stewart. August 2014.

PEER 2014/11 *Reference-Rock Site Conditions for Central and Eastern North America: Part I - Velocity Definition*. Youssef M.A. Hashash, Albert R. Kottke, Jonathan P. Stewart, Kenneth W. Campbell, Byungmin Kim, Ellen M. Rathje, Walter J. Silva, Sissy Nikolaou, and Cheryl Moss. August 2014.

PEER 2014/10 *Evaluation of Collapse and Non-Collapse of Parallel Bridges Affected by Liquefaction and Lateral Spreading*. Benjamin Turner, Scott J. Brandenberg, and Jonathan P. Stewart. August 2014.

PEER 2014/09 *PEER Arizona Strong-Motion Database and GMPEs Evaluation*. Tadahiro Kishida, Robert E. Kayen, Olga-Joan Ktenidou, Walter J. Silva, Robert B. Darragh, and Jennie Watson-Lamprey. June 2014.

PEER 2014/08 *Unbonded Pretensioned Bridge Columns with Rocking Detail*. Jeffrey A. Schaefer, Bryan Kennedy, Marc O. Eberhard, and John F. Stanton. June 2014.

PEER 2014/07 *Northridge 20 Symposium Summary Report: Impacts, Outcomes, and Next Steps*. May 2014.

PEER 2014/06 *Report of the Tenth Planning Meeting of NEES/E-Defense Collaborative Research on Earthquake Engineering*. December 2013.

PEER 2014/05 *Seismic Velocity Site Characterization of Thirty-One Chilean Seismometer Stations by Spectral Analysis of Surface Wave Dispersion*. Robert Kayen, Brad D. Carkin, Skye Corbet, Camilo Pinilla, Allan Ng, Edward Gorbis, and Christine Truong. April 2014.

PEER 2014/04 Effect of Vertical Acceleration on Shear Strength of Reinforced Concrete Columns. Hyerin Lee and Khalid M. Mosalam. April 2014.

PEER 2014/03 *Retest of Thirty-Year-Old Neoprene Isolation Bearings.* James M. Kelly and Niel C. Van Engelen. March 2014.

PEER 2014/02 *Theoretical Development of Hybrid Simulation Applied to Plate Structures.* Ahmed A. Bakhaty, Khalid M. Mosalam, and Sanjay Govindjee. January 2014.

PEER 2014/01 *Performance-Based Seismic Assessment of Skewed Bridges.* Peyman Kaviani, Farzin Zareian, and Ertugrul Taciroglu. January 2014.

PEER 2013/26 *Urban Earthquake Engineerin*g. Proceedings of the U.S.-Iran Seismic Workshop. December 2013.

PEER 2013/25 *Earthquake Engineering for Resilient Communities: 2013 PEER Internship Program Research Report Collection.* Heidi Tremayne (Editor), Stephen A. Mahin (Editor), Jorge Archbold Monterossa, Matt Brosman, Shelly Dean, Katherine deLaveaga, Curtis Fong, Donovan Holder, Rakeeb Khan, Elizabeth Jachens, David Lam, Daniela Martinez Lopez, Mara Minner, Geffen Oren, Julia Pavicic, Melissa Quinonez, Lorena Rodriguez, Sean Salazar, Kelli Slaven, Vivian Steyert, Jenny Taing, and Salvador Tena. December 2013.

PEER 2013/24 *NGA-West2 Ground Motion Prediction Equations for Vertical Ground Motions*. September 2013.

PEER 2013/23 *Coordinated Planning and Preparedness for Fire Following Major Earthquakes*. Charles Scawthorn. November 2013.

PEER 2013/22 *GEM-PEER Task 3 Project: Selection of a Global Set of Ground Motion Prediction Equations.* Jonathan P. Stewart, John Douglas, Mohammad B. Javanbarg, Carola Di Alessandro, Yousef Bozorgnia, Norman A. Abrahamson, David M. Boore, Kenneth W. Campbell, Elise Delavaud, Mustafa Erdik, and Peter J. Stafford. December 2013.

PEER 2013/21 *Seismic Design and Performance of Bridges with Columns on Rocking Foundations*. Grigorios Antonellis and Marios Panagiotou. September 2013.

PEER 2013/20 *Experimental and Analytical Studies on the Seismic Behavior of Conventional and Hybrid Braced Frames*. Jiun-Wei Lai and Stephen A. Mahin. September 2013.

PEER 2013/19 *Toward Resilient Communities: A Performance-Based Engineering Framework for Design and Evaluation of the Built Environment.* Michael William Mieler, Bozidar Stojadinovic, Robert J. Budnitz, Stephen A. Mahin, and Mary C. Comerio. September 2013.

PEER 2013/18 *Identification of Site Parameters that Improve Predictions of Site Amplification*. Ellen M. Rathje and Sara Navidi. July 2013.

PEER 2013/17 *Response Spectrum Analysis of Concrete Gravity Dams Including Dam-Water-Foundation Interaction*. Arnkjell Løkke and Anil K. Chopra. July 2013.

PEER 2013/16 *Effect of Hoop Reinforcement Spacing on the Cyclic Response of Large Reinforced Concrete Special Moment Frame Beams.* Marios Panagiotou, Tea Visnjic, Grigorios Antonellis, Panagiotis Galanis, and Jack P. Moehle. June 2013.

PEER 2013/15 *A Probabilistic Framework to Include the Effects of Near-Fault Directivity in Seismic Hazard Assessment.* Shrey Kumar Shahi, Jack W. Baker. October 2013.

PEER 2013/14 *Hanging-Wall Scaling using Finite-Fault Simulations.* Jennifer L. Donahue and Norman A. Abrahamson. September 2013.

PEER 2013/13 *Semi-Empirical Nonlinear Site Amplification and its Application in NEHRP Site Factors*. Jonathan P. Stewart and Emel Seyhan. November 2013.

PEER 2013/12 *Nonlinear Horizontal Site Response for the NGA-West2 Project.* Ronnie Kamai, Norman A. Abramson, Walter J. Silva. May 2013.

PEER 2013/11 *Epistemic Uncertainty for NGA-West2 Models.* Linda Al Atik and Robert R. Youngs. May 2013.

PEER 2013/10 *NGA-West 2 Models for Ground-Motion Directionality*. Shrey K. Shahi and Jack W. Baker. May 2013.

PEER 2013/09 *Final Report of the NGA-West2 Directivity Working Group.* Paul Spudich, Jeffrey R. Bayless, Jack W. Baker, Brian S.J. Chiou, Badie Rowshandel, Shrey Shahi, and Paul Somerville. May 2013.

PEER 2013/08 *NGA-West2 Model for Estimating Average Horizontal Values of Pseudo-Absolute Spectral Accelerations Generated by Crustal Earthquakes*. I. M. Idriss. May 2013.

PEER 2013/07 *Update of the Chiou and Youngs NGA Ground Motion Model for Average Horizontal Component of Peak Ground Motion and Response Spectra*. Brian Chiou and Robert Youngs. May 2013.

PEER 2013/06 *NGA-West2 Campbell-Bozorgnia Ground Motion Model for the Horizontal Components of PGA, PGV, and 5%-Damped Elastic Pseudo-Acceleration Response Spectra for Periods Ranging from 0.01 to 10 sec*. Kenneth W. Campbell and Yousef Bozorgnia. May 2013.

PEER 2013/05 *NGA-West 2 Equations for Predicting Response Spectral Accelerations for Shallow Crustal Earthquakes*. David M. Boore, Jonathan P. Stewart, Emel Seyhan, and Gail M. Atkinson. May 2013.

PEER 2013/04 *Update of the AS08 Ground-Motion Prediction Equations Based on the NGA-West2 Data Set*. Norman Abrahamson, Walter Silva, and Ronnie Kamai. May 2013.

PEER 2013/03 *PEER NGA-West2 Database*. Timothy D. Ancheta, Robert B. Darragh, Jonathan P. Stewart, Emel Seyhan, Walter J. Silva, Brian S.J. Chiou, Katie E. Wooddell, Robert W. Graves, Albert R. Kottke, David M. Boore, Tadahiro Kishida, and Jennifer L. Donahue. May 2013.

PEER 2013/02 *Hybrid Simulation of the Seismic Response of Squat Reinforced Concrete Shear Walls*. Catherine A. Whyte and Bozidar Stojadinovic. May 2013.

PEER 2013/01 *Housing Recovery in Chile: A Qualitative Mid-program Review*. Mary C. Comerio. February 2013.

PEER 2012/08 *Guidelines for Estimation of Shear Wave Velocity.* Bernard R. Wair, Jason T. DeJong, and Thomas Shantz. December 2012.

PEER 2012/07 *Earthquake Engineering for Resilient Communities: 2012 PEER Internship Program Research Report Collection.* Heidi Tremayne (Editor), Stephen A. Mahin (Editor), Collin Anderson, Dustin Cook, Michael Erceg, Carlos Esparza, Jose Jimenez, Dorian Krausz, Andrew Lo, Stephanie Lopez, Nicole McCurdy, Paul Shipman, Alexander Strum, Eduardo Vega. December 2012.

PEER 2012/06 *Fragilities for Precarious Rocks at Yucca Mountain.* Matthew D. Purvance, Rasool Anooshehpoor, and James N. Brune. December 2012.

PEER 2012/05 *Development of Simplified Analysis Procedure for Piles in Laterally Spreading Layered Soils.* Christopher R. McGann, Pedro Arduino, and Peter Mackenzie–Helnwein. December 2012.

PEER 2012/04 *Unbonded Pre-Tensioned Columns for Bridges in Seismic Regions.* Phillip M. Davis, Todd M. Janes, Marc O. Eberhard, and John F. Stanton. December 2012.

PEER 2012/03 *Experimental and Analytical Studies on Reinforced Concrete Buildings with Seismically Vulnerable Beam-Column Joints*. Sangjoon Park and Khalid M. Mosalam. October 2012.

PEER 2012/02 *Seismic Performance of Reinforced Concrete Bridges Allowed to Uplift during Multi-Directional Excitation*. Andres Oscar Espinoza and Stephen A. Mahin. July 2012.

PEER 2012/01 *Spectral Damping Scaling Factors for Shallow Crustal Earthquakes in Active Tectonic Regions.* Sanaz Rezaeian, Yousef Bozorgnia, I. M. Idriss, Kenneth Campbell, Norman Abrahamson, and Walter Silva. July 2012.

PEER 2011/10 *Earthquake Engineering for Resilient Communities: 2011 PEER Internship Program Research Report Collection*. Heidi Faison and Stephen A. Mahin, Editors. December 2011.

PEER 2011/09 *Calibration of Semi-Stochastic Procedure for Simulating High-Frequency Ground Motions*. Jonathan P. Stewart, Emel Seyhan, and Robert W. Graves. December 2011.

PEER 2011/08 *Water Supply in regard to Fire Following Earthquake*. Charles Scawthorn. November 2011.

PEER 2011/07 *Seismic Risk Management in Urban Areas*. Proceedings of a U.S.-Iran-Turkey Seismic Workshop. September 2011.

PEER 2011/06 *The Use of Base Isolation Systems to Achieve Complex Seismic Performance Objectives*. Troy A. Morgan and Stephen A. Mahin. July 2011.

PEER 2011/05 *Case Studies of the Seismic Performance of Tall Buildings Designed by Alternative Means.* Task 12 Report for the Tall Buildings Initiative. Jack Moehle, Yousef Bozorgnia, Nirmal Jayaram, Pierson Jones, Mohsen Rahnama, Nilesh Shome, Zeynep Tuna, John Wallace, Tony Yang, and Farzin Zareian. July 2011.

PEER 2011/04 *Recommended Design Practice for Pile Foundations in Laterally Spreading Ground.* Scott A. Ashford, Ross W. Boulanger, and Scott J. Brandenberg. June 2011.

PEER 2011/03 *New Ground Motion Selection Procedures and Selected Motions for the PEER Transportation Research Program*. Jack W. Baker, Ting Lin, Shrey K. Shahi, and Nirmal Jayaram. March 2011.

PEER 2011/02 *A Bayesian Network Methodology for Infrastructure Seismic Risk Assessment and Decision Support*. Michelle T. Bensi, Armen Der Kiureghian, and Daniel Straub. March 2011.

PEER 2011/01 *Demand Fragility Surfaces for Bridges in Liquefied and Laterally Spreading Ground.* Scott J. Brandenberg, Jian Zhang, Pirooz Kashighandi, Yili Huo, and Minxing Zhao. March 2011.

PEER 2010/05 *Guidelines for Performance-Based Seismic Design of Tall Buildings.* Developed by the Tall Buildings Initiative. November 2010.

PEER 2010/04 *Application Guide for the Design of Flexible and Rigid Bus Connections between Substation Equipment Subjected to Earthquakes.* Jean-Bernard Dastous and Armen Der Kiureghian. September 2010.

PEER 2010/03 *Shear Wave Velocity as a Statistical Function of Standard Penetration Test Resistance and Vertical Effective Stress at Caltrans Bridge Sites.* Scott J. Brandenberg, Naresh Bellana, and Thomas Shantz. June 2010.

PEER 2010/02 *Stochastic Modeling and Simulation of Ground Motions for Performance-Based Earthquake Engineering.* Sanaz Rezaeian and Armen Der Kiureghian. June 2010.

PEER 2010/01 *Structural Response and Cost Characterization of Bridge Construction Using Seismic Performance Enhancement Strategies.* Ady Aviram, Božidar Stojadinović, Gustavo J. Parra-Montesinos, and Kevin R. Mackie. March 2010.

PEER 2009/03 *The Integration of Experimental and Simulation Data in the Study of Reinforced Concrete Bridge Systems Including Soil-Foundation-Structure Interaction.* Matthew Dryden and Gregory L. Fenves. November 2009.

PEER 2009/02 *Improving Earthquake Mitigation through Innovations and Applications in Seismic Science, Engineering, Communication, and Response*. Proceedings of a U.S.-Iran Seismic Workshop. October 2009.

PEER 2009/01 *Evaluation of Ground Motion Selection and Modification Methods: Predicting Median Interstory Drift Response of Buildings*. Curt B. Haselton, Editor. June 2009.

PEER 2008/10 *Technical Manual for Strata.* Albert R. Kottke and Ellen M. Rathje. February 2009.

PEER 2008/09 *NGA Model for Average Horizontal Component of Peak Ground Motion and Response Spectra.* Brian S.-J. Chiou and Robert R. Youngs. November 2008.

PEER 2008/08 *Toward Earthquake-Resistant Design of Concentrically Braced Steel Structures*. Patxi Uriz and Stephen A. Mahin. November 2008.

PEER 2008/07 *Using OpenSees for Performance-Based Evaluation of Bridges on Liquefiable Soils*. Stephen L. Kramer, Pedro Arduino, and HyungSuk Shin. November 2008.

PEER 2008/06 *Shaking Table Tests and Numerical Investigation of Self-Centering Reinforced Concrete Bridge Columns*. Hyung IL Jeong, Junichi Sakai, and Stephen A. Mahin. September 2008.

PEER 2008/05 *Performance-Based Earthquake Engineering Design Evaluation Procedure for Bridge Foundations Undergoing Liquefaction-Induced Lateral Ground Displacement*. Christian A. Ledezma and Jonathan D. Bray. August 2008.

PEER 2008/04 *Benchmarking of Nonlinear Geotechnical Ground Response Analysis Procedures.* Jonathan P. Stewart, Annie On-Lei Kwok, Youssef M. A. Hashash, Neven Matasovic, Robert Pyke, Zhiliang Wang, and Zhaohui Yang. August 2008.

PEER 2008/03 *Guidelines for Nonlinear Analysis of Bridge Structures in California.* Ady Aviram, Kevin R. Mackie, and Božidar Stojadinović. August 2008.

PEER 2008/02 *Treatment of Uncertainties in Seismic-Risk Analysis of Transportation Systems*. Evangelos Stergiou and Anne S. Kiremidjian. July 2008.

PEER 2008/01 *Seismic Performance Objectives for Tall Buildings.* William T. Holmes, Charles Kircher, William Petak, and Nabih Youssef. August 2008.

PEER 2007/12 *An Assessment to Benchmark the Seismic Performance of a Code-Conforming Reinforced Concrete Moment-Frame Building.* Curt Haselton, Christine A. Goulet, Judith Mitrani-Reiser, James L. Beck, Gregory G. Deierlein, Keith A. Porter, Jonathan P. Stewart, and Ertugrul Taciroglu. August 2008.

PEER 2007/11 *Bar Buckling in Reinforced Concrete Bridge Columns.* Wayne A. Brown, Dawn E. Lehman, and John F. Stanton. February 2008.

PEER 2007/10 *Computational Modeling of Progressive Collapse in Reinforced Concrete Frame Structures*. Mohamed M. Talaat and Khalid M. Mosalam. May 2008.

PEER 2007/09 *Integrated Probabilistic Performance-Based Evaluation of Benchmark Reinforced Concrete Bridges*. Kevin R. Mackie, John-Michael Wong, and Božidar Stojadinović. January 2008.

PEER 2007/08 *Assessing Seismic Collapse Safety of Modern Reinforced Concrete Moment-Frame Buildings*. Curt B. Haselton and Gregory G. Deierlein. February 2008.

PEER 2007/07 *Performance Modeling Strategies for Modern Reinforced Concrete Bridge Columns*. Michael P. Berry and Marc O. Eberhard. April 2008.

PEER 2007/06 *Development of Improved Procedures for Seismic Design of Buried and Partially Buried Structures*. Linda Al Atik and Nicholas Sitar. June 2007.

PEER 2007/05 *Uncertainty and Correlation in Seismic Risk Assessment of Transportation Systems*. Renee G. Lee and Anne S. Kiremidjian. July 2007.

PEER 2007/04 *Numerical Models for Analysis and Performance-Based Design of Shallow Foundations Subjected to Seismic Loading.* Sivapalan Gajan, Tara C. Hutchinson, Bruce L. Kutter, Prishati Raychowdhury, José A. Ugalde, and Jonathan P. Stewart. May 2008.

PEER 2007/03 *Beam-Column Element Model Calibrated for Predicting Flexural Response Leading to Global Collapse of RC Frame Buildings*. Curt B. Haselton, Abbie B. Liel, Sarah Taylor Lange, and Gregory G. Deierlein. May 2008.

PEER 2007/02 *Campbell-Bozorgnia NGA Ground Motion Relations for the Geometric Mean Horizontal Component of Peak and Spectral Ground Motion Parameters*. Kenneth W. Campbell and Yousef Bozorgnia. May 2007.

PEER 2007/01 *Boore-Atkinson NGA Ground Motion Relations for the Geometric Mean Horizontal Component of Peak and Spectral Ground Motion Parameters*. David M. Boore and Gail M. Atkinson. May 2007.

PEER 2006/12 Societal Implications of Performance-Based Earthquake Engineering. Peter J. May. May 2007.

PEER 2006/11 *Probabilistic Seismic Demand Analysis Using Advanced Ground Motion Intensity Measures, Attenuation Relationships, and Near-Fault Effects*. Polsak Tothong and C. Allin Cornell. March 2007.

PEER 2006/10 *Application of the PEER PBEE Methodology to the I-880 Viaduct*. Sashi Kunnath. February 2007.

PEER 2006/09 *Quantifying Economic Losses from Travel Forgone Following a Large Metropolitan Earthquake*. James Moore, Sungbin Cho, Yue Yue Fan, and Stuart Werner. November 2006.

PEER 2006/08 *Vector-Valued Ground Motion Intensity Measures for Probabilistic Seismic Demand Analysis*. Jack W. Baker and C. Allin Cornell. October 2006.

PEER 2006/07 *Analytical Modeling of Reinforced Concrete Walls for Predicting Flexural and Coupled–Shear-Flexural Responses*. Kutay Orakcal, Leonardo M. Massone, and John W. Wallace. October 2006.

PEER 2006/06 *Nonlinear Analysis of a Soil-Drilled Pier System under Static and Dynamic Axial Loading*. Gang Wang and Nicholas Sitar. November 2006.

PEER 2006/05 *Advanced Seismic Assessment Guidelines.* Paolo Bazzurro, C. Allin Cornell, Charles Menun, Maziar Motahari, and Nicolas Luco. September 2006.

PEER 2006/04 *Probabilistic Seismic Evaluation of Reinforced Concrete Structural Components and Systems*. Tae Hyung Lee and Khalid M. Mosalam. August 2006.

PEER 2006/03 *Performance of Lifelines Subjected to Lateral Spreading.* Scott A. Ashford and Teerawut Juirnarongrit. July 2006.

PEER 2006/02 *Pacific Earthquake Engineering Research Center Highway Demonstration Project.* Anne Kiremidjian, James Moore, Yue Yue Fan, Nesrin Basoz, Ozgur Yazali, and Meredith Williams. April 2006.

PEER 2006/01 *Bracing Berkeley. A Guide to Seismic Safety on the UC Berkeley Campus.* Mary C. Comerio, Stephen Tobriner, and Ariane Fehrenkamp. January 2006.

PEER 2005/17 *Earthquake Simulation Tests on Reducing Residual Displacements of Reinforced Concrete Bridges.* Junichi Sakai, Stephen A Mahin, and Andres Espinoza. December 2005.

PEER 2005/16 *Seismic Response and Reliability of Electrical Substation Equipment and Systems.* Junho Song, Armen Der Kiureghian, and Jerome L. Sackman. April 2006.

PEER 2005/15 *CPT-Based Probabilistic Assessment of Seismic Soil Liquefaction Initiation.* R. E. S. Moss, R. B. Seed, R. E. Kayen, J. P. Stewart, and A. Der Kiureghian. April 2006.

PEER 2005/14 *Workshop on Modeling of Nonlinear Cyclic Load-Deformation Behavior of Shallow Foundations.* Bruce L. Kutter, Geoffrey Martin, Tara Hutchinson, Chad Harden, Sivapalan Gajan, and Justin Phalen. March 2006.

PEER 2005/13 *Stochastic Characterization and Decision Bases under Time-Dependent Aftershock Risk in Performance-Based Earthquake Engineering*. Gee Liek Yeo and C. Allin Cornell. July 2005.

PEER 2005/12 *PEER Testbed Study on a Laboratory Building: Exercising Seismic Performance Assessment.* Mary C. Comerio, Editor. November 2005.

PEER 2005/11 *Van Nuys Hotel Building Testbed Report: Exercising Seismic Performance Assessment.* Helmut Krawinkler, Editor. October 2005.

PEER 2005/10 *First NEES/E-Defense Workshop on Collapse Simulation of Reinforced Concrete Building Structures.* September 2005.

PEER 2005/09 *Test Applications of Advanced Seismic Assessment Guidelines.* Joe Maffei, Karl Telleen, Danya Mohr, William Holmes, and Yuki Nakayama. August 2006.

PEER 2005/08 *Damage Accumulation in Lightly Confined Reinforced Concrete Bridge Columns.* R. Tyler Ranf, Jared M. Nelson, Zach Price, Marc O. Eberhard, and John F. Stanton. April 2006.

PEER 2005/07 *Experimental and Analytical Studies on the Seismic Response of Freestanding and Anchored Laboratory Equipment.* Dimitrios Konstantinidis and Nicos Makris. January 2005.

PEER 2005/06 *Global Collapse of Frame Structures under Seismic Excitations*. Luis F. Ibarra and Helmut Krawinkler. September 2005.

PEER 2005//05 *Performance Characterization of Bench- and Shelf-Mounted Equipment.* Samit Ray Chaudhuri and Tara C. Hutchinson. May 2006.

PEER 2005/04 *Numerical Modeling of the Nonlinear Cyclic Response of Shallow Foundations.* Chad Harden, Tara Hutchinson, Geoffrey R. Martin, and Bruce L. Kutter. August 2005.

PEER 2005/03 *A Taxonomy of Building Components for Performance-Based Earthquake Engineering.* Keith A. Porter. September 2005.

PEER 2005/02 *Fragility Basis for California Highway Overpass Bridge Seismic Decision Making*. Kevin R. Mackie and Božidar Stojadinović. June 2005.

PEER 2005/01 *Empirical Characterization of Site Conditions on Strong Ground Motion.* Jonathan P. Stewart, Yoojoong Choi, and Robert W. Graves. June 2005.

PEER 2004/09 *Electrical Substation Equipment Interaction: Experimental Rigid Conductor Studies.* Christopher Stearns and André Filiatrault. February 2005.

PEER 2004/08 *Seismic Qualification and Fragility Testing of Line Break 550-kV Disconnect Switches.* Shakhzod M. Takhirov, Gregory L. Fenves, and Eric Fujisaki. January 2005.

PEER 2004/07 *Ground Motions for Earthquake Simulator Qualification of Electrical Substation Equipment.* Shakhzod M. Takhirov, Gregory L. Fenves, Eric Fujisaki, and Don Clyde. January 2005.

PEER 2004/06 *Performance-Based Regulation and Regulatory Regimes.* Peter J. May and Chris Koski. September 2004.

PEER 2004/05 *Performance-Based Seismic Design Concepts and Implementation: Proceedings of an International Workshop.* Peter Fajfar and Helmut Krawinkler, Editors. September 2004.

PEER 2004/04 *Seismic Performance of an Instrumented Tilt-up Wall Building.* James C. Anderson and Vitelmo V. Bertero. July 2004.

PEER 2004/03 *Evaluation and Application of Concrete Tilt-up Assessment Methodologies.* Timothy Graf and James O. Malley. October 2004.

PEER 2004/02 *Analytical Investigations of New Methods for Reducing Residual Displacements of Reinforced Concrete Bridge Columns.* Junichi Sakai and Stephen A. Mahin. August 2004.

PEER 2004/01 *Seismic Performance of Masonry Buildings and Design Implications.* Kerri Anne Taeko Tokoro, James C. Anderson, and Vitelmo V. Bertero. February 2004.

PEER 2003/18 *Performance Models for Flexural Damage in Reinforced Concrete Columns.* Michael Berry and Marc Eberhard. August 2003.

PEER 2003/17 *Predicting Earthquake Damage in Older Reinforced Concrete Beam-Column Joints.* Catherine Pagni and Laura Lowes. October 2004.

PEER 2003/16 *Seismic Demands for Performance-Based Design of Bridges.* Kevin Mackie and Božidar Stojadinović. August 2003.

PEER 2003/15 *Seismic Demands for Nondeteriorating Frame Structures and Their Dependence on Ground Motions.* Ricardo Antonio Medina and Helmut Krawinkler. May 2004.

PEER 2003/14 *Finite Element Reliability and Sensitivity Methods for Performance-Based Earthquake Engineering.* Terje Haukaas and Armen Der Kiureghian. April 2004.

PEER 2003/13 *Effects of Connection Hysteretic Degradation on the Seismic Behavior of Steel Moment-Resisting Frames.* Janise E. Rodgers and Stephen A. Mahin. March 2004.

PEER 2003/12 *Implementation Manual for the Seismic Protection of Laboratory Contents: Format and Case Studies*. William T. Holmes and Mary C. Comerio. October 2003.

PEER 2003/11 *Fifth U.S.-Japan Workshop on Performance-Based Earthquake Engineering Methodology for Reinforced Concrete Building Structures*. February 2004.

PEER 2003/10 *A Beam-Column Joint Model for Simulating the Earthquake Response of Reinforced Concrete Frames.* Laura N. Lowes, Nilanjan Mitra, and Arash Altoontash. February 2004.

PEER 2003/09 *Sequencing Repairs after an Earthquake: An Economic Approach.* Marco Casari and Simon J. Wilkie. April 2004.

PEER 2003/08 *A Technical Framework for Probability-Based Demand and Capacity Factor Design (DCFD) Seismic Formats*. Fatemeh Jalayer and C. Allin Cornell. November 2003.

PEER 2003/07 *Uncertainty Specification and Propagation for Loss Estimation Using FOSM Methods.* Jack W. Baker and C. Allin Cornell. September 2003.

PEER 2003/06 *Performance of Circular Reinforced Concrete Bridge Columns under Bidirectional Earthquake Loading*. Mahmoud M. Hachem, Stephen A. Mahin, and Jack P. Moehle. February 2003.

PEER 2003/05 *Response Assessment for Building-Specific Loss Estimation.* Eduardo Miranda and Shahram Taghavi. September 2003.

PEER 2003/04 *Experimental Assessment of Columns with Short Lap Splices Subjected to Cyclic Loads*. Murat Melek, John W. Wallace, and Joel Conte. April 2003.

PEER 2003/03 *Probabilistic Response Assessment for Building-Specific Loss Estimation*. Eduardo Miranda and Hesameddin Aslani. September 2003.

PEER 2003/02 *Software Framework for Collaborative Development of Nonlinear Dynamic Analysis Program*. Jun Peng and Kincho H. Law. September 2003.

PEER 2003/01 *Shake Table Tests and Analytical Studies on the Gravity Load Collapse of Reinforced Concrete Frames.* Kenneth John Elwood and Jack P. Moehle. November 2003.

PEER 2002/24 *Performance of Beam to Column Bridge Joints Subjected to a Large Velocity Pulse.* Natalie Gibson, André Filiatrault, and Scott A. Ashford. April 2002.

PEER 2002/23 *Effects of Large Velocity Pulses on Reinforced Concrete Bridge Columns.* Greg L. Orozco and Scott A. Ashford. April 2002.

PEER 2002/22 *Characterization of Large Velocity Pulses for Laboratory Testing.* Kenneth E. Cox and Scott A. Ashford. April 2002.

PEER 2002/21 *Fourth U.S.-Japan Workshop on Performance-Based Earthquake Engineering Methodology for Reinforced Concrete Building Structures*. December 2002.

PEER 2002/20 *Barriers to Adoption and Implementation of PBEE Innovations.* Peter J. May. August 2002.

PEER 2002/19 *Economic-Engineered Integrated Models for Earthquakes: Socioeconomic Impacts.* Peter Gordon, James E. Moore II, and Harry W. Richardson. July 2002.

PEER 2002/18 *Assessment of Reinforced Concrete Building Exterior Joints with Substandard Details.* Chris P. Pantelides, Jon Hansen, Justin Nadauld, and Lawrence D. Reaveley. May 2002.

PEER 2002/17 *Structural Characterization and Seismic Response Analysis of a Highway Overcrossing Equipped with Elastomeric Bearings and Fluid Dampers: A Case Study*. Nicos Makris and Jian Zhang. November 2002.

PEER 2002/16 *Estimation of Uncertainty in Geotechnical Properties for Performance-Based Earthquake Engineering*. Allen L. Jones, Steven L. Kramer, and Pedro Arduino. December 2002.

PEER 2002/15 *Seismic Behavior of Bridge Columns Subjected to Various Loading Patterns*. Asadollah Esmaeily-Gh. and Yan Xiao. December 2002.

PEER 2002/14 *Inelastic Seismic Response of Extended Pile Shaft Supported Bridge Structures.* T.C. Hutchinson, R.W. Boulanger, Y.H. Chai, and I.M. Idriss. December 2002.

PEER 2002/13 *Probabilistic Models and Fragility Estimates for Bridge Components and Systems.* Paolo Gardoni, Armen Der Kiureghian, and Khalid M. Mosalam. June 2002.

PEER 2002/12 *Effects of Fault Dip and Slip Rake on Near-Source Ground Motions: Why Chi-Chi Was a Relatively Mild M7.6 Earthquake*. Brad T. Aagaard, John F. Hall, and Thomas H. Heaton. December 2002.

PEER 2002/11 *Analytical and Experimental Study of Fiber-Reinforced Strip Isolators*. James M. Kelly and Shakhzod M. Takhirov. September 2002.

PEER 2002/10 *Centrifuge Modeling of Settlement and Lateral Spreading with Comparisons to Numerical Analyses***.** Sivapalan Gajan and Bruce L. Kutter. January 2003.

PEER 2002/09 *Documentation and Analysis of Field Case Histories of Seismic Compression during the 1994 Northridge, California, Earthquake*. Jonathan P. Stewart, Patrick M. Smith, Daniel H. Whang, and Jonathan D. Bray. October 2002.

PEER 2002/08 *Component Testing, Stability Analysis and Characterization of Buckling-Restrained Unbonded Braces™*. Cameron Black, Nicos Makris, and Ian Aiken. September 2002.

PEER 2002/07 *Seismic Performance of Pile-Wharf Connections.* Charles W. Roeder, Robert Graff, Jennifer Soderstrom, and Jun Han Yoo. December 2001.

PEER 2002/06 *The Use of Benefit-Cost Analysis for Evaluation of Performance-Based Earthquake Engineering Decisions*. Richard O. Zerbe and Anthony Falit-Baiamonte. September 2001.

PEER 2002/05 *Guidelines, Specifications, and Seismic Performance Characterization of Nonstructural Building Components and Equipment*. André Filiatrault, Constantin Christopoulos, and Christopher Stearns. September 2001.

PEER 2002/04 *Consortium of Organizations for Strong-Motion Observation Systems and the Pacific Earthquake Engineering Research Center Lifelines Program: Invited Workshop on Archiving and Web Dissemination of Geotechnical Data, 4–5 October 2001*. September 2002.

PEER 2002/03 *Investigation of Sensitivity of Building Loss Estimates to Major Uncertain Variables for the Van Nuys Testbed*. Keith A. Porter, James L. Beck, and Rustem V. Shaikhutdinov. August 2002.

PEER 2002/02 *The Third U.S.-Japan Workshop on Performance-Based Earthquake Engineering Methodology for Reinforced Concrete Building Structures*. July 2002.

PEER 2002/01 *Nonstructural Loss Estimation: The UC Berkeley Case Study.* Mary C. Comerio and John C. Stallmeyer. December 2001.

PEER 2001/16 *Statistics of SDF-System Estimate of Roof Displacement for Pushover Analysis of Buildings.* Anil K. Chopra, Rakesh K. Goel, and Chatpan Chintanapakdee. December 2001.

PEER 2001/15 *Damage to Bridges during the 2001 Nisqually Earthquake.* R. Tyler Ranf, Marc O. Eberhard, and Michael P. Berry. November 2001.

PEER 2001/14 *Rocking Response of Equipment Anchored to a Base Foundation.* Nicos Makris and Cameron J. Black. September 2001.

PEER 2001/13 *Modeling Soil Liquefaction Hazards for Performance-Based Earthquake Engineering*. Steven L. Kramer and Ahmed-W. Elgamal. February 2001.

PEER 2001/12 *Development of Geotechnical Capabilities in OpenSees*. Boris Jeremić. September 2001.

PEER 2001/11 *Analytical and Experimental Study of Fiber-Reinforced Elastomeric Isolators*. James M. Kelly and Shakhzod M. Takhirov. September 2001.

PEER 2001/10 *Amplification Factors for Spectral Acceleration in Active Regions.* Jonathan P. Stewart, Andrew H. Liu, Yoojoong Choi, and Mehmet B. Baturay. December 2001.

PEER 2001/09 *Ground Motion Evaluation Procedures for Performance-Based Design.* Jonathan P. Stewart, Shyh-Jeng Chiou, Jonathan D. Bray, Robert W. Graves, Paul G. Somerville, and Norman A. Abrahamson. September 2001.

PEER 2001/08 *Experimental and Computational Evaluation of Reinforced Concrete Bridge Beam-Column Connections for Seismic Performance*. Clay J. Naito, Jack P. Moehle, and Khalid M. Mosalam. November 2001.

PEER 2001/07 *The Rocking Spectrum and the Shortcomings of Design Guidelines.* Nicos Makris and Dimitrios Konstantinidis. August 2001.

PEER 2001/06 *Development of an Electrical Substation Equipment Performance Database for Evaluation of Equipment Fragilities*. Thalia Agnanos. April 1999.

PEER 2001/05 *Stiffness Analysis of Fiber-Reinforced Elastomeric Isolators.* Hsiang-Chuan Tsai and James M. Kelly. May 2001.

PEER 2001/04 *Organizational and Societal Considerations for Performance-Based Earthquake Engineering*. Peter J. May. April 2001.

PEER 2001/03 *A Modal Pushover Analysis Procedure to Estimate Seismic Demands for Buildings: Theory and Preliminary Evaluation*. Anil K. Chopra and Rakesh K. Goel. January 2001.

PEER 2001/02 *Seismic Response Analysis of Highway Overcrossings Including Soil-Structure Interaction*. Jian Zhang and Nicos Makris. March 2001.

PEER 2001/01 *Experimental Study of Large Seismic Steel Beam-to-Column Connections.* Egor P. Popov and Shakhzod M. Takhirov. November 2000.

PEER 2000/10 *The Second U.S.-Japan Workshop on Performance-Based Earthquake Engineering Methodology for Reinforced Concrete Building Structures*. March 2000.

PEER 2000/09 *Structural Engineering Reconnaissance of the August 17, 1999 Earthquake: Kocaeli (Izmit), Turkey*. Halil Sezen, Kenneth J. Elwood, Andrew S. Whittaker, Khalid Mosalam, John J. Wallace, and John F. Stanton. December 2000.

PEER 2000/08 *Behavior of Reinforced Concrete Bridge Columns Having Varying Aspect Ratios and Varying Lengths of Confinement*. Anthony J. Calderone, Dawn E. Lehman, and Jack P. Moehle. January 2001.

PEER 2000/07 *Cover-Plate and Flange-Plate Reinforced Steel Moment-Resisting Connections.* Taejin Kim, Andrew S. Whittaker, Amir S. Gilani, Vitelmo V. Bertero, and Shakhzod M. Takhirov. September 2000.

PEER 2000/06 *Seismic Evaluation and Analysis of 230-kV Disconnect Switches.* Amir S. J. Gilani, Andrew S. Whittaker, Gregory L. Fenves, Chun-Hao Chen, Henry Ho, and Eric Fujisaki. July 2000.

PEER 2000/05 *Performance-Based Evaluation of Exterior Reinforced Concrete Building Joints for Seismic Excitation*. Chandra Clyde, Chris P. Pantelides, and Lawrence D. Reaveley. July 2000.

PEER 2000/04 *An Evaluation of Seismic Energy Demand: An Attenuation Approach*. Chung-Che Chou and Chia-Ming Uang. July 1999.

PEER 2000/03 *Framing Earthquake Retrofitting Decisions: The Case of Hillside Homes in Los Angeles.* Detlof von Winterfeldt, Nels Roselund, and Alicia Kitsuse. March 2000.

PEER 2000/02 *U.S.-Japan Workshop on the Effects of Near-Field Earthquake Shaking*. Andrew Whittaker, Editor. July 2000.

PEER 2000/01 *Further Studies on Seismic Interaction in Interconnected Electrical Substation Equipment.* Armen Der Kiureghian, Kee-Jeung Hong, and Jerome L. Sackman. November 1999.

PEER 1999/14 *Seismic Evaluation and Retrofit of 230-kV Porcelain Transformer Bushings*. Amir S. Gilani, Andrew S. Whittaker, Gregory L. Fenves, and Eric Fujisaki. December 1999.

PEER 1999/13 *Building Vulnerability Studies: Modeling and Evaluation of Tilt-up and Steel Reinforced Concrete Buildings*. John W. Wallace, Jonathan P. Stewart, and Andrew S. Whittaker, Editors. December 1999.

PEER 1999/12 *Rehabilitation of Nonductile RC Frame Building Using Encasement Plates and Energy-Dissipating Devices*. Mehrdad Sasani, Vitelmo V. Bertero, James C. Anderson. December 1999.

PEER 1999/11 *Performance Evaluation Database for Concrete Bridge Components and Systems under Simulated Seismic Loads*. Yael D. Hose and Frieder Seible. November 1999.

PEER 1999/10 *U.S.-Japan Workshop on Performance-Based Earthquake Engineering Methodology for Reinforced Concrete Building Structures*. December 1999.

PEER 1999/09 *Performance Improvement of Long Period Building Structures Subjected to Severe Pulse-Type Ground Motions*. James C. Anderson, Vitelmo V. Bertero, and Raul Bertero. October 1999.

PEER 1999/08 *Envelopes for Seismic Response Vectors.* Charles Menun and Armen Der Kiureghian. July 1999.

PEER 1999/07 *Documentation of Strengths and Weaknesses of Current Computer Analysis Methods for Seismic Performance of Reinforced Concrete Members*. William F. Cofer. November 1999.

PEER 1999/06 *Rocking Response and Overturning of Anchored Equipment under Seismic Excitations*. Nicos Makris and Jian Zhang. November 1999.

PEER 1999/05 *Seismic Evaluation of 550 kV Porcelain Transformer Bushings.* Amir S. Gilani, Andrew S. Whittaker, Gregory L. Fenves, and Eric Fujisaki. October 1999.

PEER 1999/04 *Adoption and Enforcement of Earthquake Risk-Reduction Measures.* Peter J. May, Raymond J. Burby, T. Jens Feeley, and Robert Wood. August 1999.

PEER 1999/03 *Task 3 Characterization of Site Response General Site Categories*. Adrian Rodriguez-Marek, Jonathan D. Bray and Norman Abrahamson. February 1999.

PEER 1999/02 *Capacity-Demand-Diagram Methods for Estimating Seismic Deformation of Inelastic Structures: SDF Systems*. Anil K. Chopra and Rakesh Goel. April 1999.

PEER 1999/01 *Interaction in Interconnected Electrical Substation Equipment Subjected to Earthquake Ground Motions*. Armen Der Kiureghian, Jerome L. Sackman, and Kee-Jeung Hong. February 1999.

PEER 1998/08 *Behavior and Failure Analysis of a Multiple-Frame Highway Bridge in the 1994 Northridge Earthquake*. Gregory L. Fenves and Michael Ellery. December 1998.

PEER 1998/07 *Empirical Evaluation of Inertial Soil-Structure Interaction Effects.* Jonathan P. Stewart, Raymond B. Seed, and Gregory L. Fenves. November 1998.

PEER 1998/06 *Effect of Damping Mechanisms on the Response of Seismic Isolated Structures*. Nicos Makris and Shih-Po Chang. November 1998.

PEER 1998/05 *Rocking Response and Overturning of Equipment under Horizontal Pulse-Type Motions*. Nicos Makris and Yiannis Roussos. October 1998.

PEER 1998/04 *Pacific Earthquake Engineering Research Invitational Workshop Proceedings, May 14–15, 1998: Defining the Links between Planning, Policy Analysis, Economics and Earthquake Engineering*. Mary Comerio and Peter Gordon. September 1998.

PEER 1998/03 *Repair/Upgrade Procedures for Welded Beam to Column Connections*. James C. Anderson and Xiaojing Duan. May 1998.

PEER 1998/02 *Seismic Evaluation of 196 kV Porcelain Transformer Bushings.* Amir S. Gilani, Juan W. Chavez, Gregory L. Fenves, and Andrew S. Whittaker. May 1998.

PEER 1998/01 *Seismic Performance of Well-Confined Concrete Bridge Columns.* Dawn E. Lehman and Jack P. Moehle. December 2000.

PEER REPORTS: ONE HUNDRED SERIES

PEER 2012/103 *Performance-Based Seismic Demand Assessment of Concentrically Braced Steel Frame Buildings.* Chui-Hsin Chen and Stephen A. Mahin. December 2012.

PEER 2012/102 *Procedure to Restart an Interrupted Hybrid Simulation: Addendum to PEER Report 2010/103.* Vesna Terzic and Bozidar Stojadinovic. October 2012.

PEER 2012/101 *Mechanics of Fiber Reinforced Bearings.* James M. Kelly and Andrea Calabrese. February 2012.

PEER 2011/107 *Nonlinear Site Response and Seismic Compression at Vertical Array Strongly Shaken by 2007 Niigata-ken Chuetsu-oki Earthquake.* Eric Yee, Jonathan P. Stewart, and Kohji Tokimatsu. December 2011.

PEER 2011/106 *Self Compacting Hybrid Fiber Reinforced Concrete Composites for Bridge Columns.* Pardeep Kumar, Gabriel Jen, William Trono, Marios Panagiotou, and Claudia Ostertag. September 2011.

PEER 2011/105 *Stochastic Dynamic Analysis of Bridges Subjected to Spacially Varying Ground Motions.* Katerina Konakli and Armen Der Kiureghian. August 2011.

PEER 2011/104 *Design and Instrumentation of the 2010 E-Defense Four-Story Reinforced Concrete and Post-Tensioned Concrete Buildings.* Takuya Nagae, Kenichi Tahara, Taizo Matsumori, Hitoshi Shiohara, Toshimi Kabeyasawa, Susumu Kono, Minehiro Nishiyama (Japanese Research Team) and John Wallace, Wassim Ghannoum, Jack Moehle, Richard Sause, Wesley Keller, Zeynep Tuna (U.S. Research Team). June 2011.

PEER 2011/103 *In-Situ Monitoring of the Force Output of Fluid Dampers: Experimental Investigation.* Dimitrios Konstantinidis, James M. Kelly, and Nicos Makris. April 2011.

PEER 2011/102 *Ground-Motion Prediction Equations 1964–2010.* John Douglas. April 2011.

PEER 2011/101 *Report of the Eighth Planning Meeting of NEES/E-Defense Collaborative Research on Earthquake Engineering.* Convened by the Hyogo Earthquake Engineering Research Center (NIED), NEES Consortium, Inc. February 2011.

PEER 2010/111 *Modeling and Acceptance Criteria for Seismic Design and Analysis of Tall Buildings.* Task 7 Report for the Tall Buildings Initiative - Published jointly by the Applied Technology Council. October 2010.

PEER 2010/110 *Seismic Performance Assessment and Probabilistic Repair Cost Analysis of Precast Concrete Cladding Systems for Multistory Buildlings.* Jeffrey P. Hunt and Božidar Stojadinovic. November 2010.

PEER 2010/109 *Report of the Seventh Joint Planning Meeting of NEES/E-Defense Collaboration on Earthquake Engineering. Held at the E-Defense, Miki, and Shin-Kobe, Japan, September 18–19, 2009.* August 2010.

PEER 2010/108 *Probabilistic Tsunami Hazard in California.* Hong Kie Thio, Paul Somerville, and Jascha Polet, preparers. October 2010.

PEER 2010/107 *Performance and Reliability of Exposed Column Base Plate Connections for Steel Moment-Resisting Frames.* Ady Aviram, Božidar Stojadinovic, and Armen Der Kiureghian. August 2010.

PEER 2010/106 *Verification of Probabilistic Seismic Hazard Analysis Computer Programs.* Patricia Thomas, Ivan Wong, and Norman Abrahamson. May 2010.

PEER 2010/105 *Structural Engineering Reconnaissance of the April 6, 2009, Abruzzo, Italy, Earthquake, and Lessons Learned.* M. Selim Günay and Khalid M. Mosalam. April 2010.

PEER 2010/104 *Simulating the Inelastic Seismic Behavior of Steel Braced Frames, Including the Effects of Low-Cycle Fatigue.* Yuli Huang and Stephen A. Mahin. April 2010.

PEER 2010/103 *Post-Earthquake Traffic Capacity of Modern Bridges in California.* Vesna Terzic and Božidar Stojadinović. March 2010.

PEER 2010/102 *Analysis of Cumulative Absolute Velocity (CAV) and JMA Instrumental Seismic Intensity (I_{JMA}) Using the PEER–NGA Strong Motion Database.* Kenneth W. Campbell and Yousef Bozorgnia. February 2010.

PEER 2010/101 *Rocking Response of Bridges on Shallow Foundations.* Jose A. Ugalde, Bruce L. Kutter, and Boris Jeremic. April 2010.

PEER 2009/109 *Simulation and Performance-Based Earthquake Engineering Assessment of Self-Centering Post-Tensioned Concrete Bridge Systems.* Won K. Lee and Sarah L. Billington. December 2009.

PEER 2009/108 *PEER Lifelines Geotechnical Virtual Data Center.* J. Carl Stepp, Daniel J. Ponti, Loren L. Turner, Jennifer N. Swift, Sean Devlin, Yang Zhu, Jean Benoit, and John Bobbitt. September 2009.

PEER 2009/107 *Experimental and Computational Evaluation of Current and Innovative In-Span Hinge Details in Reinforced Concrete Box-Girder Bridges: Part 2: Post-Test Analysis and Design Recommendations.* Matias A. Hube and Khalid M. Mosalam. December 2009.

PEER 2009/106 *Shear Strength Models of Exterior Beam-Column Joints without Transverse Reinforcement.* Sangjoon Park and Khalid M. Mosalam. November 2009.

PEER 2009/105 *Reduced Uncertainty of Ground Motion Prediction Equations through Bayesian Variance Analysis.* Robb Eric S. Moss. November 2009.

PEER 2009/104 *Advanced Implementation of Hybrid Simulation.* Andreas H. Schellenberg, Stephen A. Mahin, Gregory L. Fenves. November 2009.

PEER 2009/103 *Performance Evaluation of Innovative Steel Braced Frames.* T. Y. Yang, Jack P. Moehle, and Božidar Stojadinovic. August 2009.

PEER 2009/102 *Reinvestigation of Liquefaction and Nonliquefaction Case Histories from the 1976 Tangshan Earthquake.* Robb Eric Moss, Robert E. Kayen, Liyuan Tong, Songyu Liu, Guojun Cai, and Jiaer Wu. August 2009.

PEER 2009/101 *Report of the First Joint Planning Meeting for the Second Phase of NEES/E-Defense Collaborative Research on Earthquake Engineering.* Stephen A. Mahin et al. July 2009.

PEER 2008/104 *Experimental and Analytical Study of the Seismic Performance of Retaining Structures.* Linda Al Atik and Nicholas Sitar. January 2009.

PEER 2008/103 *Experimental and Computational Evaluation of Current and Innovative In-Span Hinge Details in Reinforced Concrete Box-Girder Bridges. Part 1: Experimental Findings and Pre-Test Analysis.* Matias A. Hube and Khalid M. Mosalam. January 2009.

PEER 2008/102 *Modeling of Unreinforced Masonry Infill Walls Considering In-Plane and Out-of-Plane Interaction.* Stephen Kadysiewski and Khalid M. Mosalam. January 2009.

PEER 2008/101 *Seismic Performance Objectives for Tall Buildings.* William T. Holmes, Charles Kircher, William Petak, and Nabih Youssef. August 2008.

PEER 2007/101 *Generalized Hybrid Simulation Framework for Structural Systems Subjected to Seismic Loading*. Tarek Elkhoraibi and Khalid M. Mosalam. July 2007.

PEER 2007/100 *Seismic Evaluation of Reinforced Concrete Buildings Including Effects of Masonry Infill Walls*. Alidad Hashemi and Khalid M. Mosalam. July 2007.

The Pacifi c Earthquake Engineering Research Center (PEER) is a multi-institutional research and education center with headquarters at the University of California, Berkeley. Investigators from over 20 universities, several consulting companies, and researchers at various state and federal government agencies contribute to research programs focused on performance-based earthquake engineering.

These research programs aim to identify and reduce the risks from major earthquakes to life safety and to the economy by including research in a wide variety of disciplines including structural and geotechnical engineering, geology/seismology, lifelines, transportation, architecture, economics, risk management, and public policy.

PEER is supported by federal, state, local, and regional agencies, together with industry partners.

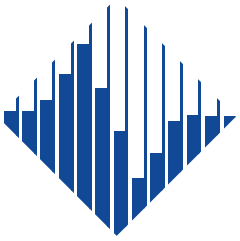

PEER Core Institutions

University of California, Berkeley (Lead Institution)
California Institute of Technology
Oregon State University
Stanford University
University of California, Davis
University of California, Irvine
University of California, Los Angeles
University of California, San Diego
University of Nevada, Reno
University of Southern California
University of Washington

PEER reports can be ordered at https://peer.berkeley.edu/peer-reports or by contacting

Pacific Earthquake Engineering Research Center
University of California, Berkeley
325 Davis Hall, Mail Code 1792
Berkeley, CA 94720-1792
Tel: 510-642-3437
Email: peer_center@berkeley.edu

ISSN 2770-8314
https://doi.org/10.55461/RYNQ3624